Title
KINETICS OF SULFUR DIOXIDE FLUORESCENCE

Author
Martin, Douglas R.

Publication Date
1973-03-01

LBL-1199

KINETICS OF SULFUR DIOXIDE FLUORESCENCE

Douglas R. Martin
(Ph.D. thesis)

March 1973

Prepared for the U. S. Atomic Energy Commission
under Contract W-7405-ENG-48

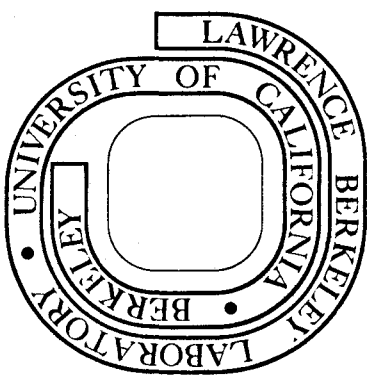

LBL-1199

DISCLAIMER

KINETICS OF SULFUR DIOXIDE FLUORESCENCE

Table of Contents

KINETICS OF SULFUR DIOXIDE FLUORESCENCE

Douglas R. Martin

Inorganic Materials Research Division, Lawrence Berkeley Laboratory and Department of Chemistry; University of California, Berkeley, California

ABSTRACT

The fluorescence lifetime of gas phase sulfur dioxide in the first excited singlet state has been measured over a range of excitation and observation wavelengths and SO_2 pressures. Measurements were made by the phase shift method. The radiative lifetime of SO_2 has been determined at low pressure (less then 0.2 mTorr) for various excitation wavelengths (10 Å FWHM, full width at half maximum) from 2500-3150 Å and observation over the range 3300-4000 Å. The radiative lifetime was observed to vary between 35 and 57 μsec as compared with the lifetime of 0.2 μsec predicted from absorption measurements. These results are discussed in light of the current theory of intramolecular radiationless transitions. The apparent lifetime was measured as a function of pressure (5-20 mTorr) and observation wavelength (16 Å FWHM) for four excitation wavelengths (about 25 Å bandwidth). For a given excitation wavelength a linear relationship is observed in graphs of (1/apparent lifetime) versus SO_2 pressure. The slopes of such graphs, the apparent quenching rate constants, decrease with increasing difference between excitation and observation energies. The apparent quenching constant for observation energies slightly less than the excitation energy is about gas kinetic

(3.3×10^{-10} cm^3/part-sec) for all four excitation energies. The decrease in apparent quenching rate constant with decreasing observation energy is attributed to vibrational relaxation within the fluorescing manifold of states. The collisional relaxation of excited SO_2 is interpreted in terms of a stepladder model including a channel removing excited molecules from each step of the stepladder (collisionally induced intersystem crossing). The rate constant for vibrational relaxation within the excited singlet is estimated to be at least 1.2 times as large as the rate constant for intersystem crossing. The step size of the stepladder is estimated to be 1000-2000 cm^{-1}.

I. INTRODUCTION

The relaxation dynamics of electronically excited molecules is a topic of current interest to chemists for two major reasons. (1) It has long been recognized that relaxation processes are important features in gas phase chemical reactions.[1] Unimolecular reactions proceed through vibrational activation of the reactants. Recombination reactions rely on radiation or collisional deactivation to remove energy and stabilize the newly formed molecule. (2) The dynamics of molecular states can be investigated for information on the nature of the state themselves.[2-5] Also, measurement of relaxation processes in electronically excited molecules tests theories of relaxation dynamics.[6]

Various experimental methods have been used to investigate relaxation processes. Fluorescence is one of the oldest and most widely used methods.[7] One advantage of the fluorescence method is that excited molecules can be prepared with a fairly well defined energy. In some cases the various quantum states of the excited molecule can be directly observed in emission.[5] Fluorescence also has the advantage of allowing time resolved studies, which can provide a direct measurement of the rate of energy transfer.

This experiment is an investigation into the relaxation dynamics of sulfur dioxide excited by ultraviolet radiation. Observation of the ultraviolet fluorescence provides measurements of the radiative emission rates and allows estimation of the rates and quantities of energy involved in collisional relaxation of the excited state.

The radiative lifetime of SO_2 is of interest because it has been observed to be about 100 times longer than predicted from its absorption spectrum.[8] The radiative lifetime has not been determined as a function of excitation wavelength. Standard radiation theory predicts a dependence on the emission frequency. In addition, the current theories explaining anomalous lifetimes imply that there may be significant variation of lifetime among individual quantum states.[3,4] The lifetime of nitrogen dioxide, which is also anomalously long, exhibits distinct fluctuations between various quantum states.[9] SO_2 lifetime determinations are also of interest since the existing measurements[8] may exhibit systematic error due to inadequately small cell geometry.[9]

The dynamics of collisional relaxation of sulfur dioxide have not been studied in detail experimentally. It is known that fluorescence from electronically excited sulfur dioxide is quenched efficiently,[10-11] but the path of the relaxation process is not known. The possibility of vibrational relaxation within the excited electronic state has been raised,[12] but analysis of collisional deactivation has been in terms of a single excited state,[12] i.e., the possibility of vibrational relaxation was ruled out. A determination of the extent of vibrational relaxation in the excited molecule is necessary in order to correctly interpret the results of previous single excited state analyses.

Sulfur dioxide has two excited electronic states in the energy range of this investigation, 2500-3400 Å. The lower state, a triplet, exhibits a weak absorption from 3400-3900 Å. The higher of the two

states is a singlet. It absorbs from 3385 Å to least 2280 Å.[16] A portion of its absorption spectrum, as determined in this laboratory, is shown in Fig. 1. The singlet absorption has been partially assigned,[14] with the most definite assignments in the long wavelength region of distinct vibronic transitions. The ground electronic state dissociates at about 2280 Å.[29] Much of the energy range of the excited singlet is completely encompassed by the ground electronic state. This is a key factor in the determination of the properties of electronically excited sulfur dioxide.

The state of principal interest in this study is the excited singlet. The presence of the triplet is important, however, since it could influence the dynamics of the excited singlet.

Photochemistry is of limited importance in the range of excitation wavelengths used, 2500 to 3150 Å. Dissociation does not occur in this range.[16] However, reactions are known to occur in photochemical experiments at these wavelengths involving several Torr of pure SO_2.[17-18] Experiments have indicated that the reactive species in SO_2 photolysis is the triplet state.[18] The triplet absorption does not extend to the range of excitation wavelengths used, so the triplet is not directly formed in these experiments by optical excitation of ground state SO_2. However, the triplet can be formed at these wavelengths by an indirect process in which the excited singlet molecules experience collisions with other molecules.[12] Such collision can induce spin inversion. Thus, triplet molecules are produced from excited singlets by a pressure dependent process. At the low pressures

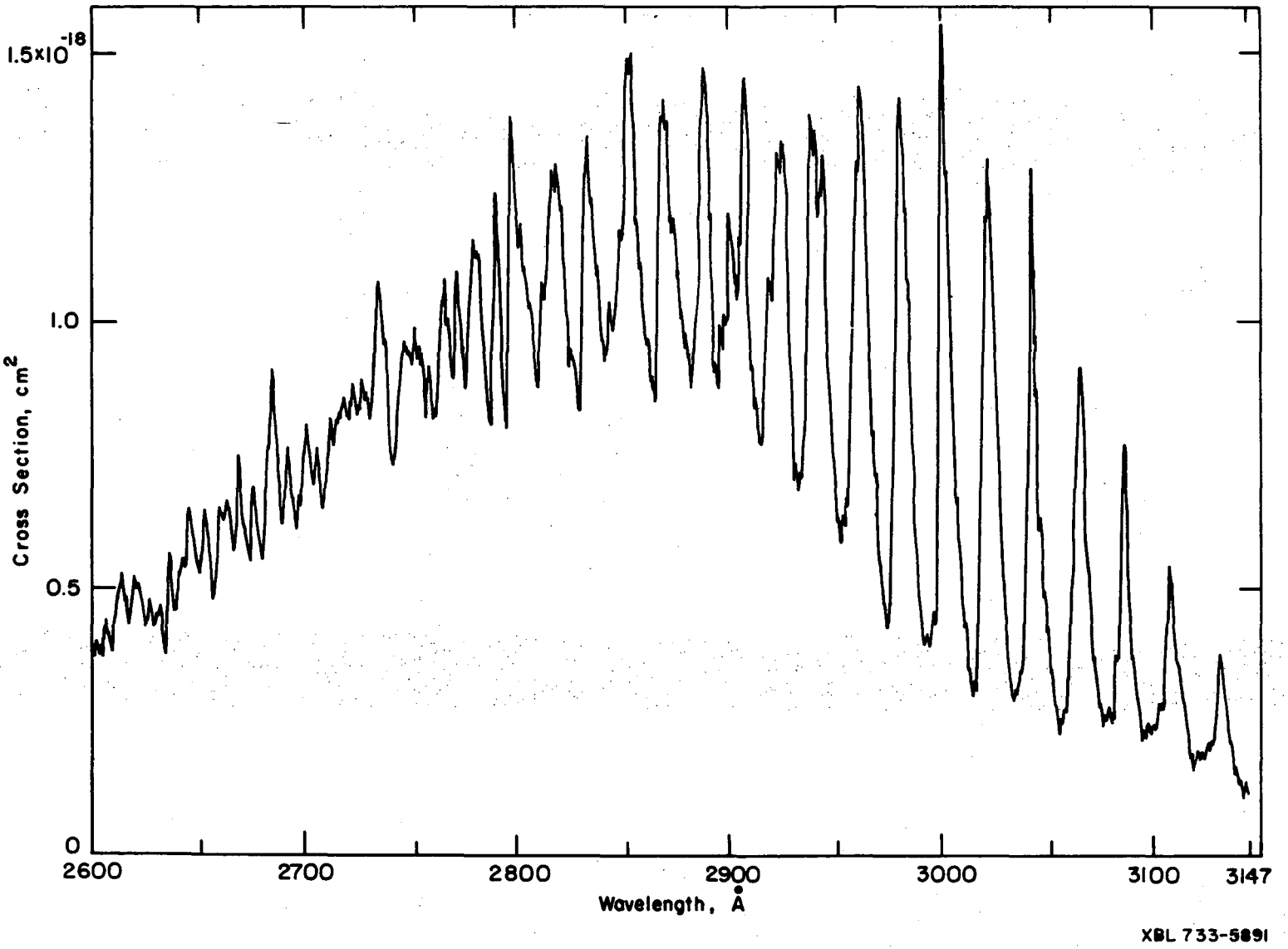

Fig. 1. Absorption spectrum of SO_2 determined in this laboratory.

used in this study, less than 20 mTorr, photochemistry due to triplet production is expected to be insignificant. No direct examination has been made of the photochemistry of pure SO_2 in the mTorr pressure range, but both Mettee[12] and Greenough and Duncan[8] could find no evidence of SO_2 decomposition during ultraviolet irradiation of several mTorr of SO_2.

SUMMARY OF PREVIOUS STUDIES OF SULFUR DIOXIDE FLUORESCENCE

Fluorescence from optical excitation of the first excited singlet of sulfur dioxide was first observed by Greenough and Duncan.[8] They excited gaseous SO_2 with light from a high pressure Hg arc. The excitation contained light from 2700 to 3100 Å. They observed a "continous" emission from about 3000 to 4400 Å. Some structure was observed in the continuum and these weak bands were correlated with known absorptions of the first excited singlet state. Superimposed on the long wavelength end of the continuum were several intense bands. These intense bands were shown to originate in the lowest level of the first excited electronic state and terminate in various levels of the ground electronic state. The lifetime of the first excited singlet state was determined in a flash-decay experiment using the filtered output of a xenon flash lamp to provide excitation from 2700 to 3100 Å. The value of the lifetime extrapolated to zero pressure was 42 μsec. From the slope of their lifetime plot, k_q, the quenching rate constant based on a single excited state model, was found to be 1×10^{-10} cm^3/part-sec. They noted that the measured lifetime was about one hundred longer than the value of 0.2 μsec they predicted from absorption data. From various considerations they identified the lower excited state as a triplet and the second excited state as its associated singlet.

Douglas[3] also determined the lifetime of SO_2 in the first excited singlet state. He reported a lifetime of about 60 μsec, supporting the anomalous nature of the lifetime. Experimental details were not given, however.

Mettee[12] observed that the triplet emission disappeared at pressures less than about 10 mTorr, while emission from the singlet remained. He concluded that the triplet was formed exclusively by intersystem crossing induced by collision with another SO_2 molecule. Mettee determined the apparent Stern-Volmer constant, the ratio of quenching rate constant to fluorescent rate constant, for six different excitation wavelengths. He noted that the Stern-Volmer constant decreased with higher excitation energy, implying that the quenching rate constant or the lifetime decreases with higher excitation energy. From theoretical considerations he decided that the change in Stern-Volmer constant was probably due to a decrease in the lifetime. This interpretation yielded lifetimes ranging from 10 μsec to 130 μsec for excitation from 3147-2650 Å. Conversely, the quenching rate constant could be interpreted as ranging from $\frac{1}{4}$ to 3 times the gas kinetic rate constant, 3.3×10^{-10} cm^3/part-sec. Mettee commented on the possibility of vibrational energy transfer within the excited singlet electronic state, but concluded that the evidence was not compelling.[12] His interpretation was based on a single excited state model.

II. EXPERIMENTAL

A. Theory of Measurements

Rate constants in this experiment were determined by use of the phase shift method. This method has been used by several other investigators in a variety of experimental contexts.[19,20] The phase shift method makes use of the fact that the response of a system to a modulated excitation is phase shifted with respect to the excitation. The magnitude of the phase shift is indicative of the rate at which the system returns to its unexcited condition. If, for instance, a system could recover virtually instantaneously from excitation it would follow the excitation closely and the phase shift would be small. Conversely, a system which recovers slowly would exhibit a large phase shift. These relationships are well known in electrical circuit analysis.[21]

We now proceed with the development of phase shift expressions in the context of fluorescence kinetics. The discussion is limited to systems described by linear differential equations, i.e., all expressions are first order in the excited state. Physically this means that all reactions between excited species are ruled out and the concentration of ground state molecules is assumed constant. These assumptions are applicable at moderate light intensities.

The simplest mechanism is that of a single excited state decaying with a single lifetime.

$$g \xrightarrow{k_a I} s \quad \text{excitation}$$

$$s \xrightarrow{k} g \quad \text{de-excitation}$$

where

g is a ground state molecule
s is an excited molecule
k_a is the absorption cross section
I is the excitation flux
k is the de-excitation rate.

The differential equation describing this system is

$$\frac{d\underset{\sim}{S}}{dt} = G k_a \underset{\sim}{I} - k\underset{\sim}{S} \tag{1}$$

where

G is the concentration of g
$\underset{\sim}{S}$ is the modulated concentration of s
$\underset{\sim}{I}$ is the modulated excitation

In some experiments the modulated excitation is a "square wave".[20] In this experiment the excitation was sinusoidal. Then

$$\underset{\sim}{I} = \frac{I_o}{2}(1+e^{i\omega t}) \tag{2}$$

where ω is the angular frequency of excitation.

Since Eq. (1) is linear, dc terms in the modulated excitation produce only a dc component in the modulated excited state. We are interested only in the ac component of the excited state so dc terms in the excitation are dropped. Then

$$\underset{\sim}{I} = I_o e^{i\omega t}$$

and

$$\frac{d\underset{\sim}{S}}{dt} = G I_o k_a e^{i\omega t} - k\underset{\sim}{S} \tag{3}$$

By use of Laplace transform methods[22] it can be shown that the solution to Eq. (1), at long times compared to k^{-1}, is

$$\underset{\sim}{S} = G I_o k_a \frac{1}{k+i\omega} e^{i\omega t} \tag{4}$$

Equation (2) can be re-written to make the phase shift between the excitation and the excited state more obvious.

$$\underset{\sim}{S} = G I_o k_a \frac{1}{(k^2+\omega^2)^{1/2}} e^{(i\omega t+\phi)} \tag{5}$$

where

$$\phi \equiv - \arctan \left(\frac{\omega}{k}\right)$$

Note that the time dependent part of Eq. (5) is of the same form as the time dependent part of Eq. (2) except that the response of the system (the excited state) has been phase shifted by the angle ϕ. The relationship defining ϕ illustrates the dependence of the phase shift on the rate constant for relaxation of the excited state. If k is very large compared to ω the phase shift will be small. As k is made very small compared to ω the phase shift approaches a value of -90°. Thus, phase shifts for a single excited state vary between 0 and -90° depending on the value of k relative to ω. If the phase, ϕ, can be measured the value of the rate constant is evaluated from

$$k = - \frac{\omega}{\tan (\phi)} \tag{6}$$

Phase information in a purely digital system can be obtained by use of two reversible counters gated in a fixed phase relationship with respect to the excitation. The signal from the excited state

(in this experiment pulses from the photomultiplier tube observing the emission) is continually fed into both counters. The counters are gated 90° apart and bear an arbitrary phase relationship to the excitation. The counting scheme is indicated diagramatially in Fig. 2. The plus and minus signs in Fig. 2 indicate whether pulses received in each particular quadrant are added or subtracted from the total on each counter. Note that counter 2 is defined as being 90° ($\frac{1}{4}$ cycle) behind counter 1. The phase between excitation and the counters is labelled ϕ_o.

After counting many cycles of the system (the number of cycles is of course determined by the integrating time necessary for the desired signal to noise) the residual values on each of the counters yield the phase between the counters and the excited state through the relationship

$$\psi = - \arctan \frac{Z2}{Z1}$$

where Z1 and Z2 are the residual values on counter 1 and counter 2 respectively. This relationship is derived in Appendix (A).

Since the counters are not necessarily in phase with the excitation the phase ψ is not the desired phase. Due to the additive nature of phase we may write

$$\phi = \psi - \phi_o$$

These phase relationships can be expressed in terms of vector diagrams as in Fig. 3. Note that Z1 and Z2 can be thought of in vector terms

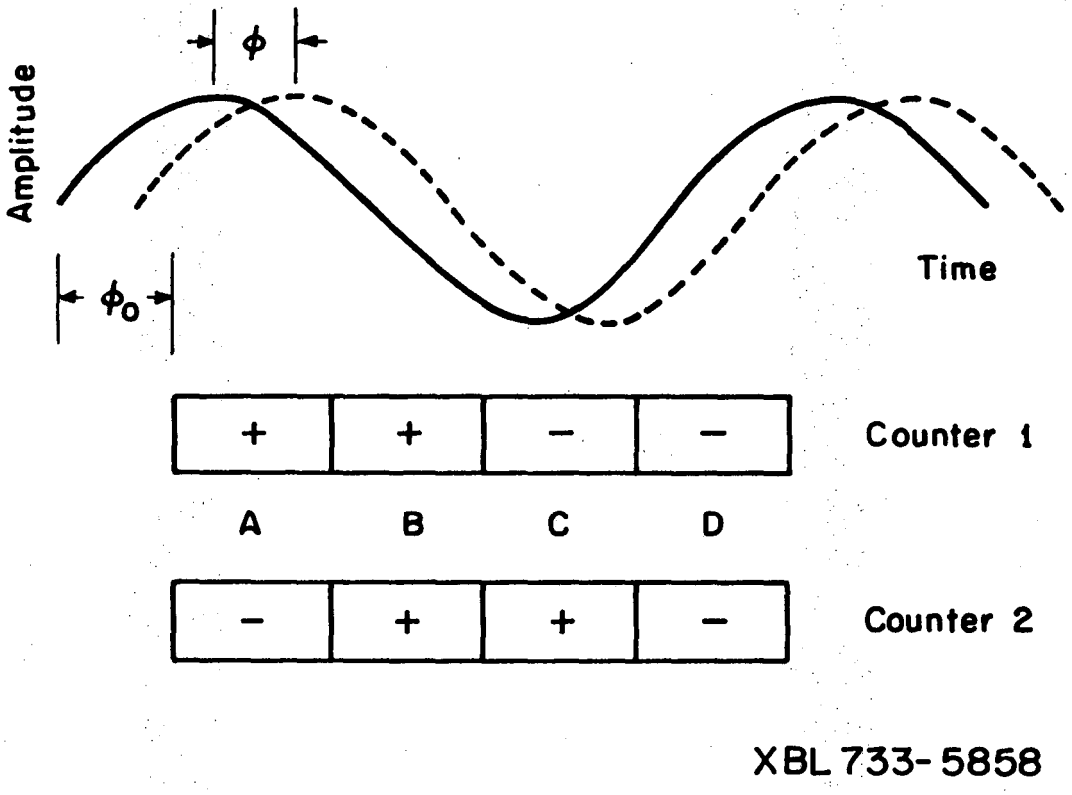

Fig. 2. Counting scheme for digital phase sensitive detection. The solid and dotted lines represent excitation and response, respectively. ϕ is the phase between excitation and response and is the phase between excitation and counters. The + and − signs indicate whether the counters are adding or subtracting in each time interval. The letters on the four quadrants are discussed in Appendix A.

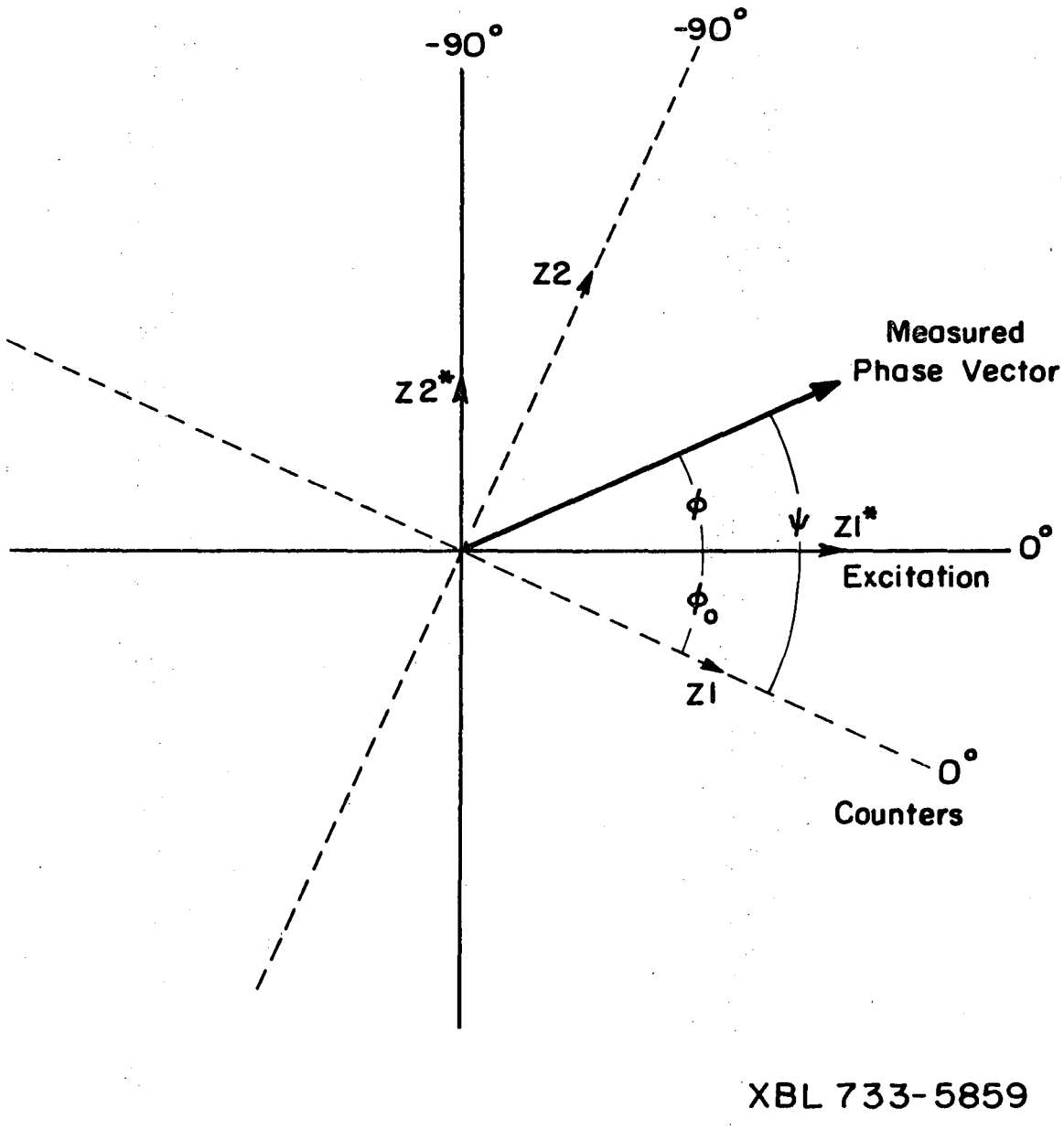

Fig. 3. Phase relationships in vector space.
The symbols are defined in the text.

as the projection of the phase vector of the two axes of the coordinate system. It is not necessary to use an orthogonal coordinate system, i.e., the counters do not have to be 90° with respect to each other. However, the expressions for ψ are simpler and the measurements more accurate for an orthogonal coordinate system.

Steady state methods have been used extensively to investigate the dynamics of fluorescence. The single excited state model, known as the Stern-Volmer model,[24] pervades much of the literature. This model applies best to atomic systems since rotation and vibrational modes are absent, but it is used frequently to analyze molecular systems. We will show that for a single excited state the information in the Stern-Volmer model is also available in the phase shift method.

The single excited state model presented earlier is now modified to reflect two physical methods of relaxation of the excited state.

$$g \xrightarrow{I_o k_a} s \qquad \text{excitation}$$

$$s \xrightarrow{k_f} g+h\upsilon \qquad \text{fluorescence}$$

$$s+M \xrightarrow{k_q} g+M \qquad \text{quenching}$$

where M is a quenching molecule which may or may not be g.

If we make the steady state approximation for this single state model

$$S = I_o k_a G \frac{1}{k_f+k_q M}$$

The emission signal is given by

$$E = \alpha k_f S$$

where α includes all detection efficiencies and is generally unknown. Then

$$E = \alpha I_o k_a G \frac{k_f}{k_f + k_q M}$$

and

$$\left(\frac{E}{G}\right)^{-1} = \alpha I_o k_a \left(1 + \frac{k_q}{k_f} M\right)$$

A "Stern-Volmer plot" is made of $(E/G)^{-1}$ vs M. The ratio of slope to intercept in such a plot is k_q/k_f. Traditionally, k_f has been measured in a flash-decay type of experiment and k_q calculated from the Stern-Volmer ratio. One important consequence of the single excited state model is that it predicts straight lines when $(E/G)^{-1}$ is plotted versus M and it predicts that the slope of those lines is independent of observation wavelength. If these predictions are not met in an experiment there is reason to believe that excited states populated by collisional relaxation from the optically populated state are partly responsible for the emission. It is important to note that multistate systems can obey the Stern-Volmer relationship at any given observation wavelength if all the measurements are made at sufficiently high pressure. This result is discussed in Appendix (B). Some investigators have taken a linear Stern-Volmer plot to indicate

single excited state behavior. Such a conclusion is not necessarily correct.

We will now show that information from the conventional dc Stern-Volmer plot is also available in the phase shift method. From Eq. (4) of Appendix (A) we have

$$Z_1^* = \frac{\text{const } Gk_f}{\omega(\omega^2+k^2)^{1/2}} \cos\phi$$

$$Z_2^* = \frac{\text{const } Gk_f}{\omega(\omega^2+k^2)^{1/2}} \sin\phi$$

It is important to note that the Z^* are not the experimental data from the counters. From Fig. 3 it is apparent that the appropriate quantities are the projections of the Z on the excitation coordinate system. The Z^* are found by a simple rotation of the phase vector through the angle ϕ.

From Eq. (1) we can write

$$Z_1^* = \text{const } G\ k\ k_f$$

$$Z_2^* = \text{const } G\ \omega\ k_f$$

For the single excited state system being considered we have $k = k_f+k_q\ M$. Then

$$\frac{(Z_1^*)^2 + (Z_2^*)^2}{Z_1^*} = \text{const } G\ \frac{k_f}{k_f+k_q\ M} \equiv E_{S-V}$$

The quantity E_{S-V} is seen to contain the same information as the conventional dc Stern-Volmer intensity.

B. Experimental Apparatus

1. General Considerations

The experimental apparatus used in this investigation is indicated schematically in Fig. 4. The apparatus was designed to provide monochromatic excitation and detection of the ultraviolet fluorescence of SO_2. The phase shift method was used to measure lifetimes in the range 5-100 μsec. The phase shift method was chosen since it allows long integration times and is readily interpreted in multistate systems. In some experiments the observation monochromator was replaced by a suitable filter, since filters give much higher collection efficiencies. In this study of SO_2 fluorescence the wavelength region of interest was so narrow that a monochromator was usually necessary to provide a sufficiently narrow band pass. The system was digital throughout. By far the greatest source of noise was the dark noise of the photomultiplier.

2. Excitation-Source

Two different lamps were used as excitation sources. One was a 1600 watt xenon arc lamp (Osram XBO 1600 W) which emits a continuum from about 2000 Å to the infrared. Power was supplied by a Christie Electric Corporation silicon rectifier. The rectifier was not stabilized. However, no significant change in voltage or current was detected during the course of an experiment of several hours duration. The output of the lamp was constant and relatively free of long term drift.

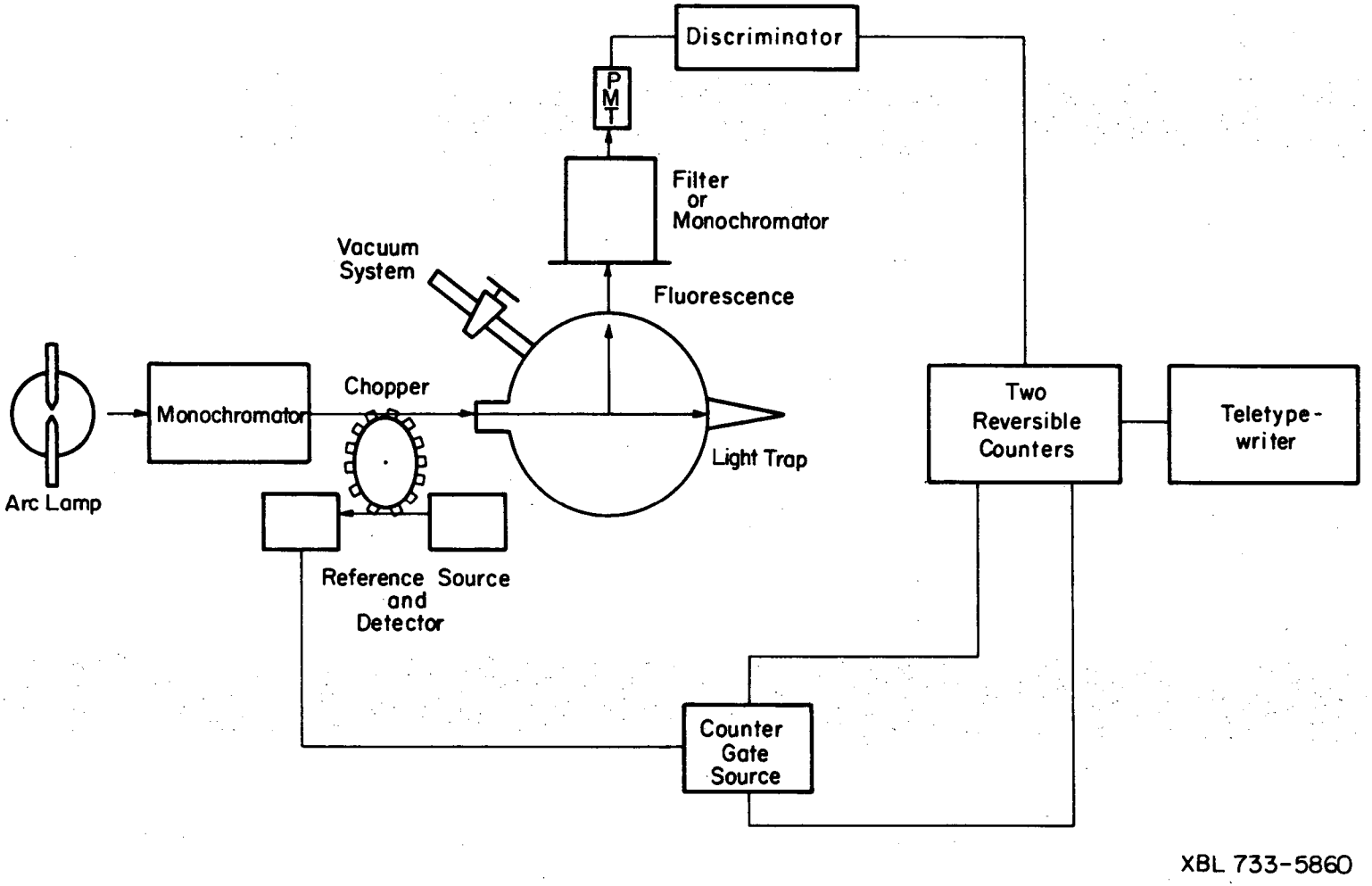

Fig. 4. Block diagram of the experimental apparatus.

Short term oscillations were less than about 5%.

The other lamp was a 500 watt PEK high pressure mercury arc lamp. Its output consisted of pressure broadened mercury lines superimposed on a continuum background. Its output was constant to about 5% over the course of several hours, but short term (1 second) changes were about 15%.

Light from either the mercury or xenon arc lamps was focussed onto the slit of a 0.5 meter Bausch & Lomb grating monochromator, model # 33-86-45. The light was focussed with a quartz collecting lens system supplied with the monochromator. The grating used in the monochromator was a 1200 line/mm grating blazed at 3000 Å.

The slit widths used varied from 2.0 mm to 0.6 mm. The excitation profile was observed with a McPherson 1 meter monochromator. In order to determine the excitation profile the beam was deflected before it entered the fluorescence cell and was focussed onto a frosted glass plate. The frosted glass plate was located about 15 cm from the entrance slit of the McPherson monochromator. The light reflected from the frosted glass plate was taken to be a representative sample of the excitation beam. Figures 5 to 9 indicate the spectral profile of the excitation-beam at the conditions listed.

The excitation beam contained a moderate amount of light of wavelengths many spectral half widths from the center wavelength of the excitation band. This scattered light was about 1% as intense as the excitation-band center. This was judged to have no significant effect on any of the experimental quantities determined. However, in

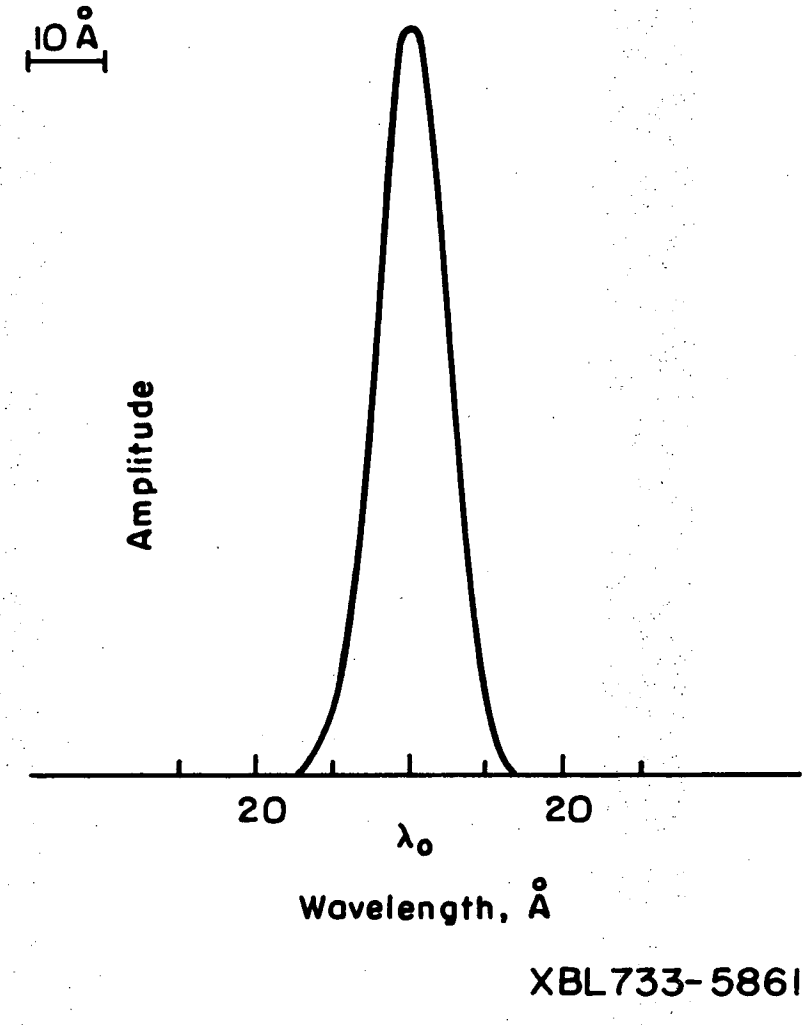

Fig. 5. A representative excitation profile in the low pressure lifetime studies.

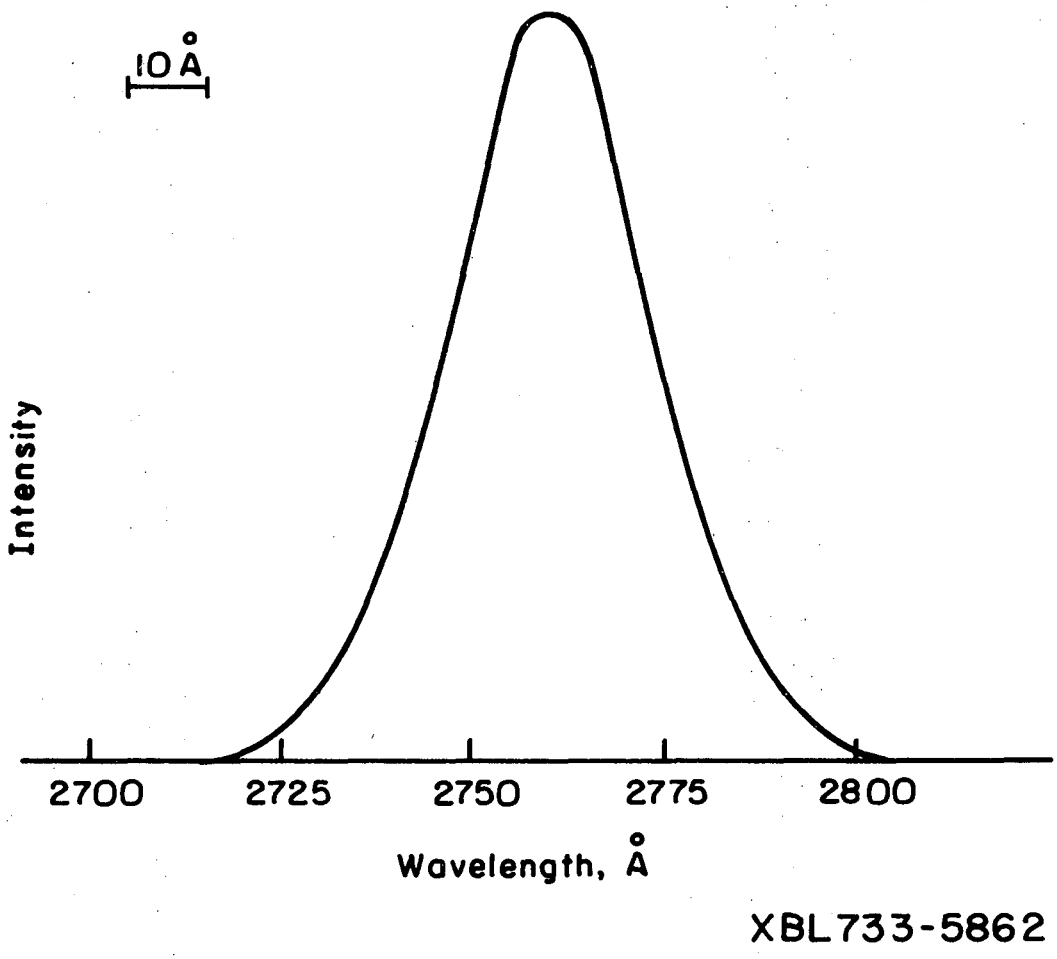

Fig. 6. Excitation profile at "2760" Å.

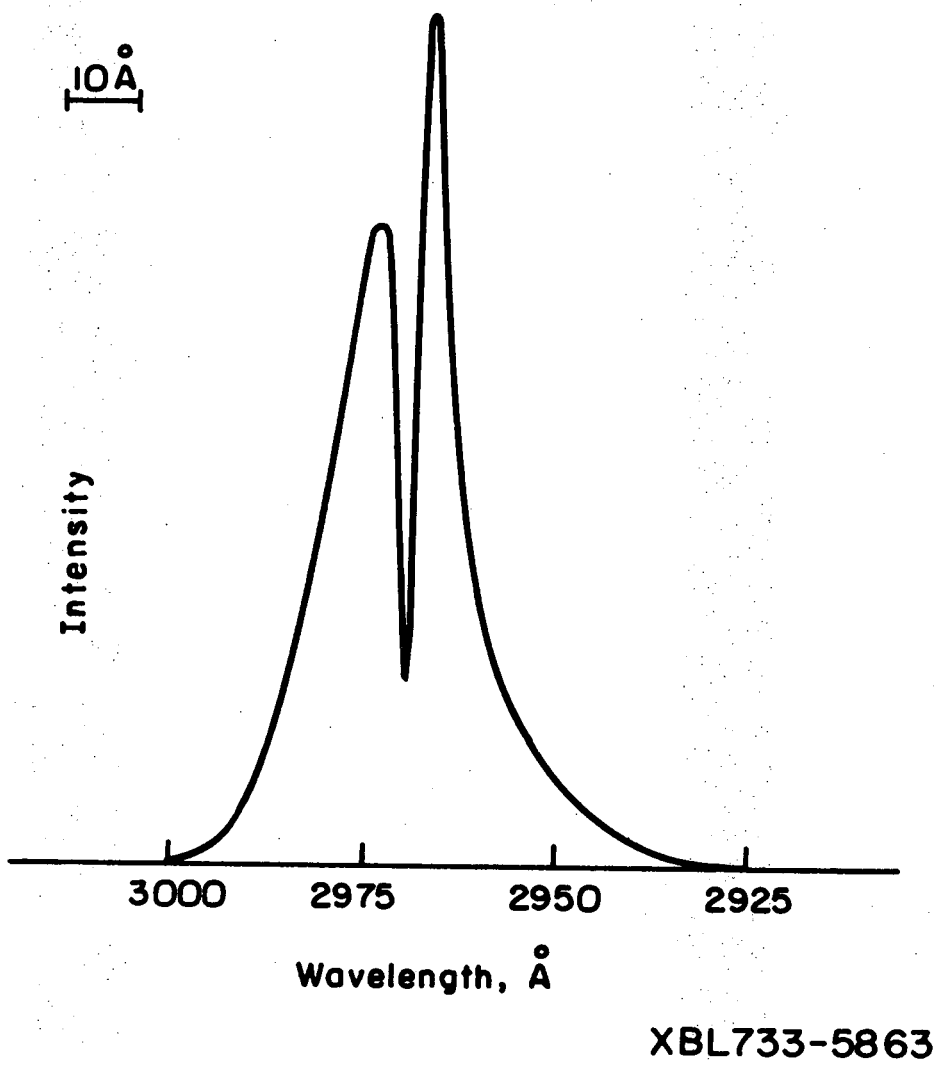

Fig. 7. Excitation profile at "2962" Å.

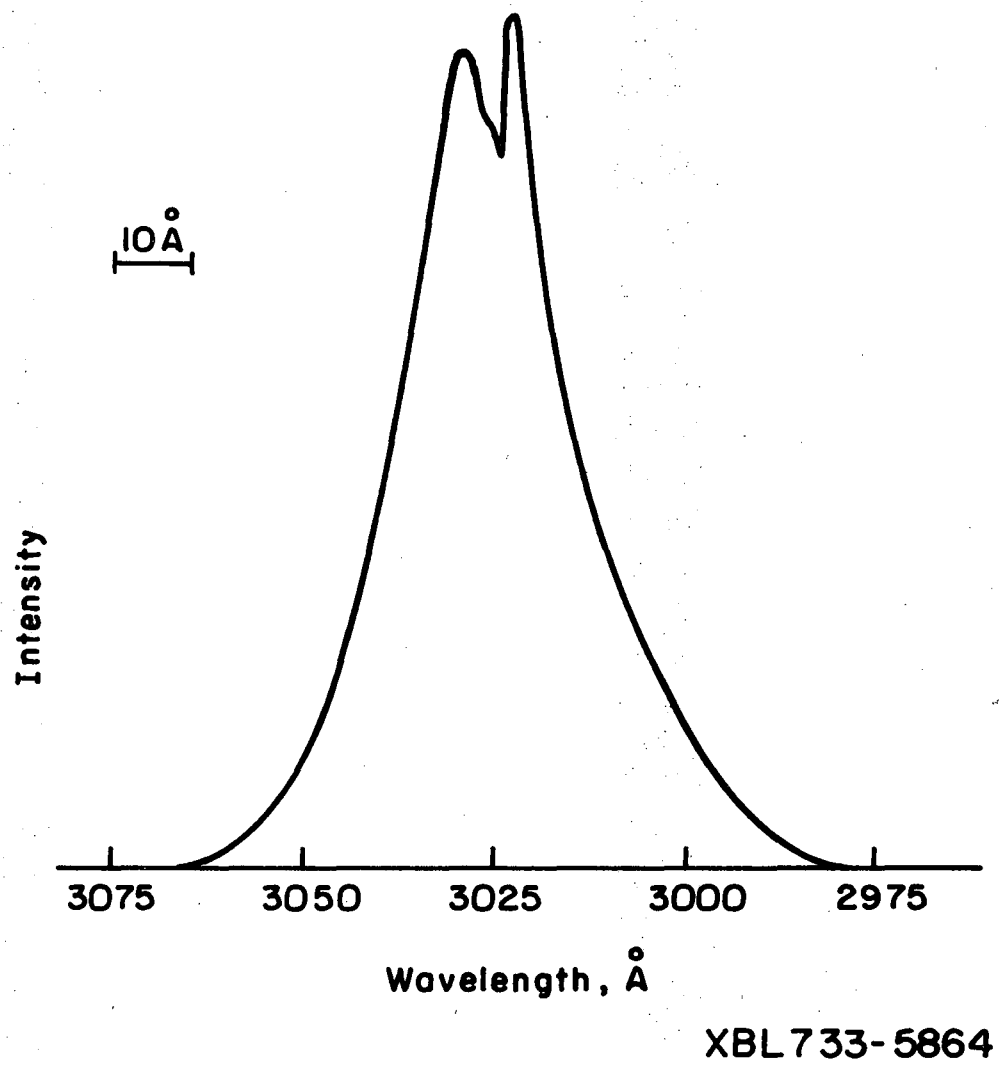

Fig. 8. Excitation profile at "3023" Å.

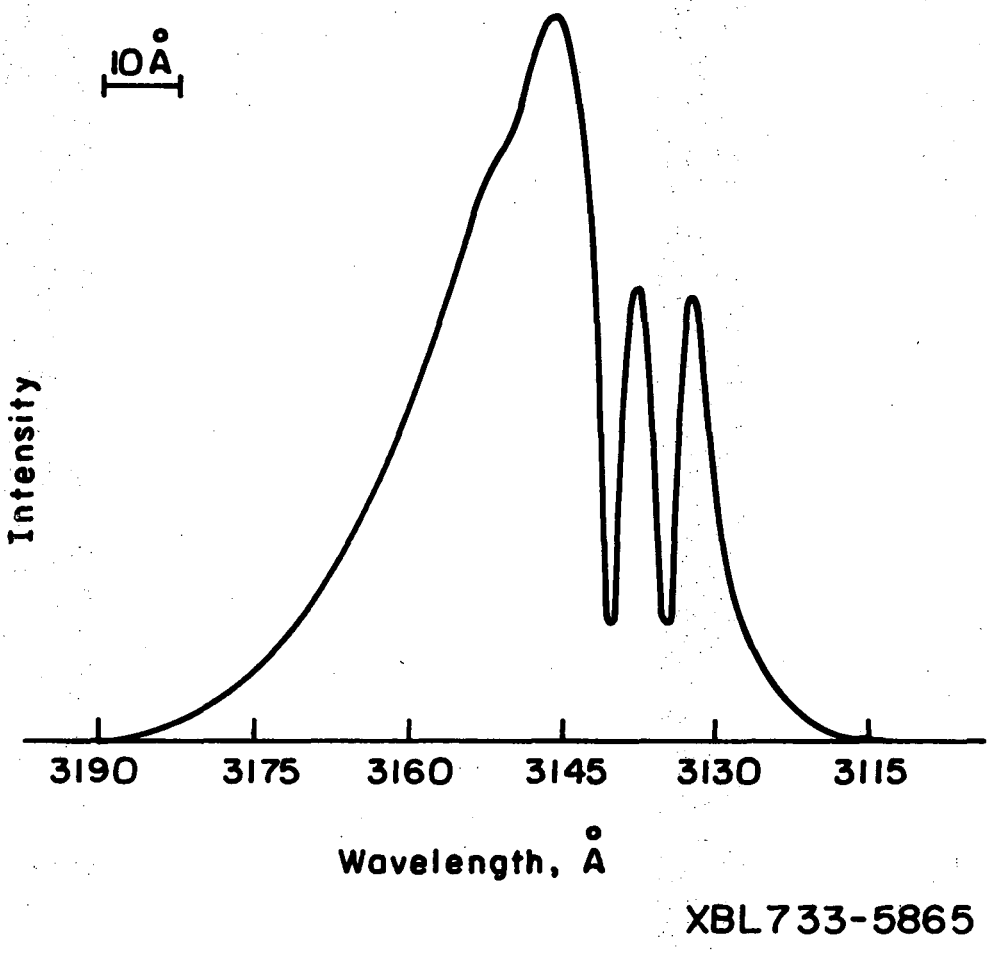

Fig. 9. Excitation profile at "3147" Å.

some of the experiments a Corning 5-54 filter, which passes ultraviolet and cuts off at about 4000 Å, was placed in the excitation beam to reduce the visible scattered light.

3. Modulator

The excitation-light was modulated by a slotted "chopper" wheel 20 cm in diameter with 60 slots along its circumference. The width of the slots at the circumference was equal to that of the blades. The wheel was turned at 3600 rpm by a 1/50 horsepower hysteresis synchronous motor (Bodine model number NCH-13). The modulation frequency was 3600±1 Hz, which was confirmed by direct count. This frequency was maintained to the accuracy of the 60 cycle line frequency.

The image of the exit slit of the excitation monochromator was focussed onto the plane of the chopping wheel, with the image in the horizontal plane of the axis of rotation of the wheel. The focussed image was about 2 mm wide and about 5 mm high. It was necessary to chop the light in the horizontal plane of the axis of rotation in order to insure that the various wavelengths in the excitation beam (which are in various vertical planes due to the dispersion of the excitation monochromator) have the same phase relation to the chopping wheel.

The harmonic content of the excitation waveform was determined by deflecting the entire modulated beam onto the cathode of an RCA 935 phototube. The output of the phototube was analyzed for its harmonic content by a wave analyzer (Hewlett Packard Model 302A). Care was taken to terminate the output of the phototube in a small enough resistance (10 k) so that the combination of the capacitance of the

cable (30 pf per foot, 0.0021 uf total) and the terminating resistor did not significantly affect the response of the system to the frequencies being measured. The optics were adjusted to alter the focussed image slightly in order to make the odd harmonics a minimum compared to the fundamental. In all the experiments performed the third harmonic was less than 1% of the fundamental, the fifth harmonic was less than 0.2%, and higher harmonics were less than 0.1%. The second harmonic was the only harmonic with significant magnitude. It was about 7% of the fundamental.

It is readily shown that the even harmonics in the excitation (2f, 4f etc.) contribute no phase information in this experiment. The odd harmonics in the excitation do contribute phase information. The odd harmonics were so small compared to the fundamental that they were assumed negligible. The modulated excitation was considered to be a pure sine wave at a frequency of 3600 cps. This assumption is discussed analytically in Appendix (A).

4. Fluorescence-Cell and Observation Geometry

Two slightly different fluorescence-cells were used. Both cells were 22 liter, 33 cm diameter, spherical pyrex bulbs. Both had quartz windows on graded seals for entrance of the excitation-beam, and light traps directly opposite the entrance to reduce scatter excitation-light. In addition, one of the bulbs had 2 inch diameter quartz windows on graded seals placed in the horizontal plane perpendicular to the axis of excitation. One of these windows was used to view fluorescence at wavelengths below the pyrex cut off at 3100 Å. This window protruded

11 cm beyond the surface of the bulb. The pair of quartz windows was used to pass a beam of light through the cell to do absorption experiments. Both bulbs had cold fingers which could be used to freeze out the SO_2 in the cell. The bulbs were closed off against the vacuum

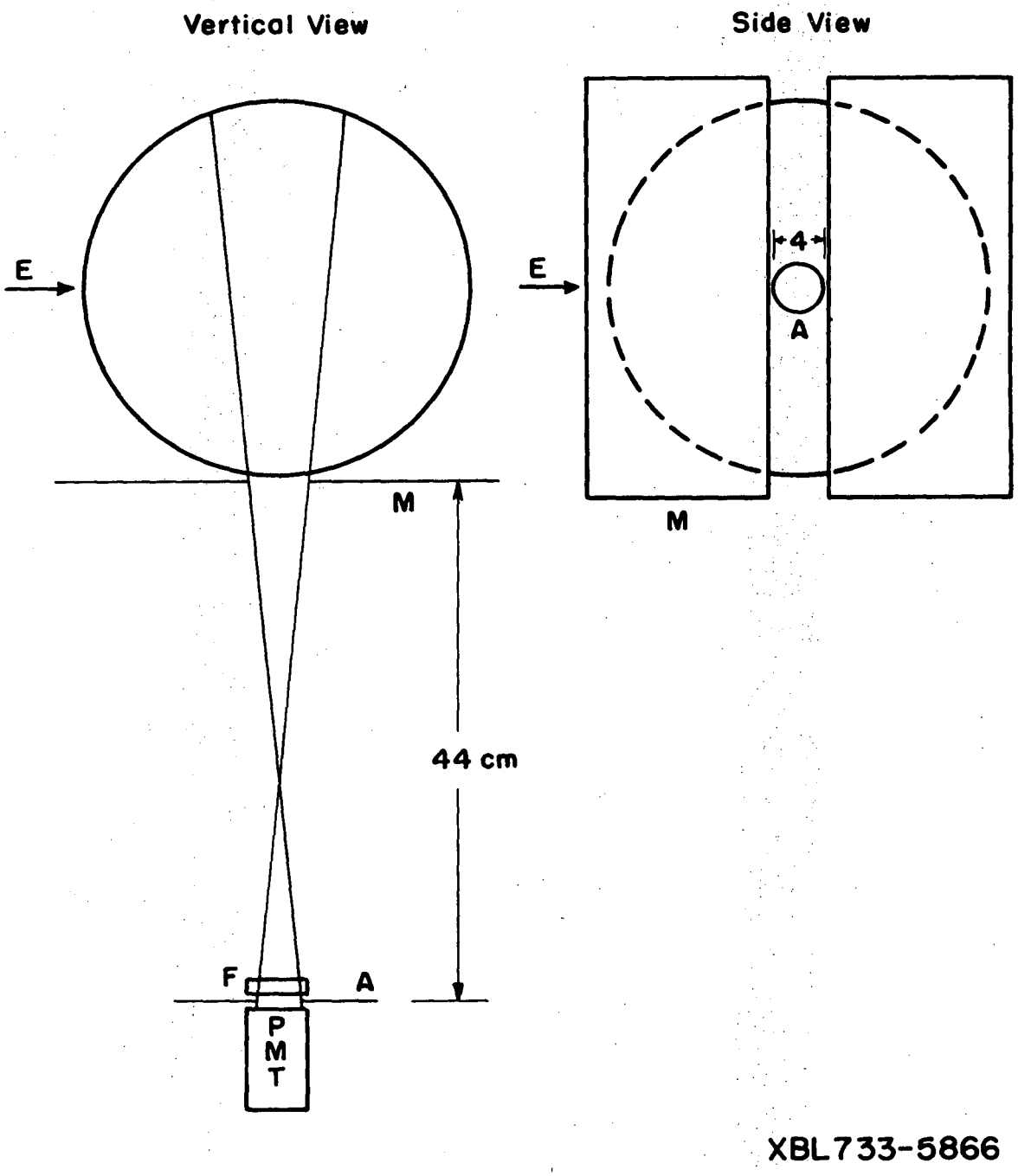

Fig. 10. Observation geometry in the low pressure lifetime experiments. A, aperture plate, 34 mm diameter; F, filter; E, axis of excitation; M, masks.

In order to have sufficient resolution in the pressure dependent studies it was necessary to use a monochromator to observe the emission. The bulb with the quartz exit window was used with the monochromator. The entrance slit of the monochromator was placed about 1 cm from the quartz window. The slit was then about 29 cm from the axis of excitation. This observation geometry is illustrated in Fig. 11. The maximum extent of the field of view of the monochromator is indicated in Fig. 11.

Consideration must be given to the question of whether the observation geometry introduced systematic error into the measurements. Schwartz[25] has considered the effect of observation geometry on measured fluorescence lifetimes. He has shown that the experimentally measured lifetimes will be within 10% of the actual lifetimes if the observation geometry includes, with equal efficiency, all the volume of the cell within a distance of $3\tau v_p$ of the axis of excitation. Sackett and Yardley[9] have commented that such an observation volume should include only a small length of the axis of excitation. At 10 mTorr the lifetime, τ, of an excited SO_2 molecule with radiative lifetime of 50 μsec and quenching constant of 1.5×10^{-10} cm^3/part-sec (roughly $\frac{1}{2}$ of the quenching constant determined in this experiment) is about 15 μsec. The most probable velocity, v_p, is about 3×10^4 cm/sec. If excitation occurred along a very thin line the excited molecules could diffuse at most about 0.5 cm, and $3\tau v_p$ would be at most 1.5 cm. The motion away from the axis of excitation would be impeded somewhat by collision. From Fig. 11 it is apparent that the

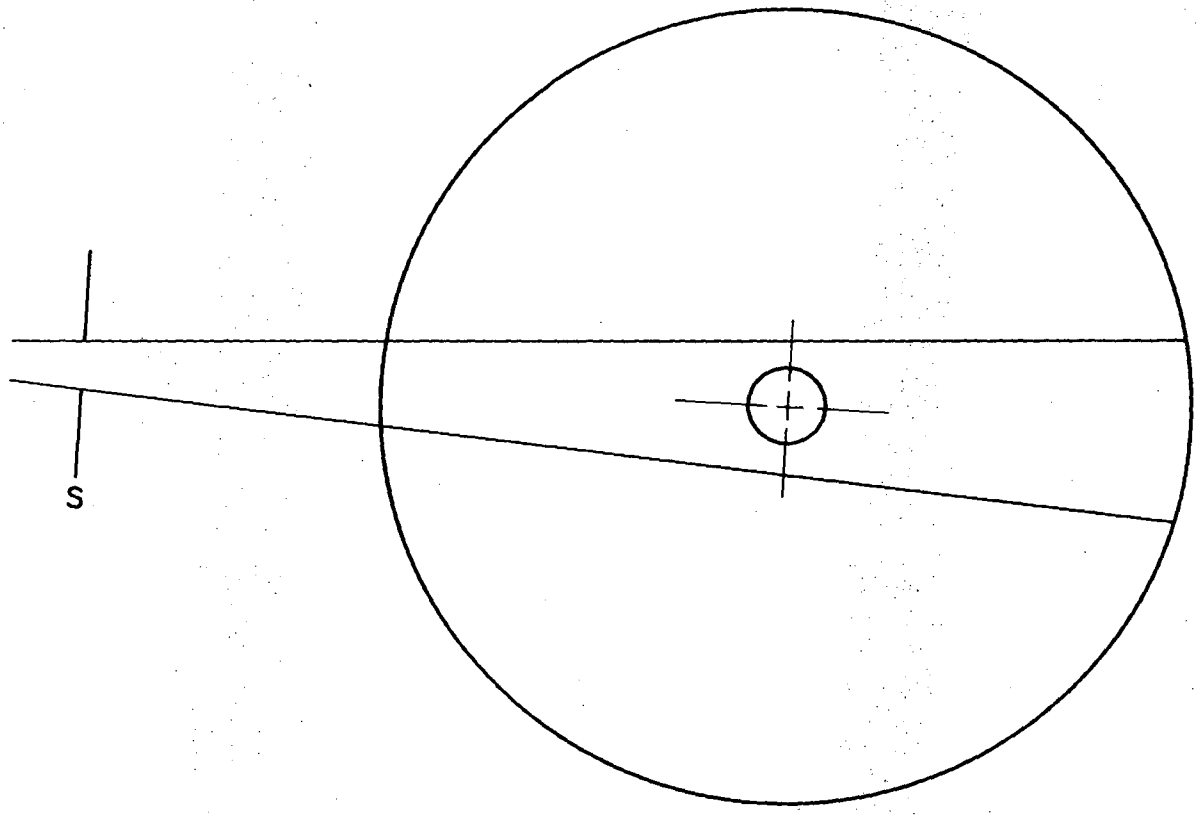

XBL 733-5867

Fig. 11. Observation geometry in pressure dependent experiments with observation monochromator. Side view with the axis of excitation perpendicular to the page. S, 2.0 cm tall slit. Enclosed area represents the maximum vertical field of view of the monochromator. Circle of 1.5 cm radius is discussed in the text.

maximum field of view of the monochromator is large enough to provide adequate observation geometry for lifetime measurements. However, all the points in the maximum field of view do not have equal collection efficiency.

An analytic solution to determine whether or not the monochromator observation geometry introduced systematic error was not attempted. Rather, correlation of some of the experimental results obtained with the monochromator with results obtained from the masked bulb geometry indicate that any systematic error introduced by use of the monochromator was of relatively small magnitude. These considerations are presented in the result section.

5. Emission Detection

A one meter monochromator (McPherson model 2051) with a 1200 line/mm grating blazed at 3000 Å was used to resolve the emission in the pressure dependent studies. The slits were 20 mm tall and were used at their maximum width, 2 mm. Resolution at this slit width was 16 Å FWHM. Wavelength calibration was checked with a Cadmium lamp at 2836.9 Å, 2980.6 Å, 3133.1 Å, 3252.5 Å and 3403.6 Å. The monochromator was always within the manufacturers stated wavelength accuracy of 0.5 Å.

Corning filter 7-51, whose spectral properties are shown in Fig. 12 was used to isolate the emission in the low pressure studies. The photomultiplier, PMT, was an EMI 9558 QA. It was cooled to -50°C by cold nitrogen boiled from a liquid nitrogen dewar. The PMT had a two inch diameter photocathode. Considerable decrease in dark noise was achieved by optically focussing the light emerging from the monochromator

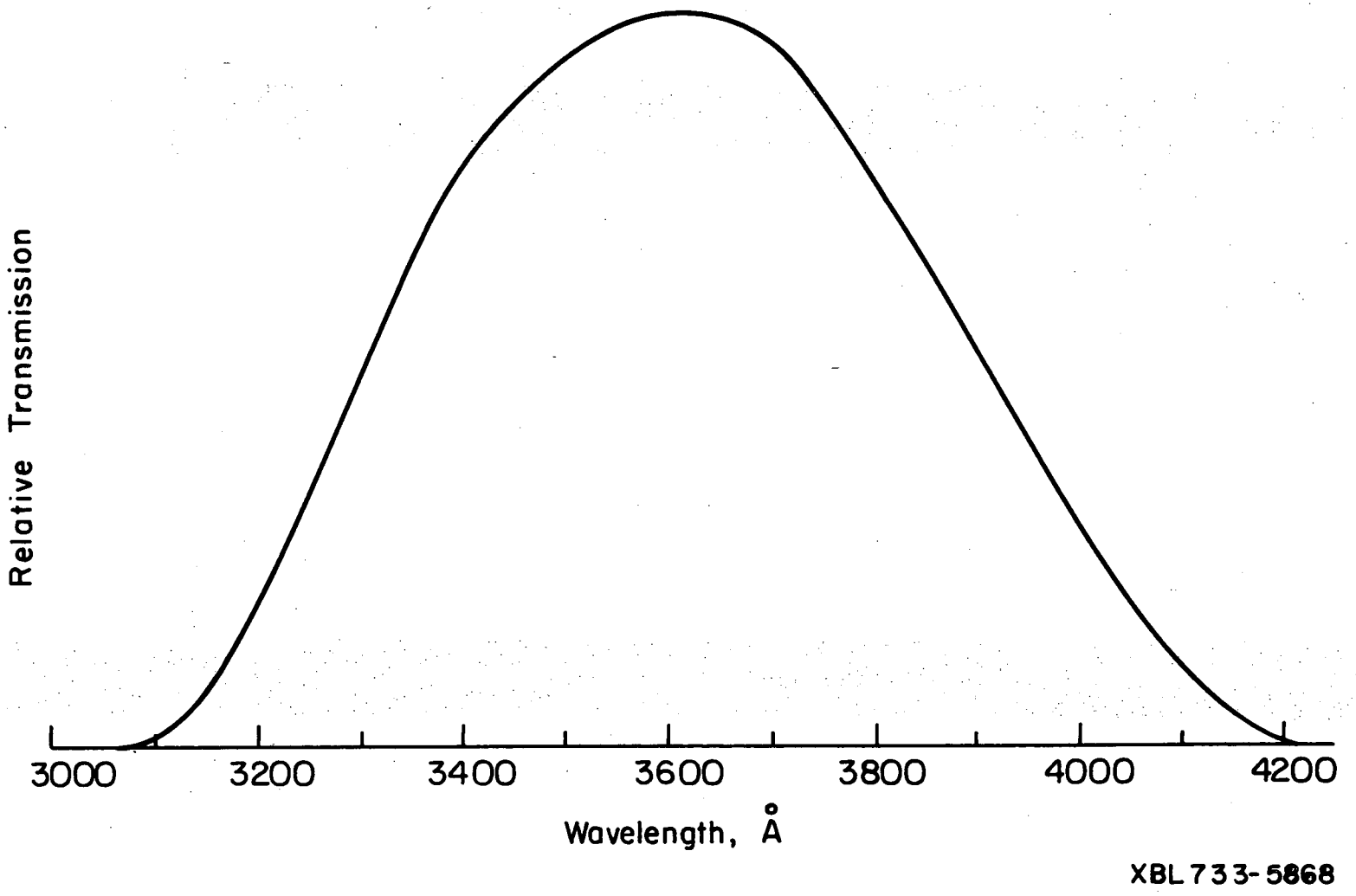

Fig. 12. Spectral transmission of filter in low pressure lifetime experiments.

onto a small area of the photocathode and using a toroidal magnet (EMI magnet type MRA) to magnetically defocus the thermal electrons emitted from the unused portion of the photocathode. The magnet assembly was stated by the company to reduce the effective photocathode to about 15 mm diameter. The PMT was operated with the anode grounded and the cathode at -1250 volts (Fluke high voltage power supply).

The PMT dark current was about 20 counts per second. The "noise" (noise is defined as one standard deviation) in a series of random events is $\sqrt{N}$ where N is the number of events. If the emission of thermal electrons were truly random we would expect a standard deviation of about 4.5 counts for an integration time of one second. The observed standard deviation was about 9 counts. This more than statistical standard deviation has been observed in other PMT detectors and is attributed to non-independent bursts of electrons emitted from the photocathode.[26] The physical origin of these bursts is not well known.

It was not necessary in this experiment to know the intensity response of the monochromator accurately, but for qualitative reasons we note that the transmittance of this particular McPherson monochromator was stated by the manufacturer to be 76% at 2537 Å, 79% at 2967 Å and 73% at 3340 Å. At longer wavelengths the transmittance typically drops off slowly. The spectral response of the PMT is given by the manufacturer as varying between 27% quantum efficiency at 2700 Å and 22% quantum efficiency at 4000 Å. The overall detection response (monochromator transmittance efficiency times detector response) varies by less than least 20% in the range 2700-3340 Å and drops slowly at higher wavelengths.

6. Electronics

The reference signal by which the counters were gated to the modulator was obtained by allowing the rotating chopper wheel to interupt light from a light emitting diode. This reference light was detected by a phototransistor and the reference signal was fed into a phase lock loop circuit designed to produce a square wave output at twice the frequency of the reference. The square wave at 2f (f is the chopping frequency) went into digital circuitry to produce two square waves at f which were ninety degrees out of phase with respect to each other.

The pulses from the photomultiplier were converted to a form suitable for subsequent digital circuitry by an amplifier/discriminator (Solid State Radiation model 1120). The high gain of this unit allowed the phototube to be run at a relatively low voltage to minimize the emission of thermal electrons.[27] The pulses from the amplifier/discriminator were fed into a pair of reversible counters. The two counters were gated ninety degrees out of phase with respect to each other through use of the f square waves generated by the reference circuit. The counters were constructed to count a preset number of excitation cycles (unusually 2^{17} or 2^{18}) then type out the residual counts in each counter on a teletype. The counters then reset themselves and went through another counting cycle. The total number of cycles was determined by consideration of the integration times necessary for a desired signal to noise ratio. Most of the data were gathered at integration times of $7\frac{1}{2}$ or 15 minutes, real time.

7. Gas Handling

The vacuum system consisted of a two inch metal oil diffusion pump, with a water cooled baffle and liquid nitrogen trap along with an all glass purification and gas storage assembly. The high vacuum manifold was connected to the fluorescence cell by a glass line. All stopcocks were of glass and teflon construction. The entire system could be pumped to 1×10^{-5} Torr as measured with an ionization gauge. Any leaks into the fluorescence cell over the time span of a typical experiment were not detectable.

Pressures in the fluorescence cell were measured by a factory calibrated capacitance pressure transducer (Datametrics Model 511-10, controller Model 1014). The linearity of this instrument was stated by the manufacturer to be 0.1% over the entire range, 0-10 Torr. The most sensitive range was 1 mTorr full scale.

Sulfur dioxide, obtained from Matheson, was stated to be 99.5% pure. It was admitted to the vacuum manifold and allowed to condense in a cold finger at -78°C. The residual gas was pumped off. The sample was distilled from -78°C to -196°C, the residue at -78°C being discarded. The sample was then pumped on, melted, recrystallized and pumped on again. The purified gas was stored at room temperature.

8. Procedure

For a given set of experimental conditions (pressure, excitation and observation wavelengths) the necessary data were the residual counts on the two counters after many cycles of excitation. In some experiments a significant amount of scattered excitation light was detected. If uncorrected this scattered light would result in measured

rate constants which would be much too large since the scattered excitation light would contribute a large in phase signal. The problem of scattered excitation was greatest in the lifetime experiment with the broad band observation filter and in some of the pressure dependent studies when the observation wavelength was close to the excitation wavelength. When significant scatter was encountered its magnitude was determined by freezing out the SO_2 in the cold finger and measuring the scatter alone. The two components of the scatter were then subtracted from the respective components of the signal measured with SO_2 present. These corrected intensities were then taken as the relevant data. To correct for scatter in this manner it is necessary to assume that the scatter is not affected by the presence of a small amount of SO_2 in the fluorescence cell. At the highest pressures used, 20 mTorr, about 2% of the excitation light was absorbed. At low pressures, where scatter was larger compared to the fluorescence signal, considerably less than 1% of the excitation light was absorbed. In many experiments employing the observation monochromator no scatter was detected and the residual counts from the counters were taken directly as the raw data.

It was necessary to determine the phase of the modulated excitation light with respect to the counters, ϕ_o. This was accomplished by measuring the apparent phase, ψ, of the fluorescence at a very high pressure of SO_2. At high enough pressure the phase shift can be regarded as zero since lifetimes are so short that the phase shift would only be a fraction of a degree. In these experiments ϕ_o was determined at pressures of at least 200 mTorr. This was demonstrated to adequately

represent zero chemical phase shift by agreement with phase measurements at much higher pressures. The instrumental phase determined in this manner was relatively constant as long as the wavelength of excitation was not changed. Changing the excitation wavelength caused changes in ϕ_o since the location of the excitation beam changed slightly with respect to the chopper when the grating in the excitation monochromator was rotated.

Experiments with a given excitation wavelength were conducted in random orders of pressure and observation wavelengths. This was done to preclude any systematic variation in the data due to phase drift in the system. During the course of a day's experimentation the instrumental phase was checked two or three times to assure that the instrumental phase was constant and that the instrument was working reliably.

III. RESULTS

A. Emission Spectra

Emission spectra were taken at four excitation wavelengths and at high and low pressures. The emission was scanned using the observation monochromator with slits set at 2.00 mm (16 Å FWHM). Emission intensities were recorded by using one counter to add the counts in a 3.5 second interval and punch the total. These totals were accumulated while the scan was in progress. About four data points were collected per spectral half width.

The low pressure spectra were all taken at pressures below 0.6 mTorr. Assuming a radiative lifetime of 50 μsec and a quenching rate constant of 3×10^{-10} cm^3/part-sec (approximately gas kinetic) it was estimated that less than 20% of the radiating molecules in the low pressure experiments suffered a quenching collision before radiating. It is unlikely that vibrational relaxation cross sections would be much larger than gas kinetic. The low pressure spectra are taken as representing emission from only the optically populated states. The high pressure limit was ascertained by comparing spectra at increasing pressures. In all cases there was no observable change between spectra taken at various pressures above about 20 mTorr. The spectra shown here were all taken at pressures greater than 100 mTorr.

The spectra are shown in Figs. 13 to 17a. Note that for each pair of high and low pressure spectra the intensity scale on the high pressure spectra is an indicated factor greater than the corresponding

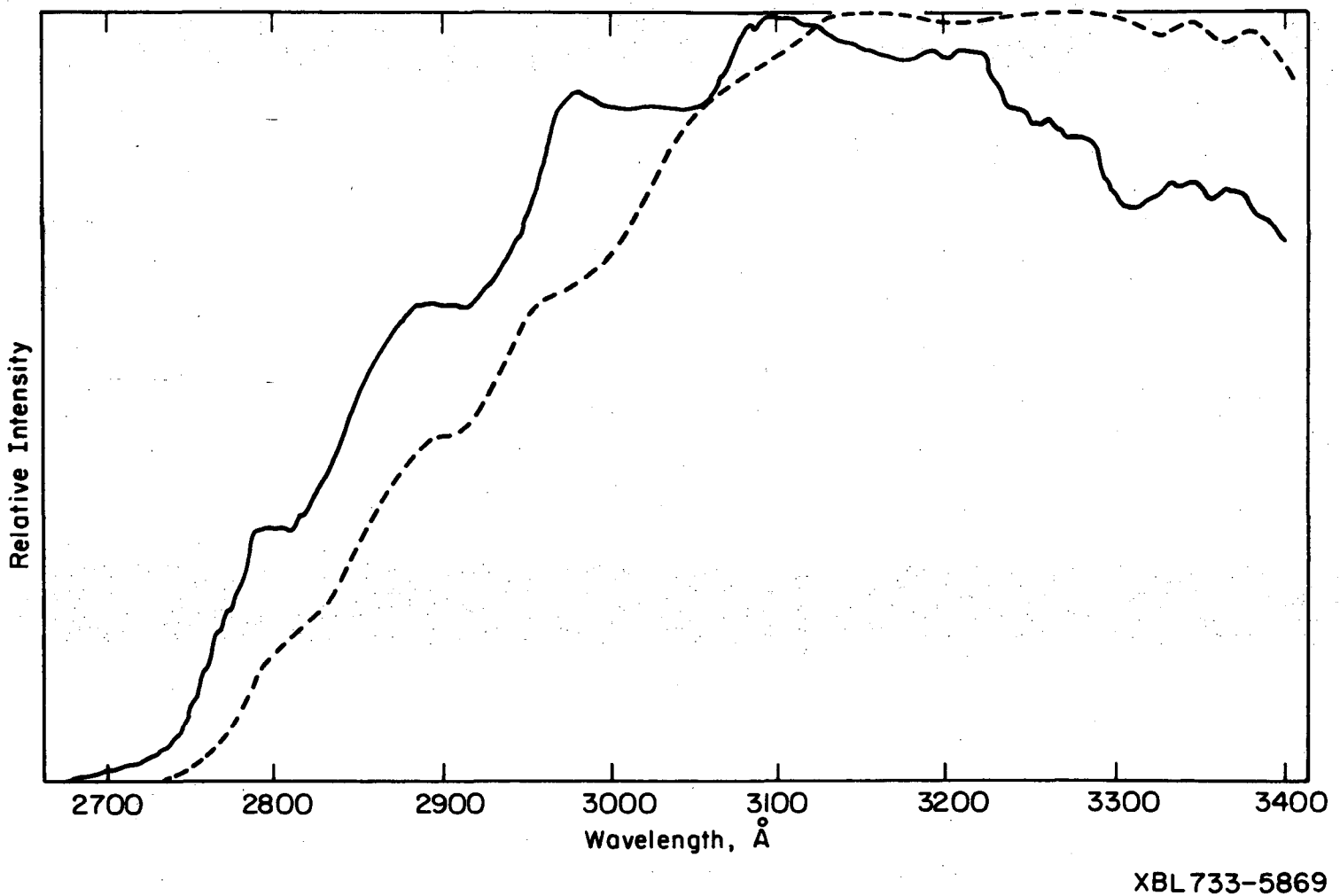

Fig. 13. Emission spectrum at λ_{ex} = 2760 Å. Solid line, low pressure; dotted line, high pressure. High pressure spectrum relative intensity is 7.8 times as great as low pressure spectrum.

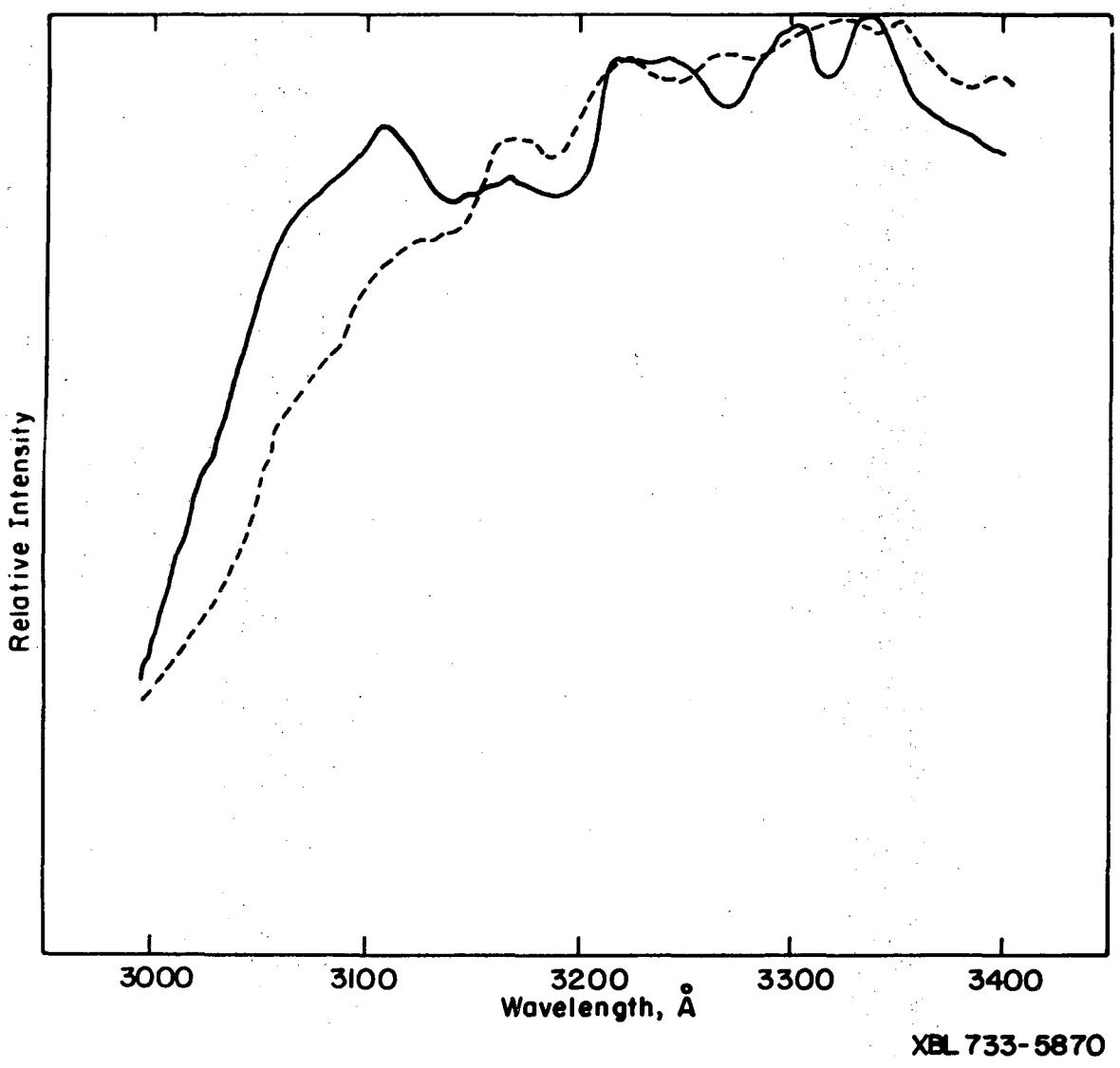

Fig. 14. Emission spectrum at λ_{ex} = 2960 Å. Solid line, low pressure; dotted line, high pressure. High pressure spectrum relative intensity is 3.9 times as great as low pressure spectrum.

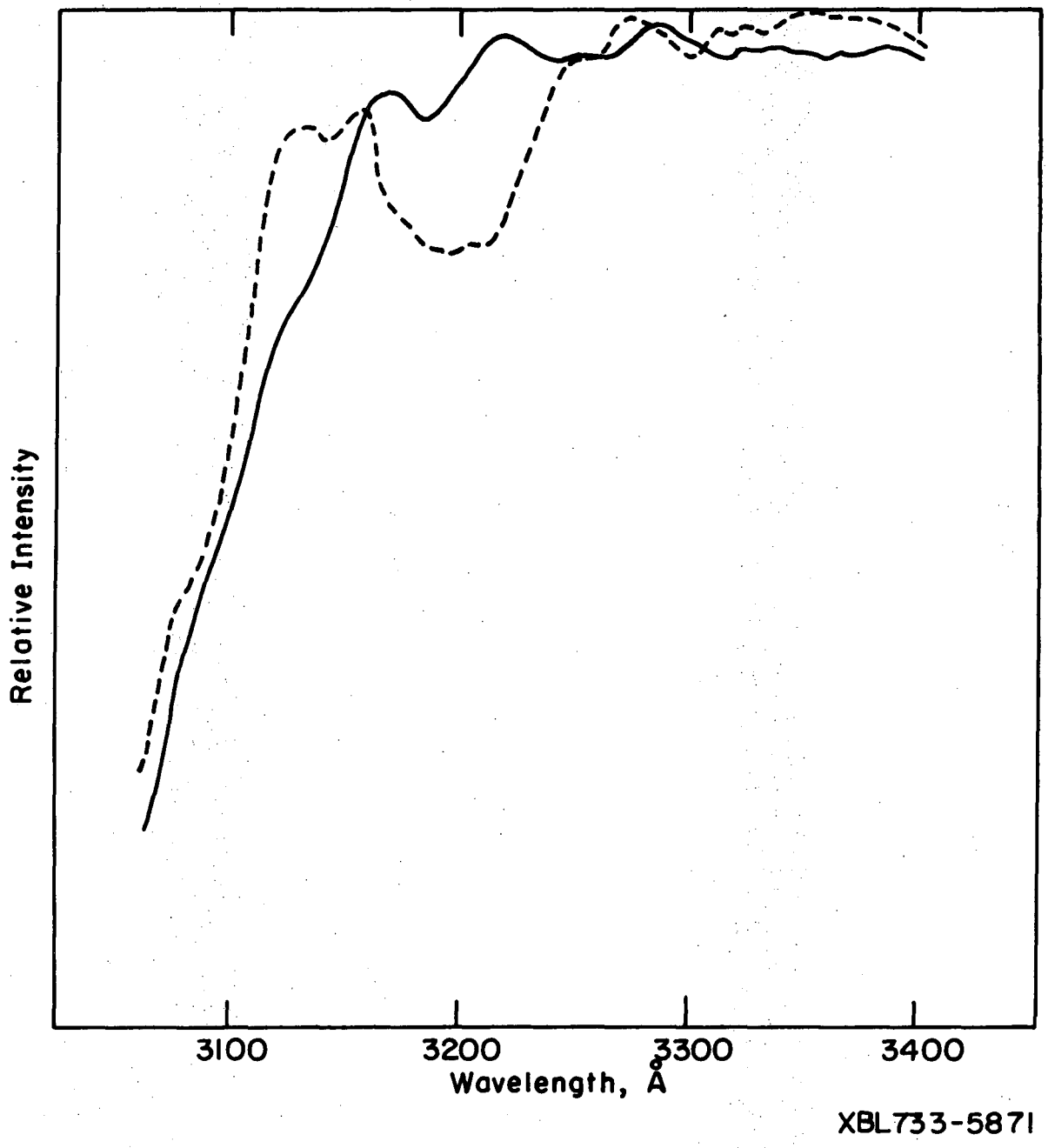

Fig. 15. Emission spectrum at λ_{ex} = 3023 Å. Solid line, low pressure; dotted line, high pressure. High pressure spectrum relative intensity is 3.0 times as great as low pressure spectrum.

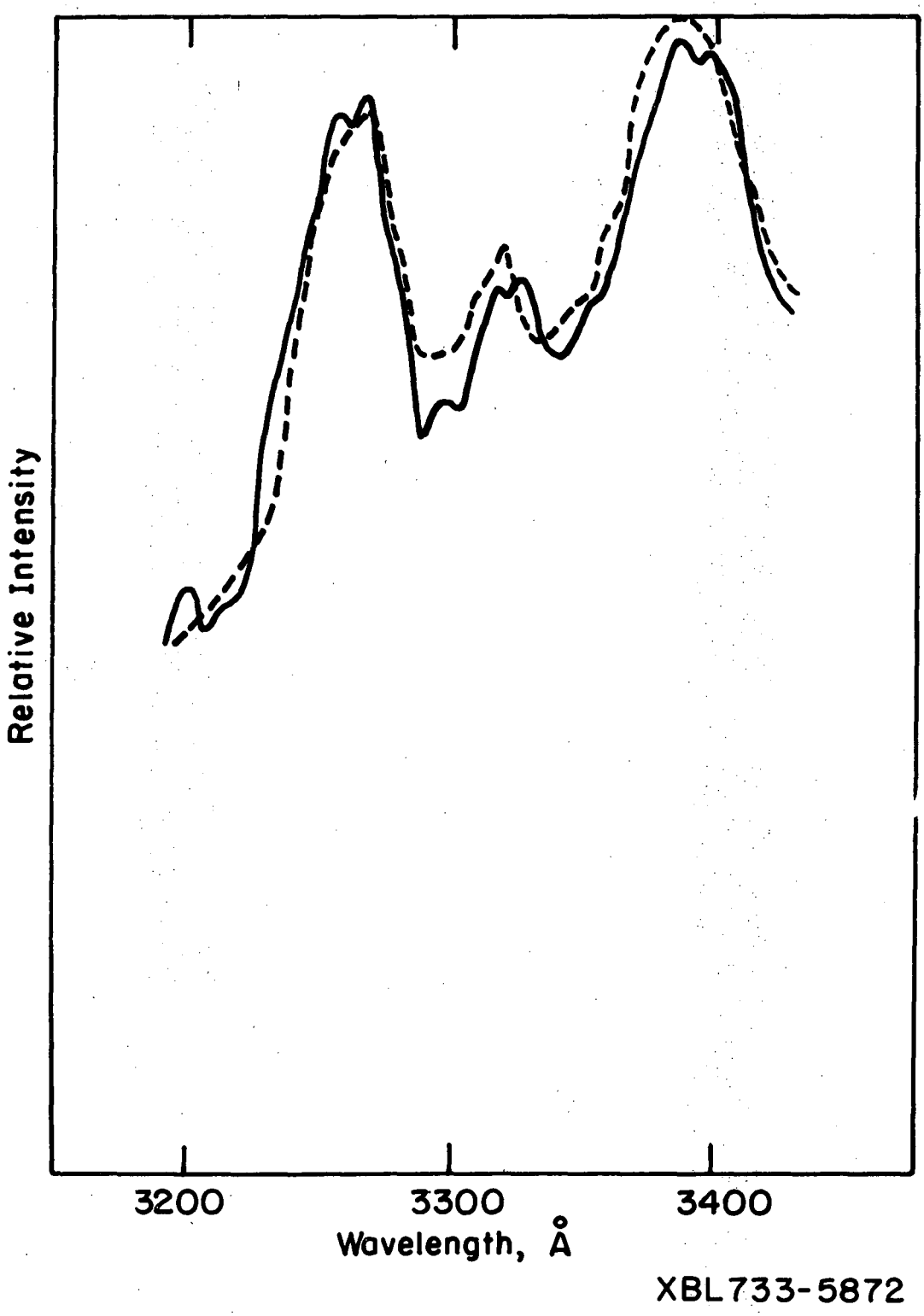

Fig. 16. Emission spectrum at λ_{ex} = 3147 Å. Solid line, low pressure; dotted line, high pressure. High pressure spectrum relative intensity is 1.2 times as great as low pressure spectrum.

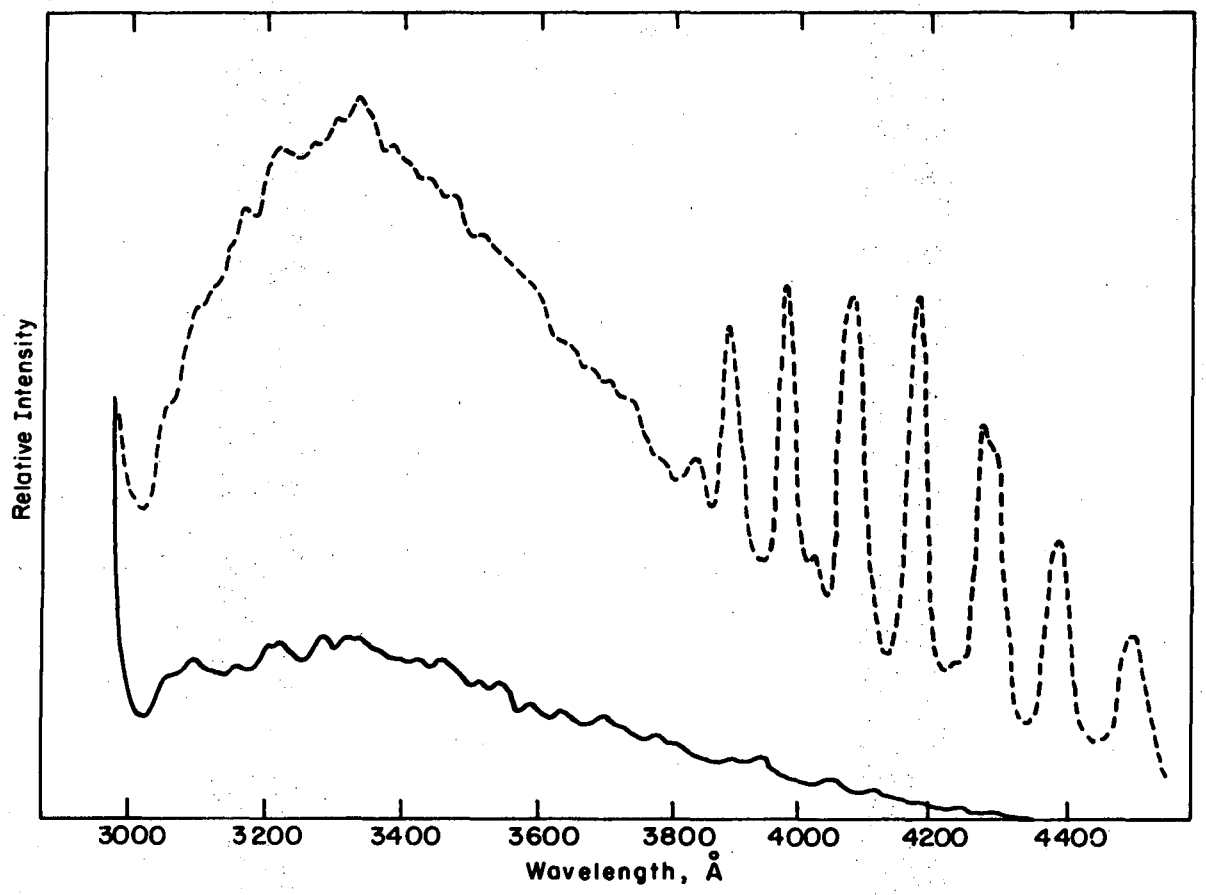

Fig. 17. Complete emission spectrum for λ_{ex} = 2960 Å. Both high and low pressure spectra are shown on the same relative intensity scale.

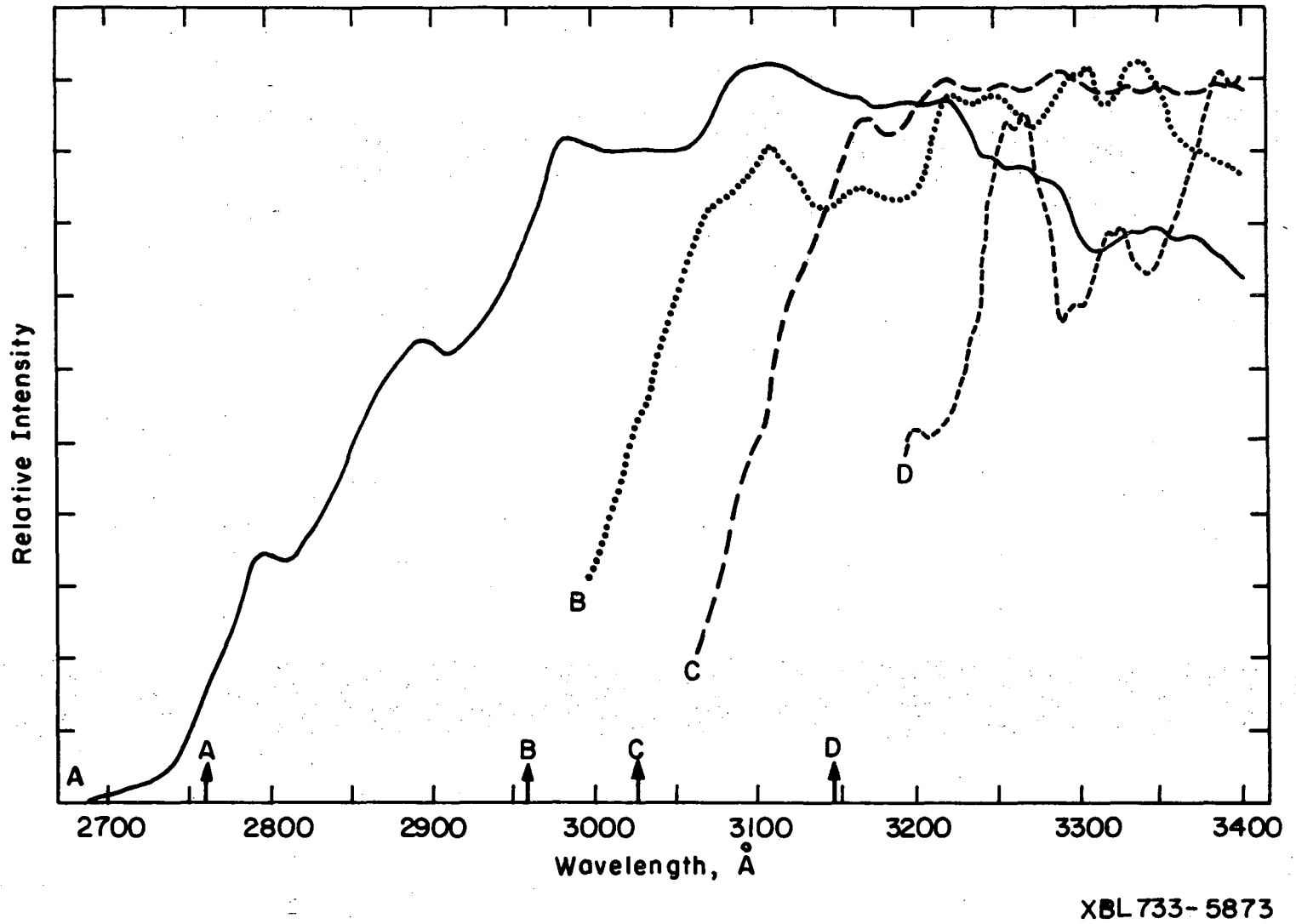

Fig. 17a. Graphs of low pressure spectra normalized to the same relative intensity. A, λ_{ex} = 2760 Å, solid line; B, λ_{ex} = 2960 Å, dotted line; C, λ_{ex} = 3023 Å, long dashes; D, λ_{ex} = 3147 Å, short dashes.

high pressures spectrum. In Fig. 17a all four low pressure spectra are plotted together to facilitate comparison. They are normalized to the same relative intensity. This allows comparison of the relative intensities of low and high pressure spectra. These spectra have not been corrected for detector response. In view of the discussion of detector correction given in the experimental section the spectra terminated at 3400 Å are taken as representing the actual fluorescence distribution. The spectra extending to 4000 Å should be multiplied by a small factor towards the red end but the spectra are still sufficiently accurate as shown to ascertain the qualitative features of interest.

Excitation at 2760 Å was with the xenon lamp. The output intensity of the lamp was constant enough so that a scan could be made with SO_2 frozen out in the cold finger on the cell and subtracted from the spectra with SO_2 present. This spectra can then be shown at wavelengths extending to the excitation wavelength. In the case of excitation at the other wavelengths the Hg lamp was used. The Hg lamp output was not sufficiently constant to allow accurate subtraction of the scattered excitation radiation. Thus, these spectra are not shown to the short wavelength limit of excitation.

The spectra at all four excitation wavelengths are shown to 3400 Å even though emission extends to about 4000 Å. The principal reason for taking emission spectra was to determine the actual emission distribution of individual states. This information is needed to analyze the results of the pressure dependent experiments. The low

pressure spectra were taken at a relatively collision free pressure (collision times longer than the lifetime of the excited molecule). The low pressure spectra represent the emission from the quantum states populated by the optical excitation. The high pressure spectra may represent the contribution of emission from states populated from the initial states by collisional processes in addition to the emission from the optically populated states themselves. The spectra were terminated at 3400 Å, or approximately the wavelength of the "vibrationless" transition (000) ← (000).

These spectra agree with those previously published. The fluorescent emission begins very weakly at the excitation wavelength. The emission rises steadily to a broad plateau at about 3200-3400 Å. The low pressure and high pressure spectra have the same general features. In molecules, such as NO_2, which are known to undergo extensive vibrational relaxation, the spectra tend to shift toward longer wavelength as the pressure is increased.[24] This "red shift" reflects the fact that molecules which lose some of their energy before fluorescing tend to fluoresce at longer wavelengths. The absence of a marked red shift in SO_2 fluorescence has been cited as evidence for the absence of vibrational relaxation in excited SO_2.[31]

The spectra excited at 2960 Å is shown extending to 4000 Å in Fig. 17. The prominent features at the long wavelength end are due to phosphorescence from the low lying triplet. Their absence at low pressure indicates that the triplet is formed only by collision. This effect has been noted previously at various other excitation wavelengths.[11]

B. Low Pressure Lifetimes

In these experiments the cell was filled with 0.2 mTorr or less of SO_2. The xenon arc lamp was used as the excitation source. A slit width of 0.6 mm on the excitation monochromator gave an excitation bandwidth of 10 Å FWHM. Fluorescence was observed through a Corning 7-51 filter. The filter transmission, which is shown in the experimental section, and the emission envelope were such that the bulk of the emission detected in these studies was of wavelengths longer than about 3300 Å and extended to the fluorescence limit of about 4000 Å. The detection configuration was that of the 33 cm bulb with the two inch vertical section open to direct view of the phototube.

Considerable scattered excitation radiation was detected along with the fluorescence. This scattered excitation, if not accounted for, would cause the apparent measured lifetimes to be considerably shorter than the actual values. The scattered radiation at each excitation wavelength was determined by performing a lifetime experiment with the SO_2 frozen out in the cold finger on the fluorescence cell. The fluorescence data was then corrected for this scattered excitation.

The measured lifetimes are shown in Fig. 18. These lifetimes were computed from the experimental quantities Z1 and Z2 through use of a single excited state model. Use of the single excited state model was felt to be adequate in view of the low pressures involved. At 0.2 mTorr there is about 670 μsec, on the average, between collisions of two SO_2 molecules. This is about 10 times longer than the approximately 50 μsec measured lifetimes. Thus, very few excited

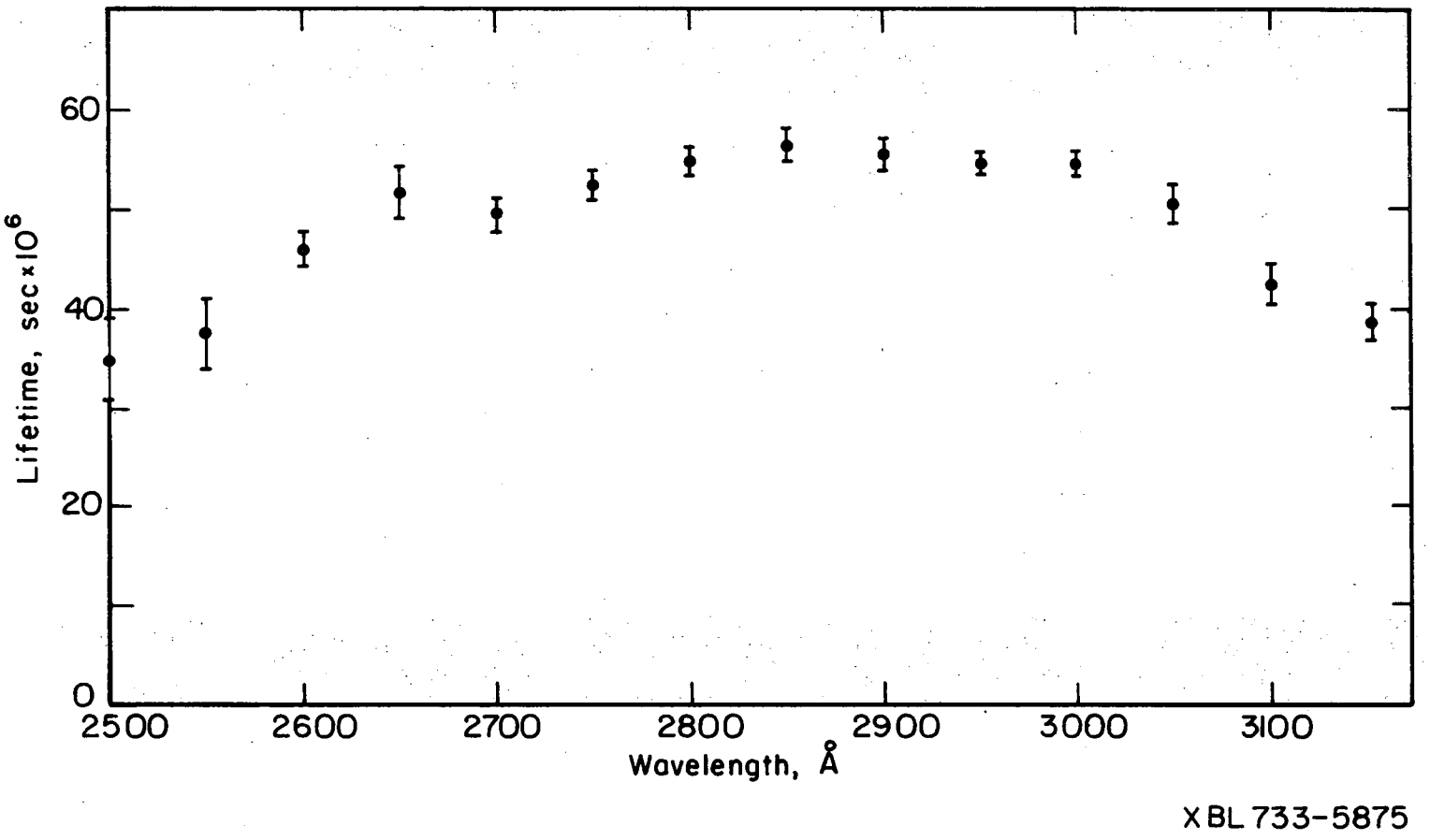

Fig. 18. Fluorescence lifetime of SO_2 at pressures less than 0.2 mTorr. Error bars represent two standard deviations determined from several experiments.

Table I. Fluorescence lifetimes for sulfur dioxide at pressures less then 0.2 mTorr.

Excitation wavelength Å	Lifetime μsec
2500	35
2550	37
2600	46
2650	52
2700	50
2750	53
2800	55
2850	57
2900	56
2950	54
3000	54
3050	51
3100	42
3150	38

Excitation bandwdith was 10 Å FWHM. Observation wavelength extended from 3300 Å to fluorescence limit at 4000 Å.

molecules experience collisions before radiating. Complications arising from collisionally induced multistate fluorescence or collisional quenching of the optically excited species are negligible. The possibility of triplet emission is also negligible at these low pressures. We can conclude that while the measured lifetimes represent only a lower bound to the actual zero pressure lifetimes, the measured values must differ by no more than 10% from the actual values.

It is pertinent to point out that the problem of measuring the lifetime at zero pressure is not necessarily dealt with adequately by extrapolation of measurements at high pressures. Even if the experimental points actually define a straight line with great accuracy it is not true that the intercept gives the correct zero pressure value. Multistate kinetics can indeed yield plots of (1/apparent lifetime) versus concentration which are straight at higher pressures but which curve appreciably at low pressures. This possibility is illustrated in Appendix (B). Measurements at pressures less than 5 mTorr may be required to detect this curvature. Nitrogen dioxide, with radiative and collisional properties similar to SO_2, exhibits curvature in such plots.[25] It was therefore decided that the most efficient use of a given amount of integrating time was to measure the lifetime at a pressure low enough to minimize quenching processes and yet high enough to give an acceptable signal to noise ratio. Low pressure lifetimes were also measured using the observation monochromator. These measurements were made in order to determine whether or not the limited observation volume of the monochromator introduced systematic error due to migration of long lived excited molecules out of the volume of the cell within the field of view of the observation

monochromator. The cell was filled with 0.6 mTorr of SO_2. The Hg arc at 2962 Å was used as the excitation-source. The lifetime was determined for various observation energies. The lifetime was observed to vary between 45 and 50 μsec for observation at various wavelength in the range 3130-3397 Å. These values compare well with the lifetime of 54 μsec measured with the extended observation volume. The good agreement between the values of the low pressure lifetime measured with the observation monochromator and the value measured with the extended observation volume indicates that large systematic error in the high pressure lifetimes was not introduced through use of the observation monochromator.

C. Pressure and Wavelength Dependence of Fluorescence Lifetime

These experiments were conducted at four excitation wavelengths; 2760, 2960, 3023 and 3147 Å (36231, 33760, 33080 and 31778 cm^{-1}). The Xe arc lamp was used as the excitation source at 2760 Å, while the Hg lamp was used for the other wavelengths. The spectral content at each nominal wavelength is shown in the experimental section. Pressure ranged from about 5-20 mTorr. The observation monochromator was used to observe the fluorescence. Observations were made approximately every 500 cm^{-1} between the excitation energy and the (000) ← (000) transition at 3397 Å. The bandpass of the observation monochromator (2.00 mm slits, 16 Å FWHM) varied between 200 cm^{-1} FWHM at 2800 Å and 130 cm^{-1} FWHM at 3400 Å.

The data at each combination of experimental parameters (excitation-wavelength, observation wavelength and pressure) was the residual counts on the two counters. In addition, the scattered excitation from a cell with SO_2 frozen out was also measured. For experiments at low pressures and observation wavelength close to the exciting wavelength there was a small amount of scattered excitation. In many experiments no scattered excitation could be observed. When scattered light was observed it was subtracted from the fluorescence signal. In all cases the scatter was small compared to the fluorescence signal.

Experiments were done in a random sequence of pressures and observation wavelengths in order to minimize the possible systematic effects of instrumental drift. The instrumental phase, ψ, was determined at least two times in the course of several hours of experimentation. The instrumental phase measured over the course of a day's experimentation was always constant, within the experimental error. The intensity of the excitation light was periodically checked for large variations. The light intensity was always constant within 10%. Since the quantities of interest were the ratios of intensities the data was not corrected for the small variations in excitation intensity.

Plots were made of the inverse apparent lifetime as a function of pressure. Figures 19-22 are plots of inverse apparent lifetimes for three observation wavelengths at each excitation wavelength. The data was fitted to straight lines by the least squares method. Points with pressure greater than about 5 mTorr were used to calculate the straight lines since points at less then 5 mTorr showed distinct

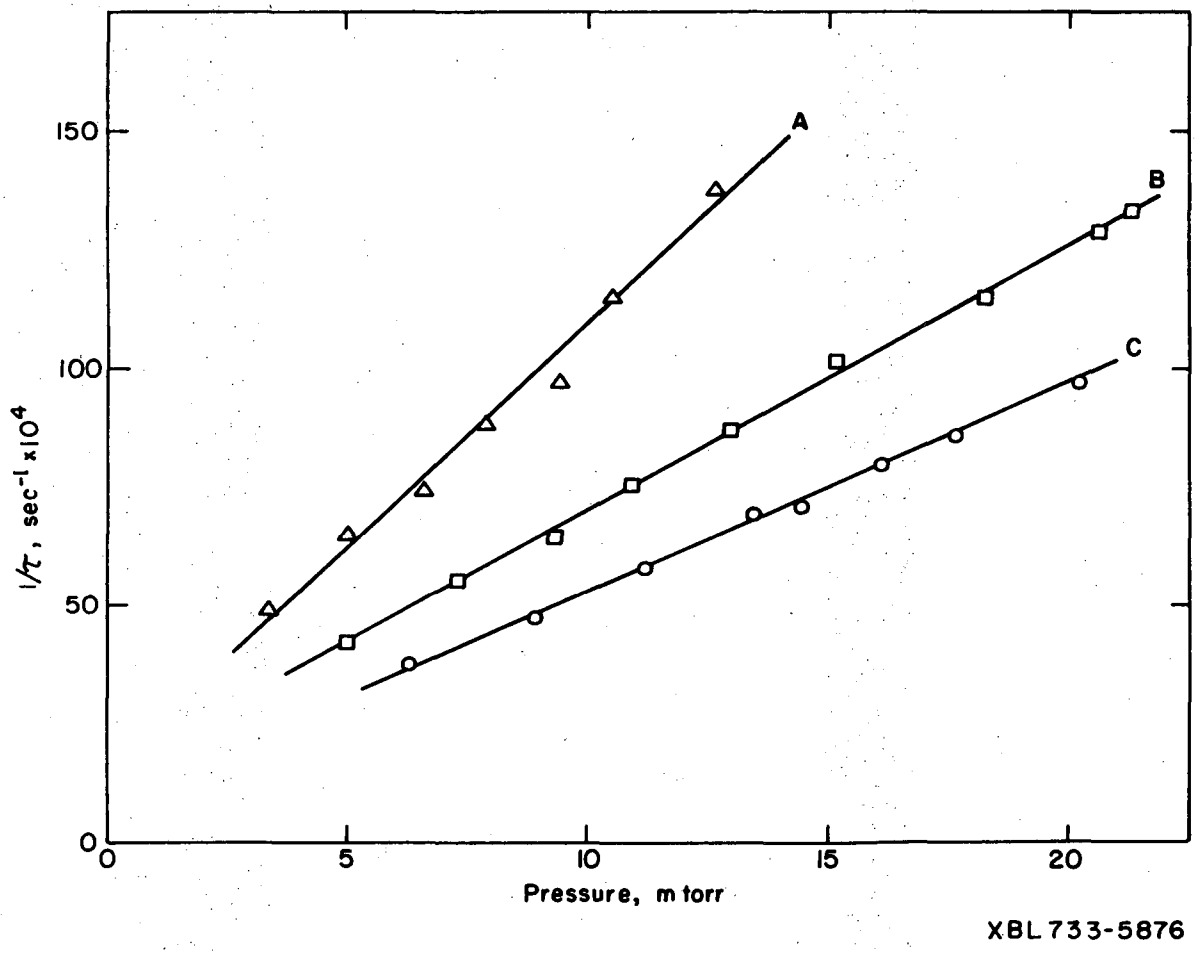

Fig. 19. Stern-Volmer graph of pressure dependent lifetime data. Excitation wavelength: 2760 Å. ΔW was: A, 770 cm^{-1}; B, 3000 cm^{-1}; C, 6500 cm^{-1}.

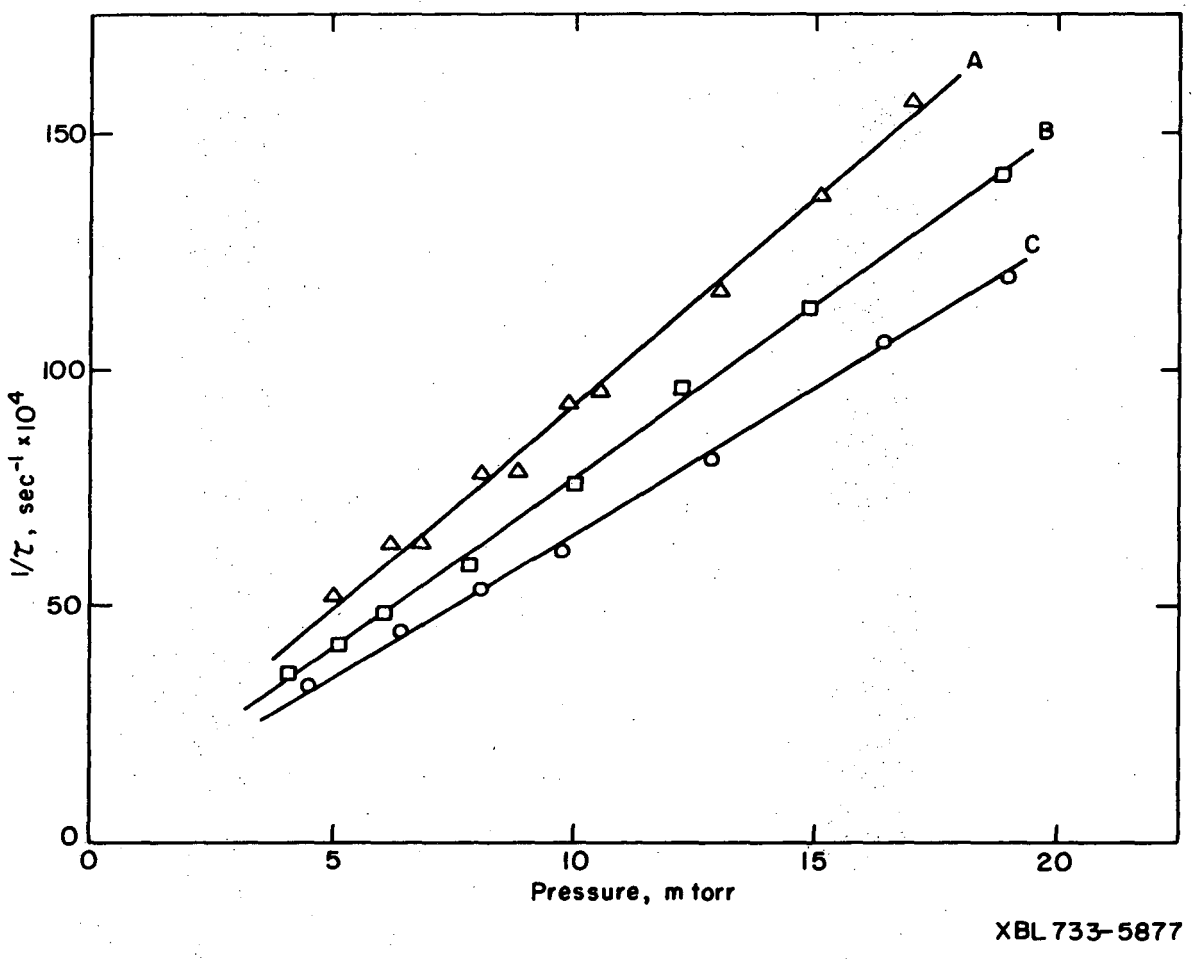

Fig. 20. Stern-Volmer graph of pressure dependent lifetime data. Excitation wavelength: 2962 Å. ΔW was: A, 910 cm^{-1}; B, 3000 cm^{-1}; C, 4321 cm^{-1}.

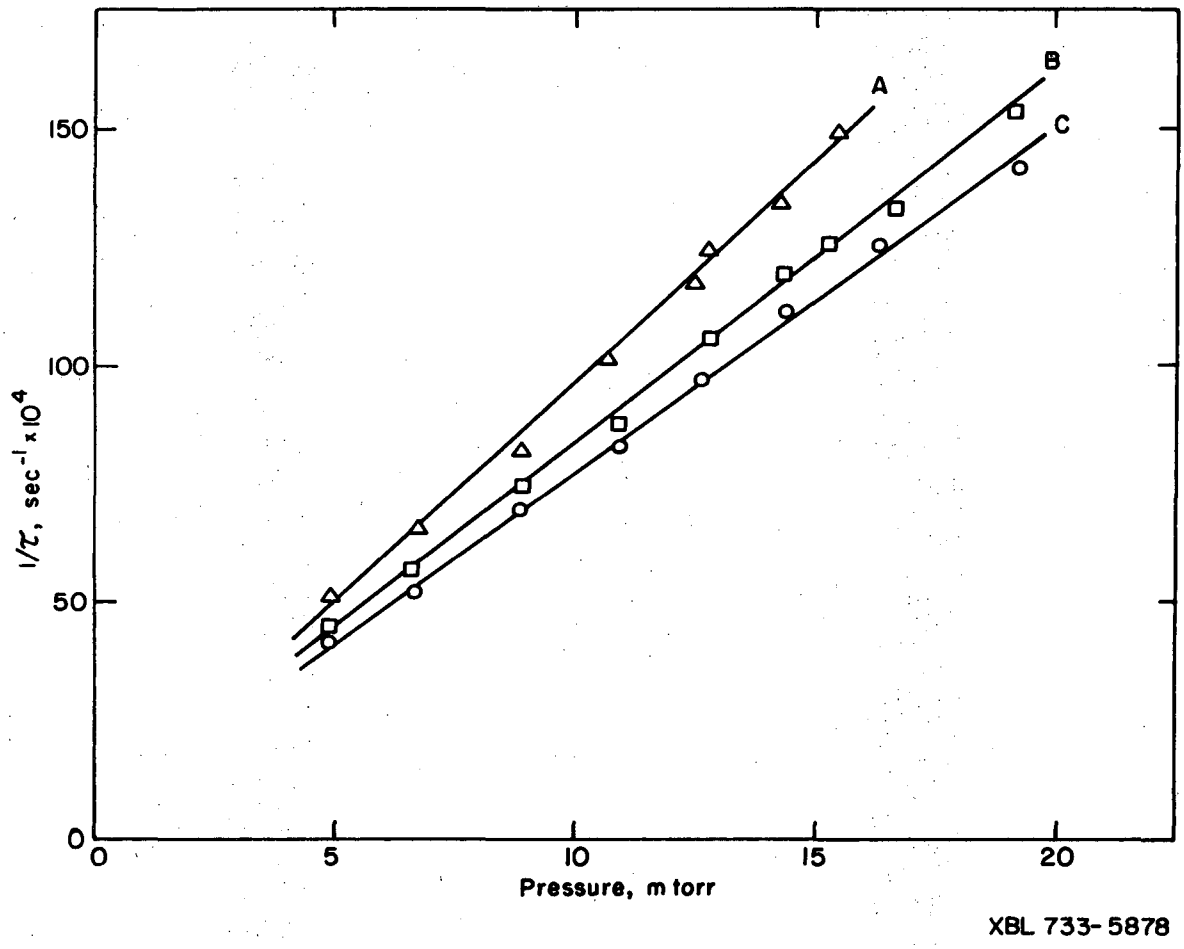

Fig. 21. Stern-Volmer graph of pressure dependent lifetime data. Excitation wavelength: 3023 Å. ΔW was: A, 703 cm^{-1}; B, 1955 cm^{-1}; C, 3641 cm^{-1}.

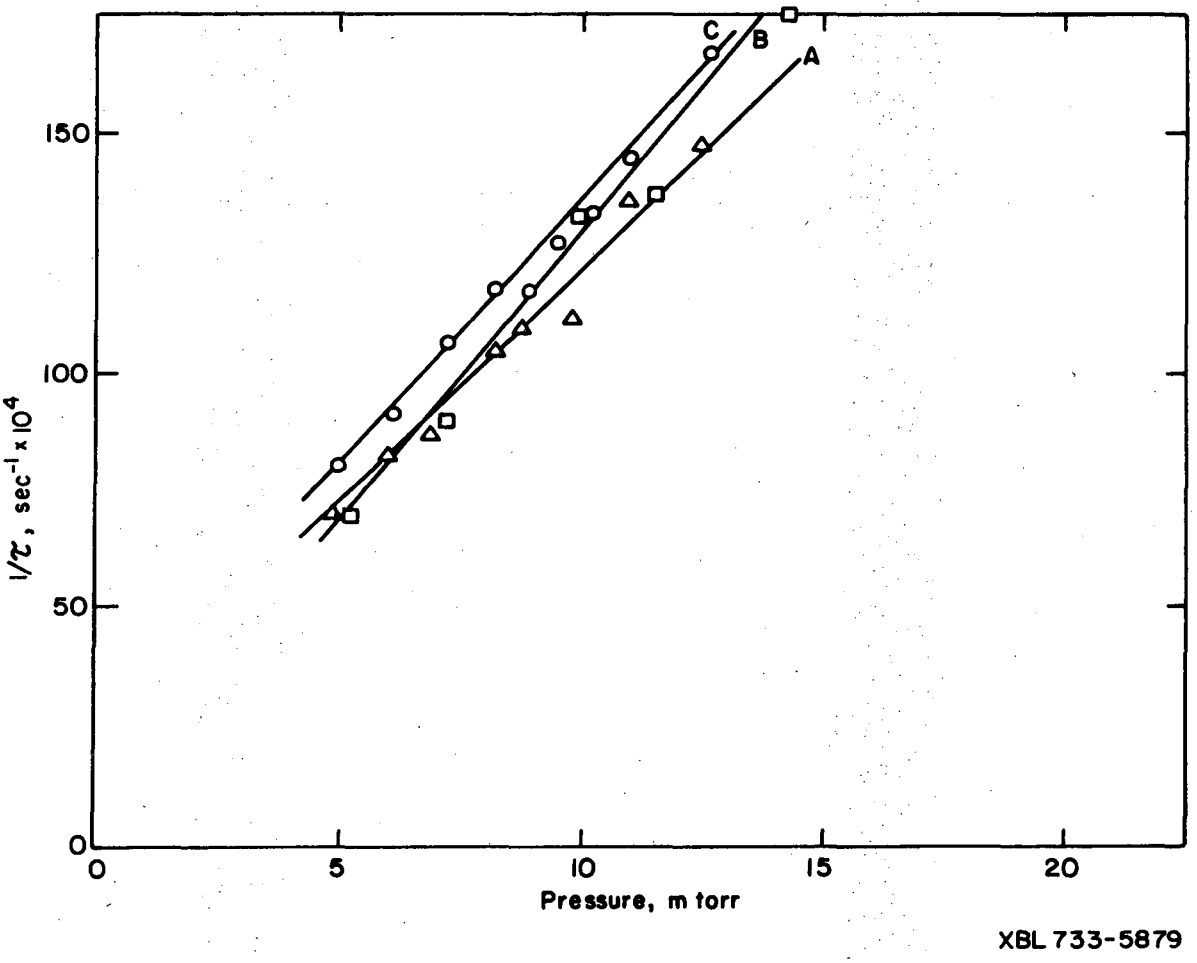

Fig. 22. Stern-Volmer graph of pressure dependent lifetime data. Excitation wavelength: 3147 Å. ΔW was: A, 638 cm^{-1}; B, 1603 cm^{-1}; C, 2339 cm^{-1}.

curvature. In all cases there was good correlation between the points above 5 mTorr and the straight line. This agrees with the development in Appendix (B) which predicts that plots of inverse apparent lifetime versus pressure should be linear for multistate kinetics at high enough pressure.

The plots in Figs. 19-22 show a significant decrease in the slope (apparent quenching rate constant) as the observation energy is lowered. This effect has been observed previously and is indicative of a multistate process.[25] This interpretation is discussed in detail in the discussion section. It is possible to rationalize these observations without assuming the presence of vibrational relaxation processes by asserting that several quantum states with different radiative and radiationless properties are populated by the excitation and that the variation of apparent quenching constant with observation wavelength is due to observing the emission from these different quantum states. Such an interpretation is unlikely in view of the regular decrease of apparent quenching constant with observation wavelength.

IV. DISCUSSION

A. Lifetime Predicted from Absorption and Emission Data

The standard Einstein relationship, which relates the integrated absorption coefficient to the radiative lifetime, is not strictly applicable to molecular systems. The Einstein relationship applies only to atomic transitions where fluorescence occurs at the same wavelength as absorption. Molecular transitions occur, in general, over a broad range of wavelengths. Strickler and Berg[28] have derived a general expression applying to molecular transitions. Their relationship allows one to calculate an appropriate value of the emission frequency. Their relationship is

$$\frac{1}{\tau_o} = 8\pi C \langle \bar{\nu}^3 \rangle \int \sigma(\bar{\nu}) \, d \, lu(\bar{\nu})$$

$$\langle \bar{\nu}^3 \rangle \equiv \frac{\int I(\bar{\nu}) \, d\bar{\nu}}{\int I(\bar{\nu}) \, \bar{\nu}^{-3} \, d\bar{\nu}}$$

where $\sigma(\bar{\nu})$ is the absorption cross section in units of cm, $\bar{\nu}$ is frequency in cm^{-1}, $I(\bar{\nu})$ is the emission intensity at frequency $\bar{\nu}$ and the integrations are performed over the entire absorption and emission spectra.

Using the data of Warneck, Marmo and Sullivan[29] for the region 2400-2600 Å and the spectrum determined in this laboratory for the region 2600-3200 Å the integrated absorption coefficient was determined by numerical integration. The exclusion of the absorption from 3200 to 3400 Å has little effect on the magnitude of the integrated absorption

coefficient since the absorption coefficients in that region are so small. The value of the integrated absorption coefficient is 3.4×10^{-19} cm^2.

The value of the frequency cubed factor was estimated in three ways:

1. The center of the absorption region was taken as the mean emission frequency. This yields a value of 44×10^{12} $(cm^{-1})^3$ for $\bar{\nu}^3$. The lifetime is predicted to be about 0.1 μsec.

2. The frequency cubed factor was calculated from data on the emission spectrum of SO + O_3 chemiluminescence.[30] This data was used in the Strickler and Berg relationship for $\langle \bar{\nu}^3 \rangle$. The frequency cubed factor is 19×10^{12} $(cm^{-1})^3$. The lifetime is predicted to be about 0.2 μsec.

3. A low pressure spectrum of SO_2 fluorescence from this study was used in the same manner as the SO_2 chemiluminescence data to calculate the frequency cubed factor. The frequency factor is 24×10^{12} $(cm^{-1})^3$, for excitation at 2960 Å. The predicted lifetime is about 0.17 μsec.

The predicted lifetime is about 0.1-0.2 μsec for all three methods of estimating the frequency factor. It is interesting that there is so little difference between the three predictions in view of the rather different methods used to estimate the frequency factor. In method 1 the value of $\bar{\nu}^3$ is probably too high since fluorescence from any given excited vibronic state can take place to high levels of the ground state. This effect would make the "average" emission frequency lower than the average absorption frequency. For this reason, the

prediction of τ_o is probably low. Method 2 suffers from the fact that the chemiluminescence experiment is done at relatively high pressure. Any relaxation processes could cause the observed chemiluminescence to originate in several different excited states, giving rise to a possible red shift in the emission spectrum. Method 3 is probably the most satisfactory since the excited states were prepared in a narrow energy range and the experiment was conducted at low enough pressure (0.6 mTorr) that relaxation was probably unimportant. This method suffers from experimental uncertainty in the relative detection efficiency at various wavelengths. The intensity of emission at long wavelengths would be increased by a detector correction factor resulting in a value of the frequency factor which is somewhat smaller than the calculated value. This correction would make the predicted lifetime longer. However, no more than about a factor of 2 change would be expected. The maximum predicted lifetime would then be about 0.3 μsec. The three methods would still agree to about a factor of 2. This is not the case for NO_2, however, where predicted lifetimes vary from 0.2-18 μsec.[25] The principal reason that the various prediction for SO_2 are very consistent is that both the absorption and emission spectra are relatively narrow compared to the overall energy of the transition. The spectra of NO_2 are quite broad making estimates of the mean emission frequency rather uncertain.

B. Quantum Yield at Zero Pressure

One important question in the interpretation of low pressure lifetimes measurements is whether the unimolecular processes depopulating the excited states are entirely radiative or whether additional non-radiative processes depopulate the excited states. If there were non-radiative processes the measured rate constant would be larger than the radiative rate constant.

The presence of non-radiative intramolecular processes is indicated by an emission quantum yield less than one in the limit of zero pressure. If there were no non-radiative intramolecular processes every absorption of a photon would result in the emission of a photon and the quantum yield would be one. The quantum yield of SO_2 fluorescence in the limit of zero pressure has been reported by Mettee[12] and Rao, Collier and Calvert (RCC).[31] Mettee reported that the quantum yield goes to unity at six exciting wavelengths from 3130 to 2650 Å. RCC report that the quantum yield is .14±0.06 for excitation at 2875 Å. These results are investigated in the following discussion.

If the quantum yield at zero pressure is 0.14 measurements of lifetimes at zero pressure could not be interpreted as the radiative lifetime. For a single excited state the quantum yield at zero pressure, Φ_o, is given by

$$\Phi_o = \frac{k_f}{k_f + k_{NR}}$$

where k_{NR} stands for the sum of all intramolecular non-radiative rate constants. If $\Phi_o = 0.14$ then $\tau_{rad} = 7.1 \times \tau_o$, where τ_{rad} is the radiative lifetime and τ_o is the zero pressure lifetime.

Experiments have shown that there are molecules which seem to have a quantum yield less than one at zero pressure. Benzene, for instance, is suggested to have a quantum yield of 0.2 at zero pressure.[32] However, it is not clear that the present theories of intramolecular relaxation in isolated molecules could account for a quantum yield less than one in a molecule as small as SO_2.[24,33,34] The proposed mechanism accounting for quantum yields less than one involves intersystem crossing from an optically active electronic state, populated by absorption, to an optically inactive electronic state. If the optically inactive electronic state has very high density of vibronic states the intersystem crossing can be considered irreversible, within the finite observation time of a physical experiment. This intramolecular radiationless transition results in an experimental quantum yield less than one at very low pressures. Moelcules having large enough level density in the optically inactive state have been categorized as being in the "statistical limit."[2] Molecules described as being in the statistical limit have generally been large organic molecules. There is even doubt that molecules as small as benzene are truly in the statistical limit.[2] Current theory indicates that SO_2 is not in the statistical limit and should have a zero pressure quantum yield of one.[33]

The experiments on quantum yields of SO_2 may be compared to determine if one experiment is more compelling than the other. Mettee stated that 20-28 quantum yield determinations in the pressure range 1-50 mTorr were used to extrapolate to the zero pressure quantum yield. RCC report that their lowest pressure used was 26 mTorr. Further, the fluorescence cell used by RCC was so small that significant quenching of emission probably occurred at the cell walls. Such quenching would give rise to a zero pressure quantum yield of less than one.

In view of the experimental uncertainties in the work of RCC and in view of the predictions of current theory the value of the zero pressure quantum yield of SO_2 is accepted as being unity. The low pressure lifetimes measured in this study are taken as the radiative lifetimes.

C. The Radiative Lifetime of Sulfur Dioxide

The radiative lifetime of SO_2 was measured for excitation in the range 2500-3150 Å. The excitation bandwidth was 10 Å FWHM. The lifetime varied from about 35 μsec at the extremes of the excitation range to about 55 μsec at intermediate wavelengths. These results agree with previous measurements[8] of 44 μsec for excitation in the range 2700-3100 Å. As has previously been pointed out the measured lifetimes are considerably longer than lifetimes predicted from absorption data. In a previous section of this study the lifetime was predicted to be 0.2±.1 μsec.

The anomalously long lifetimes of SO_2, CS_2 and NO_2 have been discussed previously. Douglas[3] has provided a qualitative model to explain the long lifetimes. His model has been investigated quantitatively by others.[33] The breakdown of the Born-Oppenheimer approximation is the key to the explanation of the long lifetimes of these molecules. If there is a significant perturbation between the upper electronic state, A, to which the transition occurs, and another electronic state, B, having a large density in the absorption region, then the B-O wavefunction of state A does not describe the actual upper state. The B-O wavefunction of state A is mixed with many levels of state B. The total transition moment from the ground state to the upper state is conserved, but it is spread out among transitions to the many actual excited states of the molecule instead of belonging to the transition from the ground state to state A. Thus the predicted lifetime is not altered by the perturbation in the molecule. However, the measured lifetime reflects the rate of emission from each of the actual excited states. If state B is not optically connected with the levels of the ground state to which emission occurs the transition moment between each of the actual excited states and the ground state is less than predicted from the total integrated absorption. That is, the oscillator strength of the transition is spread between emission from the many actual states of the molecule to which absorption occurs. The lifetime of each of these actual states is then longer than predicted.

In the case of SO_2 there are two known electronic states which can play the role of state B. The lowest triplet has levels in the energy range of excitation. There are also highly excited vibrational levels of the ground electronic state in the energy range of excitation. Both the triplet states and the highly excited vibrational states of the ground electronic state are only weakly connected with the lower levels of the ground state to which emission occurs. Both of these electronic states are potential candidates for the role of state B. The identity of state B is discussed subsequently.

One of the observable spectral characteristics of this model of lifetime lengthening is the presence of a complex absorption spectrum. In the unperturbed molecule one absorption line would be observed for a particular transition from the ground state to an excited quantum state. However, in the perturbed molecule quantum states of the upper electronic state are mixed with many states of state B giving rise to a myriad of apparently uninterpretable absorptions. Such an explanation could account for the complex spectrum of SO_2.

The relative magnitude of lifetime lengthening yields information concerning the identity of state B. The actual lifetime, τ_{exp}, is related to the lifetime predicted from absorption measurements, τ_{pred}, by $\tau_{exp} \approx N\tau_{pred}$ where N is the number of states coupled with the level of the upper state under consideration.[33] For SO_2, N is of the order of magnitude $N \approx (50/0.2) = 250$. That is, each level of the excited singlet is coupled with about 250 levels of state B. The magnitude of N is dependent on the level density of state B and the

magnitude of the coupling elements between state B and the upper state. Lacking an exact solution of the molecular hamiltonian, N is not available a priory.

The magnitude of the coupling matrix element can be estimated from the width of the well defined vibrational peaks in the absorption spectrum. Interaction with levels of state B further away than the wdith of the absorption peak would cause the peaks to be so broad that they would not be resolved. The width of the well resolved peaks is on the order of magnitude of 150 cm^{-1}. The density of states of the triplet state at 3000 Å is about 0.1 state/cm^{-1} in the harmonic approximation.[35] Thus the excited state could interact with about 15 of the triplet vibronic states. This is clearly not enough states to explain the long lifetime. The density of states of the ground electronic state is about 1 state/cm^{-1} in the region of interest. Thus, about 150 states could interact with the excited state. This is about the number of states necessary to give the lifetime observed. This argument does not pretend to be a quantitative analysis, but merely to show that only the ground state can supply the necessary number of states to produce the observed lifetime.

The measured lifetimes are expected to show variation with excitation energy since the level density of the ground state changes with energy and, presumably, the coupling between the upper state and levels of state B depends on the specific nature of the quantum states excited. The radiative lifetime of NO_2 exhibits significant variation when excited by a laser with about 0.8 Å bandwidth.[9] Lifetimes in the range 62-75 μsec were measured over a range of 100 Å in excitation

wavelength.[9] Experiments with very monochromatic laser excitation (about 0.15 Å bandwidth) have yielded lifetimes for NO_2 in the range 0.5-3.7 μsec.[36] These lifetimes are of the order of magnitude of those predicted from the integrated absorption coefficient.[25,36] These measurements presumably reflect the excitation of unperturbed levels of the $^2B_1$ Born-Oppenheimer excited state.

The radiative lifetimes for SO_2 determined in this study varied from 35-57 μsec. The variation was relatively smooth as contrasted with the irregular variation in NO_2 lifetimes. The bandwidth of excitation used in this study (10 Å FWHM, about 120 cm^{-1}) was, of course, too large to permit excitation of individual quantum states. The observed lifetime variation presumably reflects changes in the coupling perturbation and level density of the ground electronic state.

The kinetic nuclear energy operator has been shown to be the principal perturbation leading to radiationless intramolecular transition in large molecules.[37,38] Gardner and Kasha[39] have reviewed the current theory of intramolecular transitions. They have applied the theory to determine group theoretical selection rules for intramolecular transition between electronic states of various symmetries. They have shown that in order for such intramolecular processes to occur the direct product of both the electronic states and one of the normal vibrational modes of the molecule must contain the totally symmetric irreducible representation of the point group of the molecule. They have applied this rule to the investigation of "vibrationally deficient" molecules, or molecules whose symmetry species of the vibrational modes

do not span all of the irreducible representations of the molecular point group. SO_2 is identified as a vibrationally deficient molecule since its normal modes transform as A_1 or B_2. SO_2 lacks vibrations transforming as the remaining representations in the C_{2v} point group.

We may apply Gardner and Kasha's selection rule to the ground state, $^1A_1$, and the lowest singlet excited state, $^1B_1$, of SO_2. The direct products of the two electronic states and each of the vibrational modes do not transform as A_1. To first order at least, the nuclear kinetic energy operator is not responsible for coupling the excited state with the ground state.

It has been suggested that the coriolis effect breakdown of the B. O. approximation may be responsible for coupling the electronic states.[3,40] If this were the case one would expect a temperature dependent radiative lifetime since the coriolis forces depend on the rotational velocity of the molecule. Such an experiment could be of great value in elucidating the coupling mechanism in these small molecules.

D. Collisional Relaxation in Excited SO_2

In this section the energetics and rates of the collisional processes removing or redistributing energy in excited SO_2 are considered. The observation of strong phosphorescence at high pressures indicates that collisionally induced triplet ← singlet transitions play a role in quenching the singlet. There is also ample evidence from the pressure dependent experiments in this study to indicate that fluorescence occurs from a multi-state system.

The quenching behavior of excited SO_2 is discussed in terms of a hypothetical electronic state with equally spaced vibrational levels. Level 1, the optically populated level, is the highest level considered. Thus, collisionally induced transitions to higher energy are considered negligible relative to downward transitions. This assumption is subsequently justified by comparison of the magnitude of the energy difference between levels and the value of kT at room temperature.

Excited molecules are considered to be vibrationally relaxed by collisions to the next level of lower energy. Parameters to be determined to characterize the "stepladder" include the step size, ΔE, and the rate constants connecting the various levels. In addition, a process which takes molecules irreversibly out of the stepladder is included. Molecules removed from the stepledder are considered quenched as far as fluorescence is concerned. Figure 23 indicates this stepladder model schematically. The rate constant from state i to state i+1 is symbolized by b_i. The b_i are considered unequal in the most general case. The q_i are rate constants from each state out of the stepladder and are also initially considered unequal. The process removing molecules from the lowest singlet, the q_1, can be identified physically with the collisionally induced transitions from the lowest singlet to the lowest triplet electronic state.

The stepladder model has been employed previously in the discussion of vibrational relaxation in electronically excited NO_2.[25,41] It has been used in a slightly different context to analyze relaxation in chemically activated species.[42,43] Use of the stepladder model to

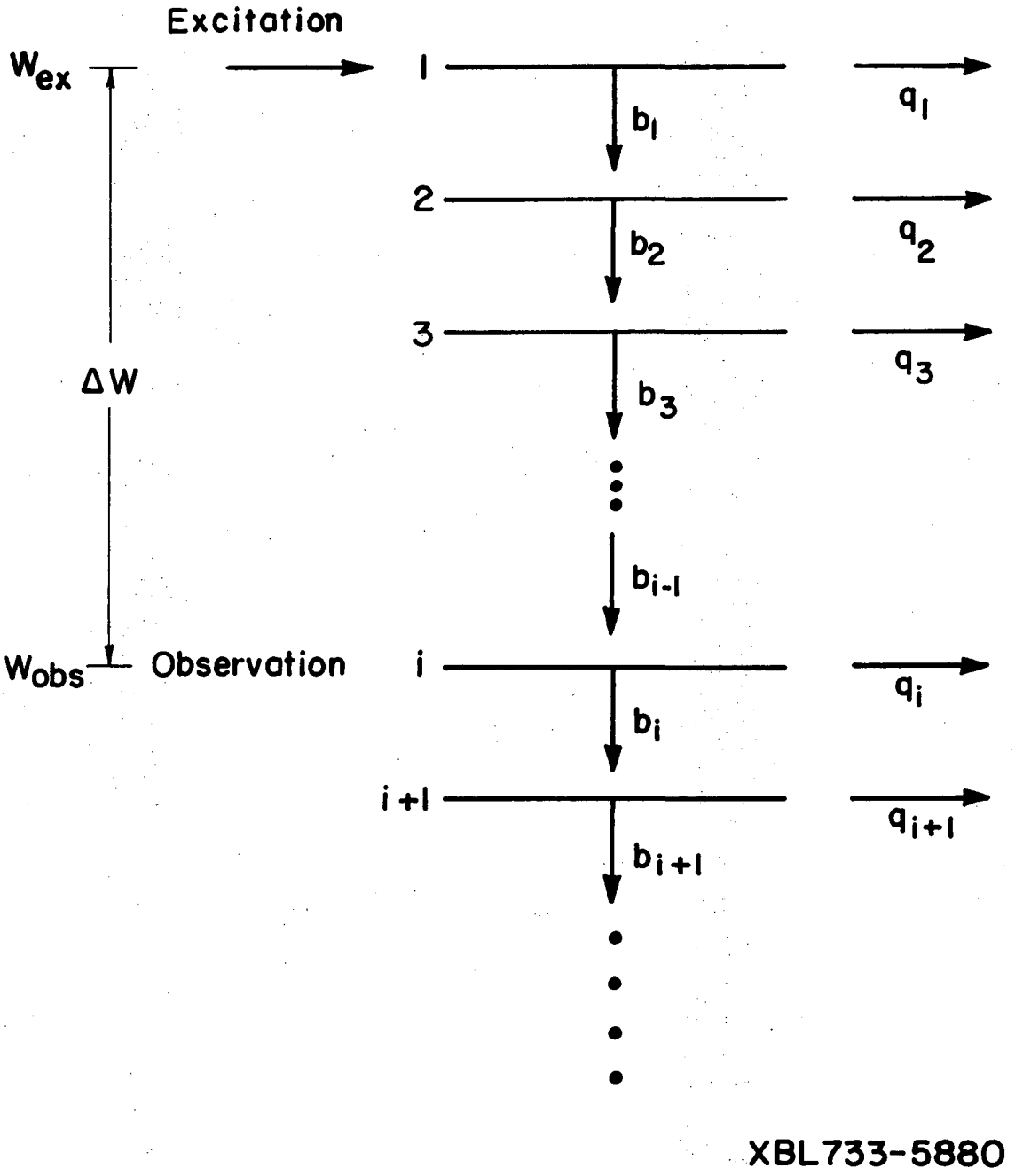

Fig. 23. Stepladder model used to analyze relaxation behavior of SO_2. Energies W_{ex} and W_{obs} are measured relative to the lowest vibrational state of the ground electronic state.

interpret experimental data does not, of course, imply that this model accurately describes the actual physical processes occurring in the excited molecule. At most the stepladder model can be said to reflect some kind of "average" process occurring in excited molecules. The proper use of such models in interpretation of experimental results is two fold; to arrive at a qualitative description of the dynamics of relaxation in excited species and as a basis of comparison between the relaxation characteristics of different species, e.g., SO_2 and NO_2.

For small value of ΔW, the difference between the excitation and observation energies, we will make the assumption that fluorescence from the initially populated state is the predominate part of the observed emission. In terms of the stepladder model this is equivalent to assuming that ΔE is larger than the small ΔW being considered. The low pressure fluorescence spectra indicate that even if ΔE is about equal to ΔW state 1 contributes more to the observed emission than states of lower energy.

With this assumption the conventional single state Stern-Volmer interpretation may be applied to the pressure dependent data at the smallest ΔW. The slope of plots of (1/lifetime) versus pressure yields an apparent quenching rate constant for the observed state. Quenching rate constants for states at each of the 4 excitation energies were calculated in this manner and are presented in Table (2). These quenching rate constants are roughly equal for each of the 4 excitation energies. In terms of the stepladder model this result indicates that (b_1+q_1) is roughly invariant to the energy of the initially

Table 2. Apparent quenching rate constants for fluorescence at energy near excitation energy.

Energy of excitation A	cm^{-1}	ΔW cm^{-1}	W_o cm^{-1}	k_q(apparent) cm^3/part-sec
2760	36231	771	6609	$(3.5\pm.3)\times10^{-10}$
2962	33760	910	4138	$(3.1\pm.2)\times10^{-10}$
3023	33080	703	3458	$(2.9\pm.2)\times10^{-10}$
3147	31778	638	1518	$(3.2\pm.5)\times10^{-10}$

ΔW is the difference between excitation and observation energies. W_o is the difference between excitation energy and the minimum in the upper state. k_q was calculated from slopes of the pressure dependent lifetimes graphs.

populated state. It is possible that changes in b_1 compensate changes in q_1 so that their sum is invariant or that either the b_i or q_i are small compared to the other and relatively large changes in the smaller rate constants does not significantly affect the sum.

Light is emitted at any observation energy, W_{obs}, by all states of energy equal to or higher than W_{obs}. The exact contribution of each state to the total signal is determined by each particular states resonant emission spectrum and population. The high pressure population of the general state n, $\hat{E}_n$, has been derived in Appendix B. Recast in the terminology of the stepladder model the population is

$$\hat{E}_n = I_o k_a G \frac{\prod_{j=1}^{j=n-1} b_j}{\prod_{j=1}^{j=n} (b_j+q_j)} \left[1 - \frac{i\omega}{M} \sum_{j=1}^{n} \frac{1}{b_j+q_j} \right] \tag{7}$$

The analysis of the high pressure quenching behavior would be particularly simple in the case of resolved emission. That is, if the emission spectra were such that each state could be observed individually. Such an experiment is obviously impossible at the resolution of this study. However, a discussion of such an analysis illuminates several points pertinent to a more realistic discussion.

In the pressure dependent studies plots were made of k_{app} versus M. Since $k_{app} = \omega(Z_1/Z_2)$ the following expression is easily found using Eq. (7).

$$k_{app}^{n} = \omega \frac{1}{\frac{\omega}{M} \sum_{j=1}^{n} \frac{1}{b_j+q_j}} = M\left[\sum_{j=1}^{n} \frac{1}{b_j+q_j}\right]^{-1} \quad (8)$$

where k_{app}^{n} stands for the apparent rate constant observed for state n. A straight line is predicted for plots of k_{app} versus M (as observed) with an apparent high pressure quenching constant, k_q^*, such that

$$(k_q^*)_n^{-1} = \sum_{j=1}^{n} \frac{1}{b_j+q_j} \quad (9)$$

This result indicates that the slope of Stern-Volmer plots (k_q^*) should decrease, as observed, as the observation energy is lowered. Equation (9) overestimates the decrease in slope since it is based on the ability to observe each state independently. In practice k_q^* decreases more gradually with ΔW since all states of energy greater than W_{obs} contribute to the emission.

If the assumption is made that the b_i are all equal and the q_i are all equal we have

$$(k_{qn}^*)^{-1} = \frac{n}{b+q} \quad (10)$$

Since (b+q) is known from Stern-Volmer plots at small ΔW a value of n can be calculated at each observation energy and the step size can be determined.

One interesting question is the possibility of resolving the sum (b+q) into individual values for b and q. Since the phase behavior of a particular state with respect to its immediate precursor (whether the precursor is the exciting light or another excited state) is a function only of the sum of the rates of the individual channels de-populating the state in question there is no information available in the resolved spectroscopy model which would enable one to resolve (b+q) into individual components. The phase behavior of the entire manifold of states is a function of (b_i+q_i) only. The individual values of b_i and q_i enter into the population distribution only. Therefore, phase information in the resolved model supplies no information to resolve (b_i+q_i) into its components.

A more realistic treatment considers the unresolved nature of the emission spectra. The observed signal at $W_{obs} = W_n$ is given by

$$S_n = \sum_{i=1}^{n} Ei\ k_{fi}^{n}\ \alpha_i \qquad (11)$$

where k_{fi}^{n} is the fluorescence rate constant which for any state i is a function of the observation energy. The various detection efficiencies are represented by α_i. The α_i can be assumed to be identical. The summation is carried out over all states of energy W_n and higher.

In the unresolved case k_{app} has a somewhat more involved form than in the resolved case.

$$k_{app} = \omega \frac{\sum_{i=1}^{n} E_i^o \, k_{fi}^n}{\sum_{i=1}^{n} E_i^{-90} \, k_{fi}^n} = M \frac{\sum_{i=1}^{n} \left\{ k_{fi}^n \left[\frac{\prod_{j=1}^{i-1} b_j}{\prod_{j=1}^{i} (b_j+q_j)} \right] \right\}}{\sum_{i=1}^{n} \left\{ k_{fi}^n \left[\frac{\prod_{j=1}^{i-1} b_j}{\prod_{j=1}^{i} (b_j+q_j)} \right] \sum_{j=1}^{i} \frac{1}{(b_j+q_j)} \right\}} \qquad (12)$$

As in the resolved case a straight line is predicted with inverse slope, $(k_{qn}^*)^{-1}$ given by

$$(k_{qn}^*)^{-1} = \frac{\sum_{i=1}^{n} \left\{ k_{fi}^n \left[\frac{\prod_{j=1}^{i-1} b_j}{\prod_{j=1}^{i} (b_j+q_j)} \right] \sum_{j=1}^{i} \frac{1}{(b_j+q_j)} \right\}}{\sum_{i=1}^{n} \left\{ k_{fi}^n \left[\frac{\prod_{j=1}^{i=1} b_j}{\prod_{j=1}^{i} (b_j+q_j)} \right] \right\}} \qquad (13)$$

In its completely general form Eq. (13) contains too many undetermined quantities to be of use in analyzing the fluorescence. Assumptions concerning the spectral distributions (the k_{fi}^n) must be made and the values of the b_j and the q_j must be restricted in order to apply Eq. (13). Model calculations were made to determine the effect of various assumptions. In particular the effects of various spectral distributions and differing values of the b_j are considered.

Schwartz and Johnston[25] used the stepladder model expressed in terms of the Rice-Rampsberger-Kassel (RRK) theory[44] of unimolecular

reactions to interpret the quenching behavior of NO_2. In this model the multiplicity of energy level j is given by

$$g_j = \frac{(J+s-1)!}{J!(s-1)!} \tag{14}$$

where s is the number of normal modes of vibration and J is the number of vibrational quanta. In the present case $J\Delta E$ is the total vibrational energy and for SO_2 s=3.

Consider a set of three adjacent, decreasing, vibrational energy levels j+1, j, and j-1 with multiplicity g_{j+1}, g_j and g_{j-1}.

$$E_{j+1} \xrightarrow{b_{j+1}M} E_j \xrightarrow{b_jM} E_{j-1}$$

The relative rate of vibrational deactivation is given by the product of an appropriate transition moment times the multiplicity of the final state.[45] If the transition moment is assumed to vary slowly with energy[46] the multiplicity is the dominant term. Then

$$\frac{b_{j+1}}{b_j} \sim \frac{g_j}{g_{j-1}} \tag{15}$$

and the complete set of the b_j are determined except for an undetermined constant. This method has been used previously to generate the b_j in the analysis of NO_2 quenching.[25]

In discussion of the long lifetime of SO_2 the excited state has been described as a superposition of the Born-Oppenheimer ground state and the B. O. excited electronic state. Each of the levels of the B.O. excited state were pictured as being mixed with about 150 highly excited vibrational levels of the ground B.O. electronic state. If this model is assumed to be correct then the excited state of SO_2 would be characterized as a highly vibrationally excited ground state molecule as far as relaxation processes are concerned. Excitation at 2960 Å would involve about 34,000 cm^{-1} of vibrational energy. On the other hand, if the excited state is considered to be adequately described by the excited B.O. electronic state excitation at 2960 Å would involve only 4000 cm^{-1} of vibrational energy, the rest going into electronic excitation. These two models of the vibrational energy of the excited state manifest themselves in very different relative values of the b_j. Figure 24 shows model calculations of $(k^*_{qn})^{-1}$ as a function of n. The step size for these model calculations was 500 cm^{-1}. In these calculations $b_1 = 2 \times 10^{-10}$ cm^3/part-sec and $q_1 = 1 \times 10^{-10}$ cm^3/part-sec. A flat spectral distribution from all states was assumed. A was calculated assuming that the b_j are all equal. B was calculated in terms of the superposition model with b_j given by Eq. (15) and C assumes that the excited state is characterized adequately in terms of the B.O. excited state with b_j given by Eq. (15).

These plots indicate that the assumption of equal b_j is relatively innocuous in the superposition model, but leads to rather large errors in the B.O. model. This is understood through consideration of the

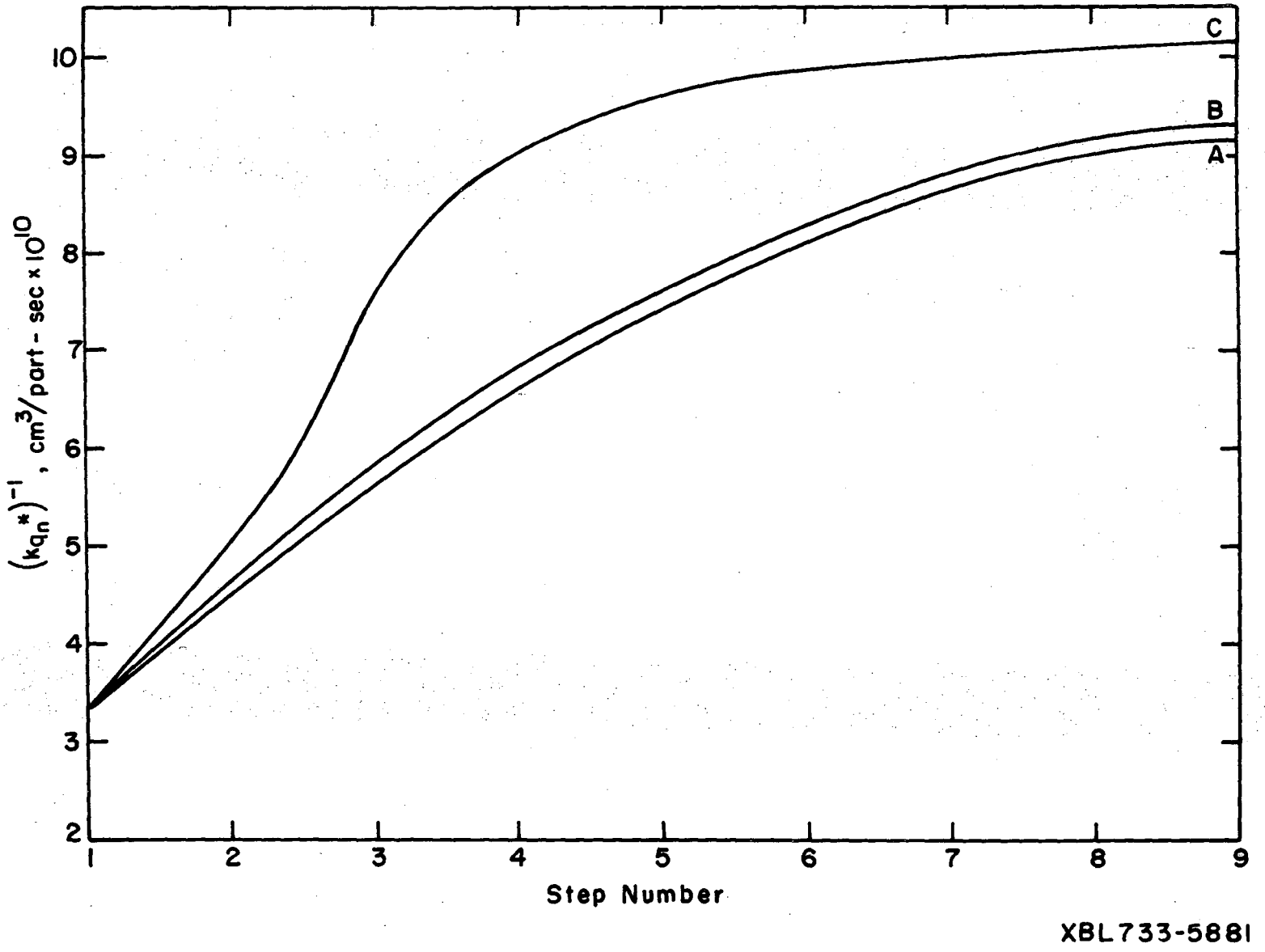

Fig. 24. Graph of $(k_{qn}^*)^{-1}$ for three models of the b_j. The models are described in the text.

relative values of the b_j in each model. Due to the large number of vibrational quanta in the superposition model the multiplicities of the energy levels considered change relatively little. At 30,000 cm^{-1} (the energy of the lowest step) there are about 60 of the hypothetical 500 cm^{-1} quanta. At 2960 Å (34,000 cm^{-1}) there are 68 such quanta. The ratio of the multiplicities is

$$\frac{\frac{(68+3-1)!}{68!\ 2!}}{\frac{(60+3-1)!}{60!\ 2!}} = 1.3$$

Thus the b_j vary by a factor of 1.3 over the whole energy range considered. In the B.O. model there are 8 quanta at 34,000 cm^{-1} and 0 at 30,000 cm^{-1}. The ratio of the degeneracies is

$$\frac{\frac{(8+3-1)!}{8!}}{\frac{(0+3-1)!}{0!\ 2!}} = 72$$

In the B. O. model the b_j vary by a factor of about 72. In view of the current theory of the nature of the excited singlet of SO_2 and the experimental result that the apparent Stern-Volmer quenching constant at small ΔW is relatively constant over a rather wide region of the energy beings considered, the superposition model seems to better describe the nature of excited SO_2. On the basis of these model calculations the assumption of equal b_j is seen to be quite acceptable. It is true that the model calculations support this conclusion only

for values of b comparable or larger than the value of q. The relative magnitude of b and q is discussed subsequently.

The effects of various model spectral distributions were investigated in similar calculations. These calculations used values of b and q of 2×10^{-10} cm^3/part-sec and 1×10^{-10} cm^3/part-sec respectively. Three spectral distributions were considered. (1) A flat distribution, i.e., uniform emission at all wavelengths considered. (2) A constantly linearly increasing distribution with unit intensity at step 1, 2 units at step 2, etc. (3) A distribution which increases for 2 steps then becomes flat. These model distributions are indicated in Fig. 25. The distribution most closely approximating the actual observed spectral distributions is the third model distribution, as comparison with Fig. 17a indicates.

Figure 26 shows a plot of calculated $(k^*_{qn})^{-1}$ versus step number for the 3 model distributions. Since model 3 is the most realistic distribution the other two distributions will be compared to it. $(k^*_{q1})^{-1}$ is not defined for model distribution (3) since there is no emission at the energy of step 1 in this model. Distribution (2) gives rise of values of $(k^*_{qn})^{-1}$ which are too low at high values of n. This is due to the fact that observation at energies corresponding to the lower energy steps is dominated by emission from the high energy steps. Thus $(k^*_{qn})^{-1}$ does not increase with n as rapidly as for distribution (3). The most interesting comparison is between distribution (2) and the flat distribution, (1). The chief characteristic of the flat distribution is that the entire curve is shifted towards lower step

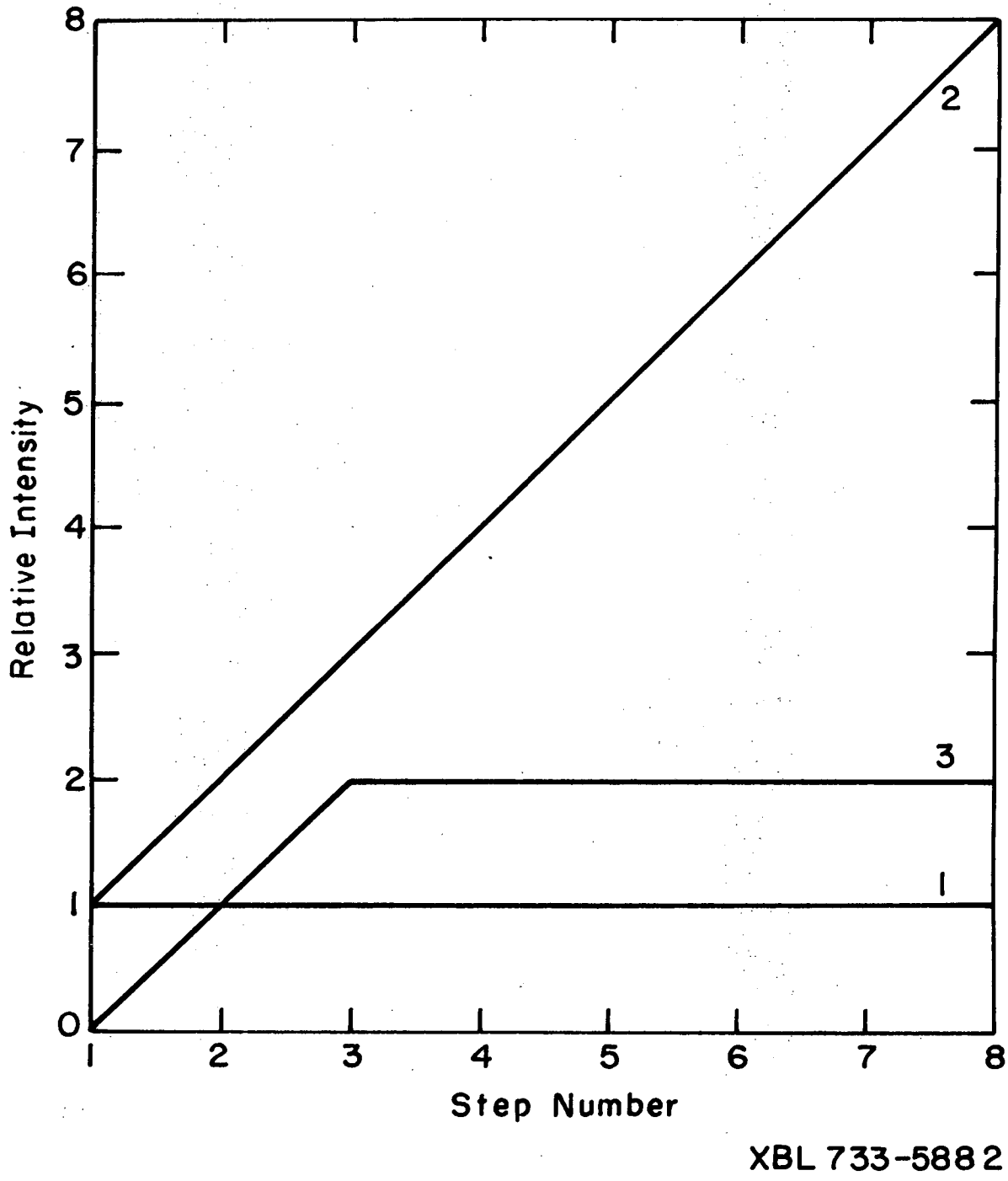

Fig. 25. Three model spectral distributions.

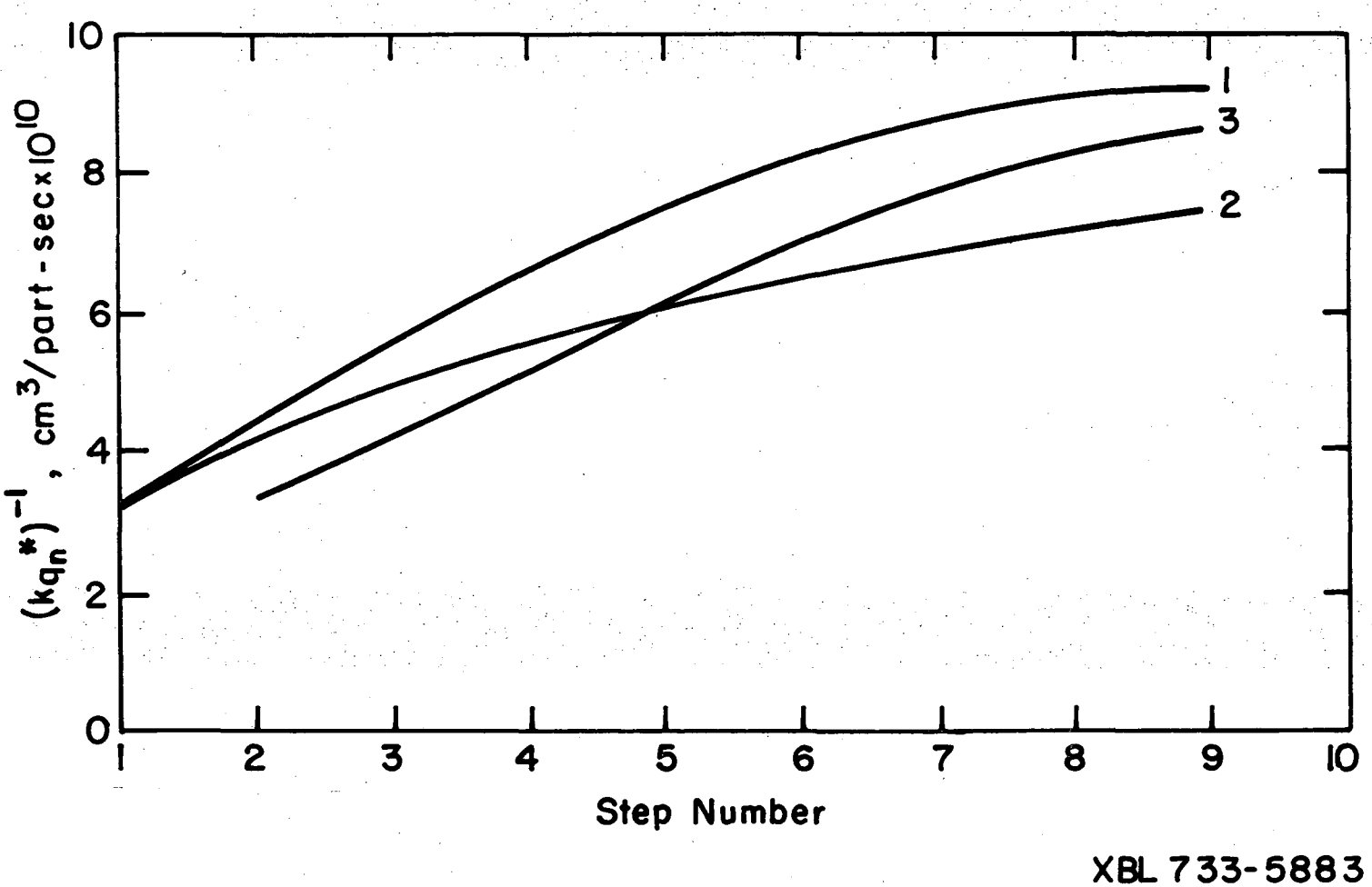

Fig. 26. Graph of $(k_{qn}^*)^{-1}$ for three model spectral distributions. The distributions and model parameters are described in the text.

numbers (higher observation energies). The overall shape of the two curves is similar. This similarity is illustrated in Fig. 27 which shows the $(k^*_{qn})^{-1}$ curves for distributions (1) and (3) plotted with the curve for (3) shifted by 1 step to lower energy. This plot demonstrates that the assumption of a flat spectral distribution is acceptable as long as it is recognized that the flat distribution tends to shift the curves of $(k^*_{qn})^{-1}$ to higher energy. This analysis is most accurate for step sizes about 1000 cm^{-1} since the typical low pressure emission spectra seem to rise for about 2000 cm^{-1} and then level off. The step size is estimated subsequently.

These model calculations and the experimental results have demonstrated that the assumption of equal b_i and q_i is probably very good. Calculations with various spectral distributions indicate that the assumption of a flat distribution does not change the shape of the $(k^*_{qn})^{-1}$ versus step number curves, but does shift them to lower energy. The relaxation behavior of excited SO_2 will be analyzed assuming that the spectral distribution is flat. The effect of shifting the $(k^*_{qn})^{-1}$ curves to lower energy can be discussed in view of the estimates of ΔE to be derived in the following analysis.

With these assumptions $(k^*_{qn})^{-1}$, Eq. (13), can be written as

$$(k^*_{qn})^{-1} = \frac{1}{b+q} \frac{\sum_{j=1}^{n} j\chi^{j-1}}{\sum_{j=1}^{n} \chi^{j-1}} \qquad (16)$$

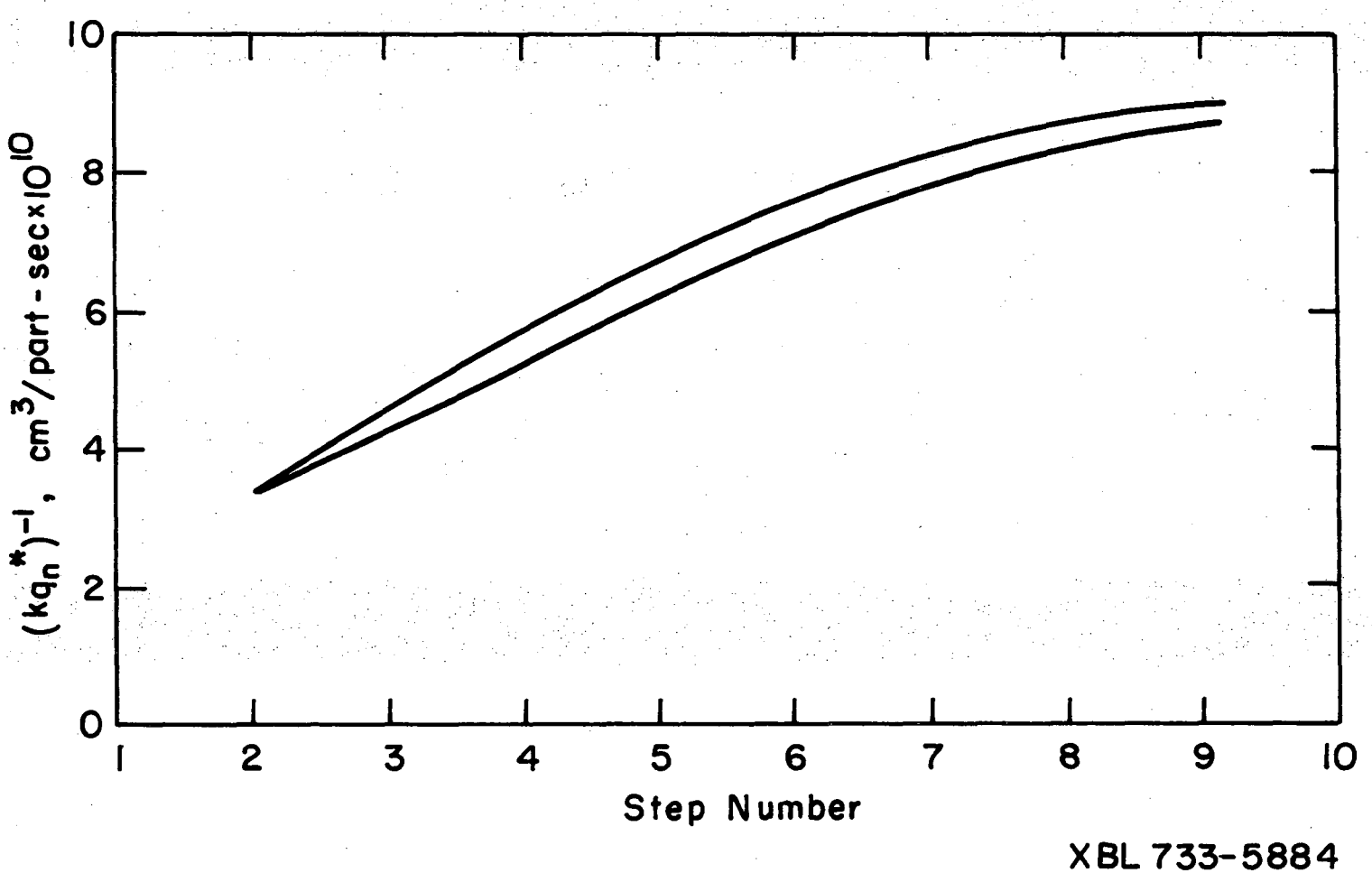

Fig. 27. Graph of $(k_{cn}^*)^{-1}$ comparing the flat and semiflat spectral distributions. The curve for the flat distribution is shifted one step to lower energy.

where

$$\chi = \frac{b}{b+q}$$

The $(k^*_{qn})^{-1}$ are plotted as a function of n for various values of χ in Fig. 28. Figure 28 also contains a plot of $(k^*_{qn})^{-1}$ is the resolved spectroscopy model. This curve is defined by Eq. (9). Several features of this family of curves are of interest. For χ=0 there is no collisional population of lower levels and conventional Stern-Volmer kinetics are observed. That is, quenching behavior does not depend of observation wavelength. For small values of χ there is some deviation from Stern-Volmer kinetics but the populations of the first few states predominate so the $(k^*_{qn})^{-1}$ quickly reach a limiting value. As χ increases the populations of the lower energy states increase causing the plateau to move to higher step number (lower energy). For $\chi = 1$ Eq. (16) takes on a particularly simple form

$$(k^*_{qn})^{-1} = \frac{1}{b} \frac{\sum_{J=1}^{n} J}{\sum_{J=1}^{n} 1} = \frac{1}{b}\left[\frac{h+1}{2}\right] \qquad (17)$$

The general form of this equation is identical to expression (10) for the resolved model. Again a straight line is predicated in the unresolved model with $\chi = 1$, but with slope of $\frac{1}{2}$ of the slope in the resolved case.

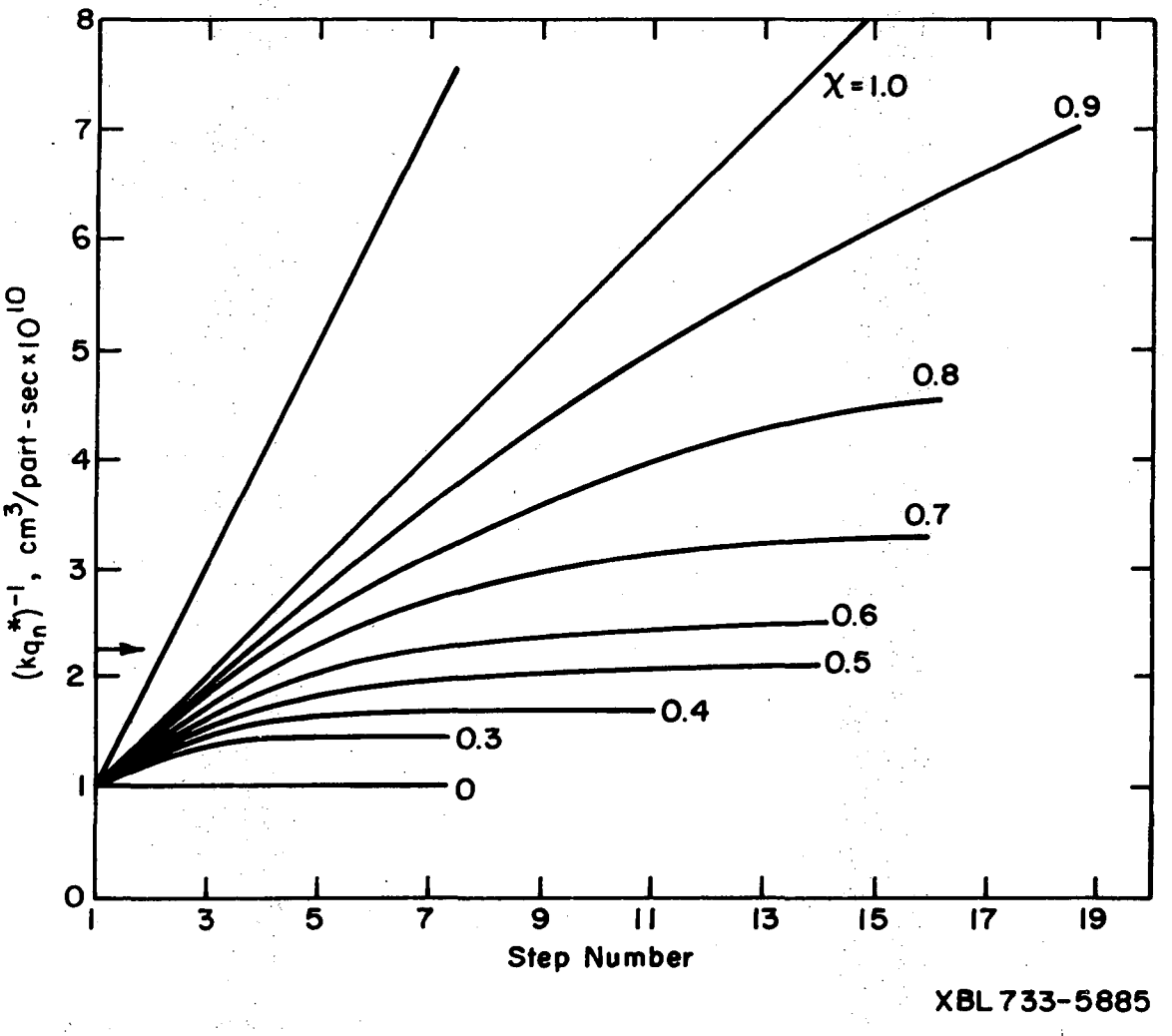

Fig. 28. Graph of $(k_{qn}^*)^{-1}$ for various values of χ.

Figures 29 - 32 are plots of the experimental high pressure apparent quenching constants, $(k_q^*)^{-1}$. They were calculated from the experimental data at each observation wavelength by fitting the high pressure plots of k_{app} vs M to the best straight line. The slope of such a plot is $(k_q^*)^{-1}$.

Figure 32 for excitation at 3147 Å covers so short an energy range and the points are so uncertain that quantitative consideration is not warranted. However, the plots at the three other excitation wavelengths show that $(k_q^*)^{-1}$ clearly increases with ΔW, although the increase is not completely monotonic. If the assumption that the b_i and q_i are single valued over the energy range of these studies is accepted, then one would expect similar curves of $(k_q^*)^{-1}$ versus ΔW for all four excitation wavelengths. The experimental curves are in general similar although the curves at lower excitation energy appear to increase slightly less rapidly.

Assuming that the four plots reflect the same relaxation behavior the curve at 2760 Å covers the largest energy range and for that reason will be analyzed in detail. The slope of the plot of $(k_q^*)^{-1}$ versus ΔW is a function of both the step size and the value of χ. A lower limit to the possible value of χ can be obtained by comparing the experimental plot of $(k_q^*)^{-1}$ to the family of calculated curves, Fig. 28. The experimental curve rises from about 3.2×10^9 to 7.3×10^9 part-sec/cm^3. Figure 28 indicates that curves with $\chi \lesssim .55$ do not increase by that much, therefore, $\chi > .55$. Since we know $(b+q) \simeq 3.3 \times 10^{10}$ cm^3/part-sec any value of χ can be solved for the individual

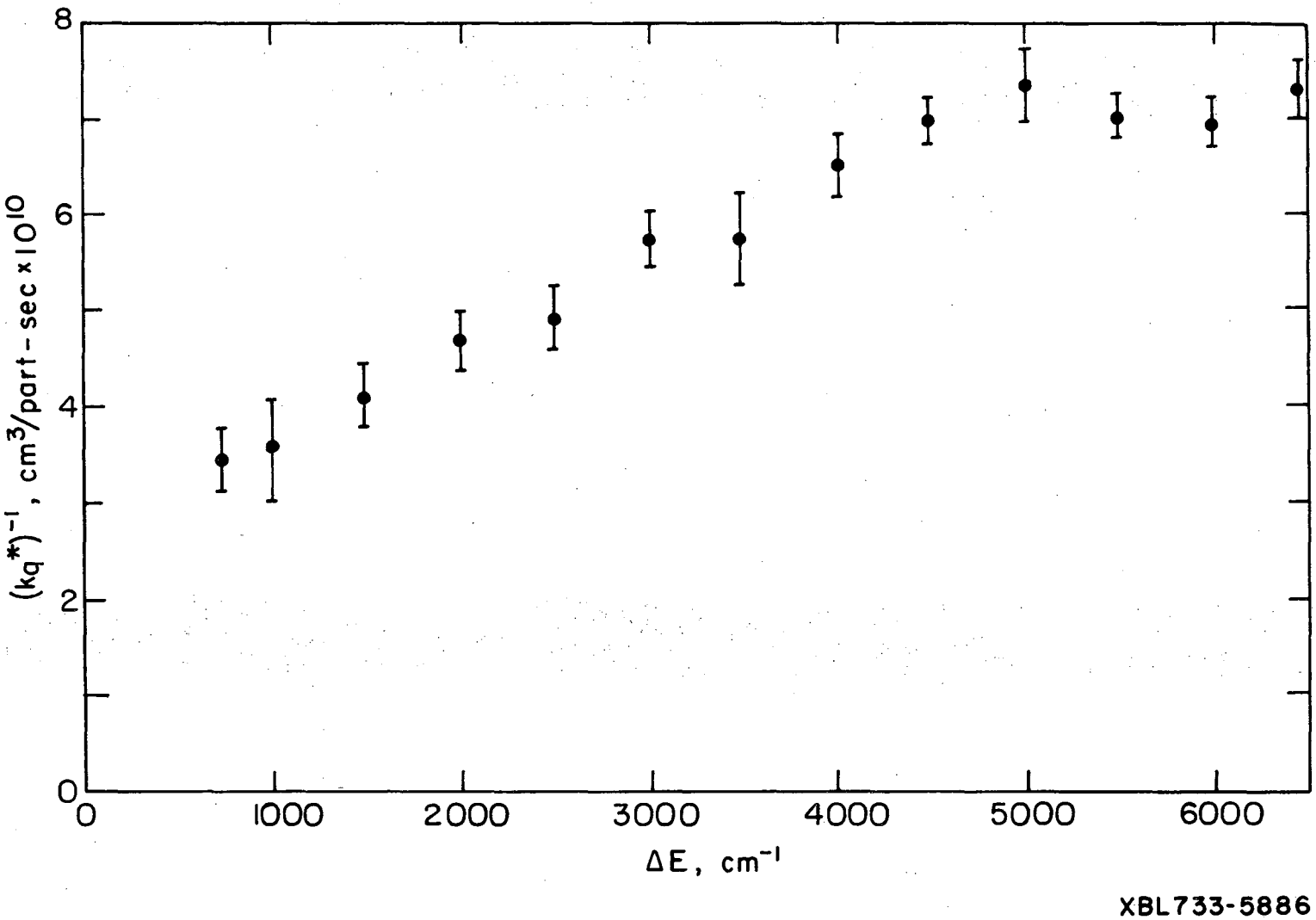

Fig. 29. Graph of experimental values of $(k_q^*)^{-1}$ for excitation at 2760 Å. Error bars represent two standard deviations of the slopes from which each of the values of $(k_q^*)^{-1}$ was calculated.

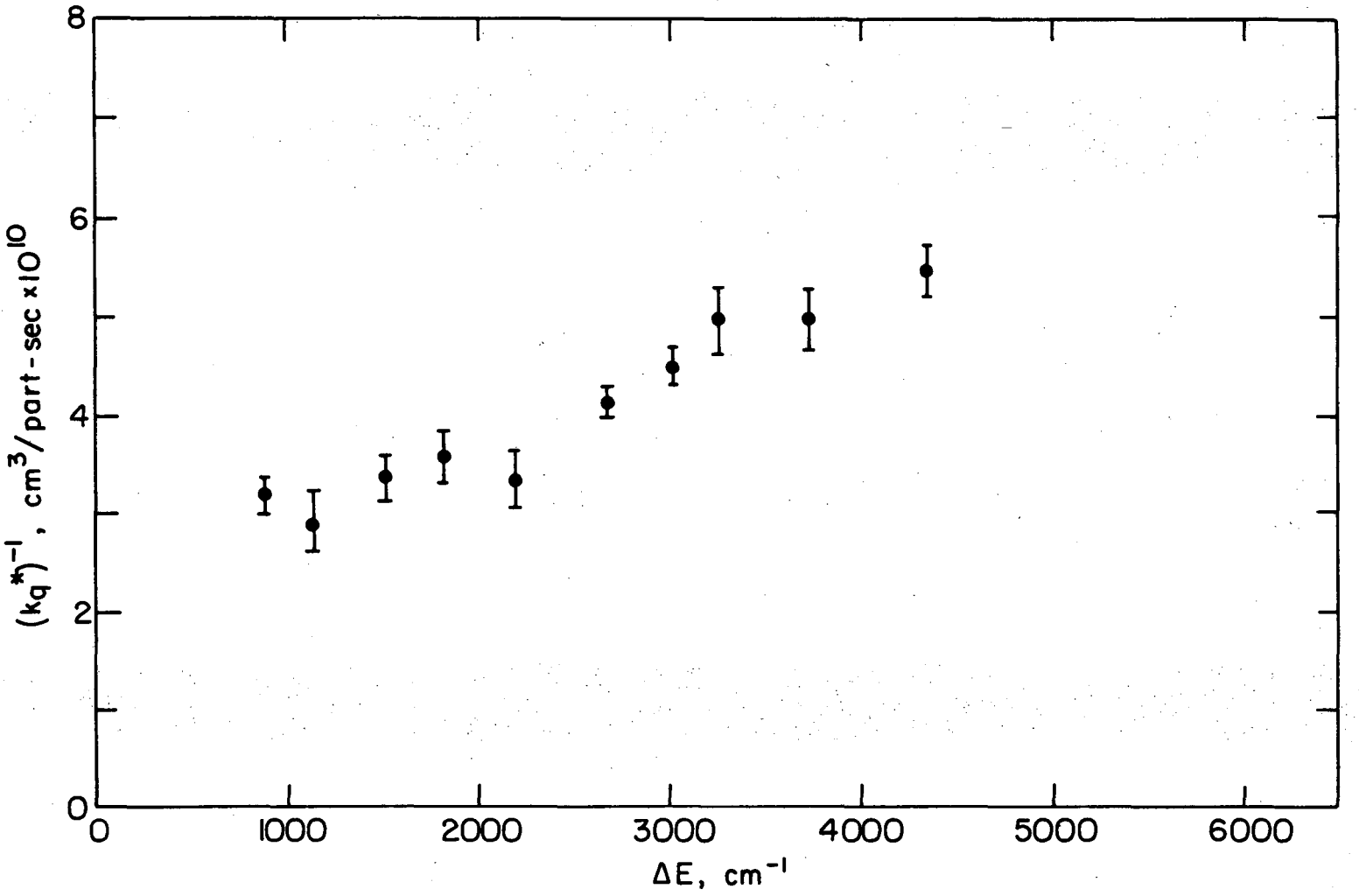

Fig. 30. Graph of experimental values of $(k_q^*)^{-1}$ for excitation at 2962 Å. Error bars represent two standard deviations of the slopes from which each value of $(k_q^*)^{-1}$ was calculated.

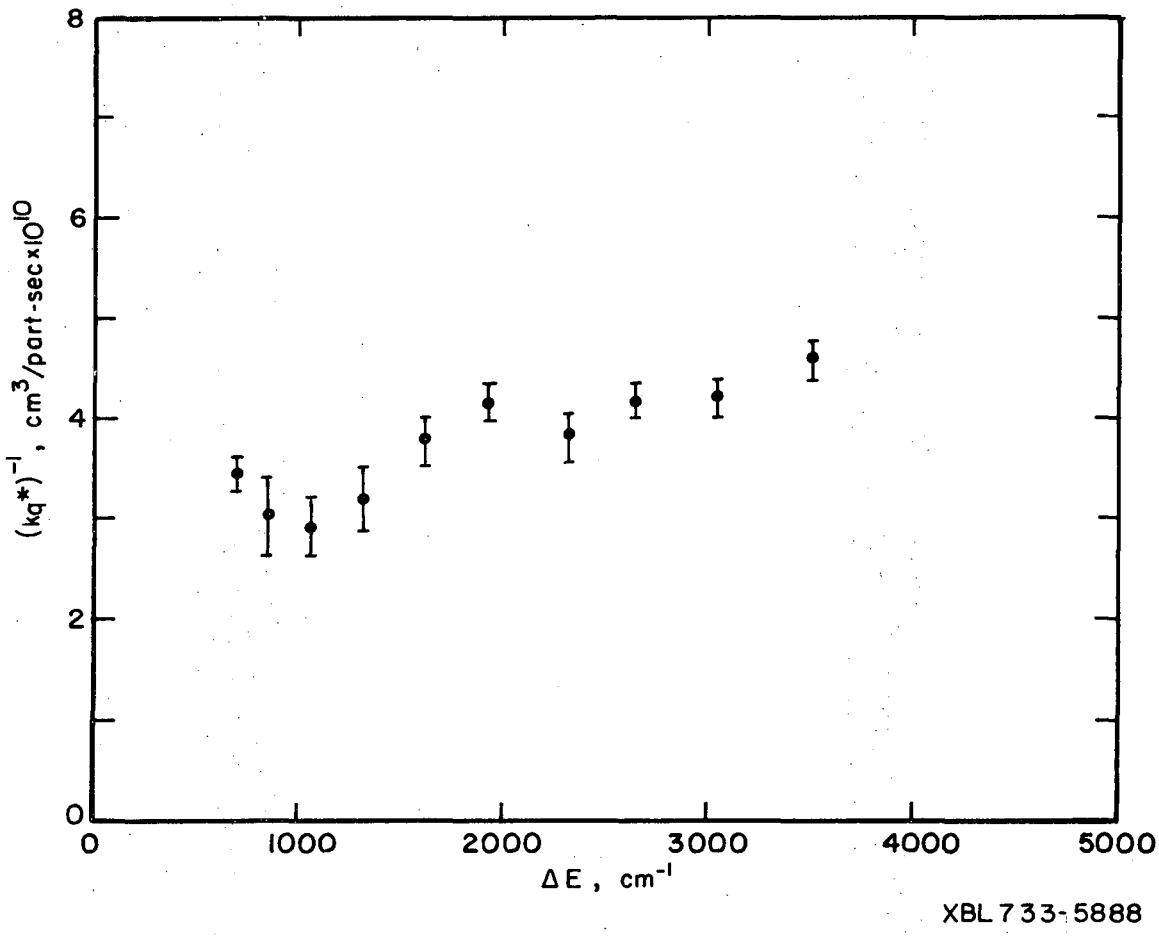

Fig. 31. Graph of experimental values of $(k_q^*)^{-1}$ for excitation at 3023 Å. Error bars represent two standard deviations of the slopes from which each value of $(k_q^*)^{-1}$ was calculated.

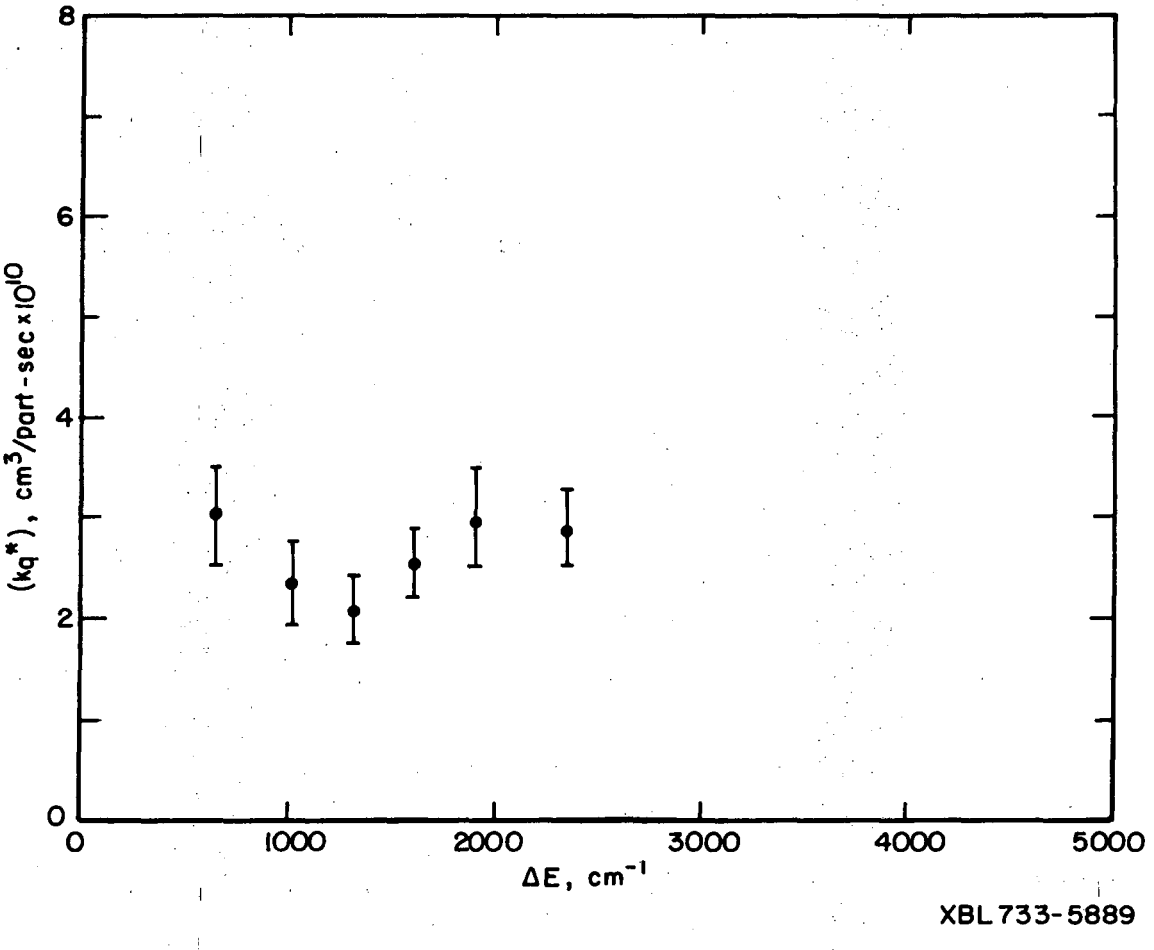

Fig. 32. Graph of experimental values of $(k_q^*)^{-1}$ for excitation at 3147 Å. Error bars represent two standard deviations of the slopes from which each value of $(k_q^*)^{-1}$ was calculated.

values of b and q.

Each assumed value of χ corresponds to a different step size. For $\chi = 0.7$ an increase of a factor of 2.25 in $(k^*_{qn})^{-1}$ occurs at about step 5. Excitation at 2760 Å involves about 6500 cm^{-1} of energy above the (000) ← (000) transition. Thus, each step would be about 6500/4 = 1625 cm^{-1}. The curves for $\chi > 0.8$ rise by a factor of 2.25 at about step 4 implying that $\Delta E \simeq 6500/3 = 2160$ cm^{-1}. Thus for $\chi > 0.7$ the step size indicated is about 2000 cm^{-1}. For $.55 < \chi < 0.7$ the analysis is more difficult, since the slowly rising plateau in these curves makes determination of the number of steps at $(k^*_{qn})^{-1} = 2.25\ (b+q)$ rather uncertain. For $\chi = .6$ there are about 6 or 7 steps before $(k^*_{qn})^{-1}$ crosses 2.25 (b+q) resulting in a step size of about 1000 cm^{-1}. If χ is less than 0.6 the step size would be substantially reduced. Thus, unless χ was very close to 0.55 the value of ΔE can be estimated to lie between 2000 and 1000 cm^{-1}.

If vibrational and electronic energies are separable, that is, if the Born-Oppenheimer approximation is applicable, then excitation at 2760 Å involves about 6500 cm^{-1} of vibrational energy and longer excitation energies involve correspondingly less. Thus vibrational energy transfer of 1000-2000 cm^{-1} per collision would be a large percentage of the total vibrational energy. However, in view of the proposed mixing of electronic states it may be more appropriate to consider the vibrational energy to be nearly the total energy above the lowest vibrational level of the ground state (32000-36000 cm^{-1}). In this interpretation, in which the excited state is viewed as a

highly vibrationally excited ground electronic state molecule, the vibrational energy transferred per collision would be on the order of 5% of the total vibrational energy.

As discussed previously phase measurements in the resolved spectroscopy model do not allow the sum (b+q) to be separated into values for b and q. It was noted that knowledge of the population distribution in the various states would supply information on b and q. In this discussion of the resolved spectroscopy model we have shown that $.55 \lesssim \chi \leqslant 1$. Essentially, a limit was placed on the possible population distributions by showing that a factor of 2.25 change in $(k_q^*)^{-1}$ was only consistent with $.55 \lesssim \chi \leqslant 1$.

It is desireable to investigate the population distributions directly from high pressure spectra. In spectra with obvious red shifts at high pressures it may be possible to derive population distributions. However, the emission spectra in this study are not greatly red shifted at high pressure. Further, the low pressure spectra are so irregular that the high pressure spectra do not warrant quantitative analysis for the population distribution. Therefore, individual values of band q are not available in this experiment.

Rao, Collier and Calvert[31] have performed experiments which allow an estimate of χ to be made. They irradiated mixtures of SO_2 and biacetyl with wideband radiation centered at 2875 Å. The biacetyl functioned as a triplet energy acceptor quenching the triplet state of SO_2, but not affecting the singlet state. By measuring the quantum yield of the sensitized biacetyl emission as a function of biacetyl

concentration they were able to arrive at the estimate that "quenching collisions of excited SO_2 with ground state SO_2 result in intersystem crossing about 8% of the time and relaxation to the ground state about 92% of the time." Their interpretation did not include the provision for vibrational relaxation within the excited singlet. Their estimate of the percentages of excited singlets which eventually find their way to the ground state and triplet state imply that in the stepladder model somewhat less than 8% of the molecules in any given level indergo intersystem crossing on collision with a ground state molecule. Their experiment indicates that χ is very close to 1.

The estimates of χ and ΔE in this study have been in terms of excitation at 2760 Å with the assumption that relaxation processes were invariant to the energy of the state considered. This assumption is supported by the estimates of (b+q) at the four excitation energies. However, from Figs. 29-32 it appears that the slope of experimental plots of $(k_q^*)^{-1}$ versus ΔW is higher for higher excitation energies. Indeed, the plot for excitation at 3147 Å could be fitted reasonably well by a flat line. Thus, it appears that relaxation at energies corresponding to 3147 Å and lower can not be characterized by the same parameters as at the higher energies considered. The flatness of the $(k_q^*)^{-1}$ curve for excitation at 3147 Å indicates single state behavior. Also, the low and high pressure emission spectra for excitation at 3147 Å show very similar structure. This may indicate that the same states are emitting in both cases. These observations could be explained in two ways; 1. Since excitation at 3147 Å involves about

2400 cm^{-1} of energy above the minimum in the excited singlet surface, collisions removing about 2400 cm^{-1} of energy would completely quench fluorescence and single state behavior would be observed. 2400 cm^{-1} is slightly larger than the maximum value estimated for ΔE. This argument can not be supported by the data at larger excitation energies, however. If this interpretation were extended to data at higher excitation energy the $(k_q^*)^{-1}$ curves would be expected to be flat for about 2400 cm^{-1} below W_{ex}. Such flatness is definitely not observed.

2. It could be asserted that the b_i for states at energies less than 3147 Å are very small. The (b_i+q_i) were determined experimentally to be constant from 2760-3147 Å. There is no experimental evidence for states of energy less than 3147 Å. However, it was pointed out that in the superposition model using states with RRK degeneracy the b_i change by only a small factor over the range of energies considered. It is possible, however, that the b_i could decrease below 3147 Å.

Neither of the explanations for the quenching behavior at 3147 Å is satisfying, but the experimental data are not compelling enough to demand an explanation.

The assumptions and conclusions of the quenching analysis will now be reviewed.

1) A stepladder model with steps of equal energy was used. Interpretation of data in terms of this model does not imply that molecules were actually deactivated according to such a scheme. Rabinovitch[42,43] has shown that in chemical activation studies consideration of models other than the step ladder model does not

effect the conclusions drastically.

2) The b_i and q_i were assumed to be constant. The constancy of (b_i+q_i) was indicated experimentally. $b/(b+q)$ was shown to be greater than .55. The possibility remains that q_i is small compared to b_i and that the q_i change by relatively large factors. However, the q_i enter into Eq. (13) for $(k^*_{qn})^{-1}$ only as part of the sum (b_i+q_i). Therefore, even if q_i changes considerably but is small, the analysis is not affected.

3) a flat spectral distribution was assumed. Model calculations showed that the effect of the flat distribution was to shift the calculated curves to higher energy by about 1 step. The step size was estimated to be between 1000 and 2000 cm^{-1}. Comparison of the low pressure spectra and the semi-flat model spectral distribution indicates that the model distribution was relatively realistic.

4) A lower limit of .55 was placed on $b/(b+q)$. It was pointed out that the individual determination of b and q depended on information on the high pressure population distribution which is not available in this study.

5) Since $b/b+q \geq .55$ the vibrational deactivation rate constant, b, is at least 1.2 times as large as the intersystem crossing rate constant, q. Thus, vibrational deactivation is shown to play a large role in the relaxation mechanism of excited SO_2.

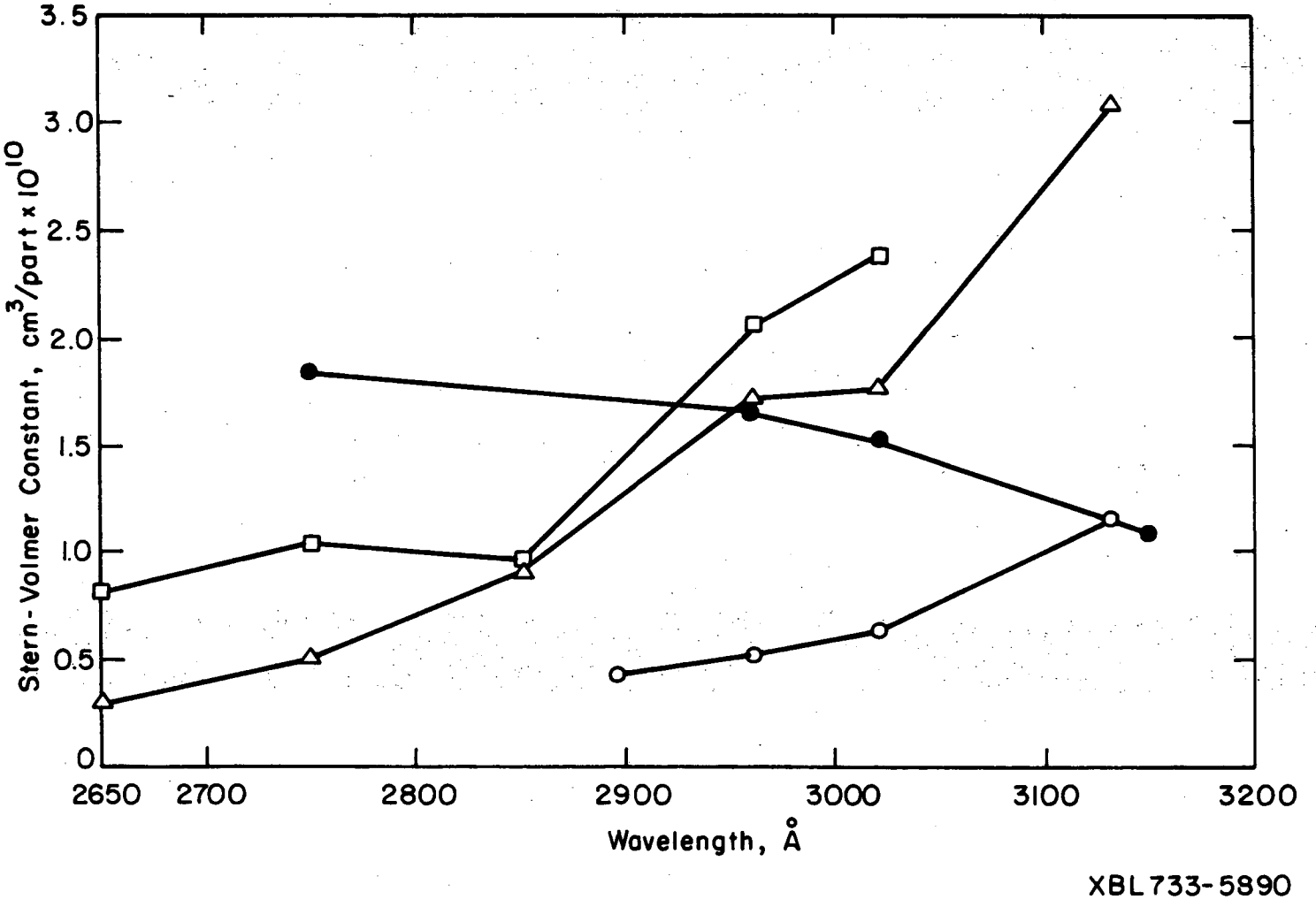

Fig. 33. Apparent Stern-Volmer constants reported by various investigators. Solid circles, this experiment; open circles, Strickler and Howell;[10] triangles, Mettee;[12] squares, Rao and Calvert.[47]

E. Comparison with Other Studies

The studies of SO_2 relaxation dynamics by previous investigators can be more fully explained in light of the results of the present experiment. Mettee,[12] Strickler and Howell[10] and Rao and Calvert[47] have all observed a decrease in the Stern-Volmer constant, k_q/k_f, with increasing excitation energy. Mettee has interpreted the change of Stern-Volmer constant in terms of an increase in k_f as the molecule is excited to higher energy, in analogy with Brewer's result for I_2.[19]

The present work, however, indicates that k_f changes by at most a factor of two over the energy range considered and the change in k_f is not monotonic as indicated in Mettee's interpretation. Furthermore, k_q, the quantity (b+q) in the stepladder model, is constant over the energy range considered. The Stern-Volmer constants calculated from the results of the present experiment are compared with those from other investigators in Fig. 33. The S-V constants from the three previous experiments all show a definite increase going to longer wavelength. The S-V constants from this experiment decrease slightly with wavelength. The increase of S-V constant with wavelength can be explained by consideration of the multistate kinetics indicated in this experiment. The results in the other three experiments[10,11,47] were interpreted on the basis of a single excited state model, not allowing for vibrational relaxation within the excited singlet electronic state. Thus, k_q is the apparent quenching constant for the entire manifold of vibrational state capable of fluorescing. If several steps of vibrational relaxation must be undergone before

fluorescence is effectively quenched the apparent quenching rate constant derived in a single state treatment is less than the rate constant for the individual relaxation steps. The higher the excitation energy, i.e., the greater the number of steps to the potential minimum, the smaller the single state quenching constant appears. This explanation then attributes the apparent decrease of S-V constant with increasing excitation energy to the incorrect single excited state treatment of SO_2 fluorescence.

Mettee[12] has shown that the quantum yield of fluorescence, measured at a given finite pressure, increases with excitation energy. This observation can be explained qualitatively within the results of the present experiment. Since higher excitation energies require more steps to deactivate the fluorescence a molecule excited to a high energy will in general pass through more steps from which it can fluoresce before it is removed from the fluorescing manifold. Thus, the overall quantum yield of fluorescence would be greater in molecules excited to relatively high energy, in agreement with experiment. Although the evidence is not compelling, Mettee has stated that it is likely that the quantum yield for triplet production is larger for higher excitation energies. This is explained by an argument similar to that explaining the quantum yield of fluorescence except that collision induced intersystem crossing to the triplet replaces fluorescence.

Calvert, et.al.,[48] (SOHCRD) have performed experiments on electronically excited sulfur dioxide which were interpreted in terms

of vibrational relaxation within the first excited singlet state. They directed a beam of light from a laser at 2662 Å along the axis of a cylindrical cell 2.5 cm in diameter. They observed the fluorescent emission in the wavelength range 3100-3950 Å. The emission decay following the laser flash was distinctly non-exponential. A distinct downward curvature was observed in plots of log(intensity) versus time. SOHCRD interpreted the initial decay rate of the emission in terms of properties of the initially excited state at 2662 Å. The lifetime at 2662 Å extrapolated to zero pressure was 36±4 μsec and the quenching rate constant was 0.6×10^{-10} cm^3/part-sec. The decay at long times after excitation (more than 400 μsec) was interpreted as arising from the vibrationally equilibrated excited singlet state. The decay curves were observed to be linear at times greater than 400 μsec and were observed to obey conventional Stern-Volmer kinetics. The lifetime at zero pressure for the vibrationally equilibrated excited state was determined to be 18±6 μsec and the quenching rate constant was about 1.3×10^{-10} cm^3/part-sec. SOHCRD discuss the variation in lifetime between the state at 2662 Å and the vibrationally equilibrated state in terms of changes in radiationless transition rates.

It is possible that the experiment of SOHCRD is seriously affected by use of a rather small fluorescence cell. Both Schwartz and Johnston[25] and Sackett and Yardley[9] have pointed out that the emission observation geometry must be large enough to encompass the migration of the excited molecules in order to prevent systematic errors in the measurements. The axis of excitation in the experiment of SOHCRD is only 1.25 cm

from the walls of the fluorescence cell. Both previous analyses[9,25] indicate that the observation geometry of SOHCRD may have introduced systematic quenching of the excited species at the walls of the fluorescence cell. Such wall deactivation could account for the downward curvature observed in plots of log(intensity) versus time. Thus, emission measured at long times after the flash is probably systematically affected and properties ascribed to a vibrationally equilibrated excited state may be in error. Further, the correlation of emission observed at long times after the excitation flash with properties of the "vibrationally equilibrated" excited state is conceptually unclear (disregarding the obvious experimental difficulties of observation at long times). Unless one postulates that the coupling between the excited singlet and the ground electronic states is negligible near the minimum of the excited state it is not clear than an equilibrated excited singlet could excist. Molecules would leave the low levels of the excited singlet by deactivation to vibrational levels of the ground state at lower energy than the minimum in the excited potential surface. A vibrationally equilibrated excited electronic state would not exist.

There is no experimental evidence available to determine the extent of the coupling between the low levels of the excited singlet and the ground state. The 18 μsec lifetime attributed by SOHCRD to a vibrationally equilibrated excited singlet is significantly longer than the 0.2 μsec predicted lifetime. Thus their interpretation does not seem consistent with their measurements.

ACKNOWLEDGMENTS

This research was conducted with the assistance of many persons. I wish to thank them all and to acknowledge that each of their individual contributions played an important role in the conduct of this experiment and dissertation. Harold Johnston was my principal research adviser. His scientific insight subtly influenced the direction of this research while he allowed me the opportunity to shape this investigation in my own fashion. I also want to thank R. Peter Frosch for helpful discussions during my first two years at Berkeley.

Steve Schmiriga and Tom Merrick provided invaluable assistance in the design and construction of the electronic apparatus. Many pieces of equipment were constructed by persons in the metal and glass shops. Alice Ramirez typed this dissertation and Gloria Pelatowski did the drawings. I wish to thank the Atomic Energy Commission for their support and use of the facilities at Lawrence Berkeley Laboratory.

APPENDIX A.

Modulation Relationships

We wish to show that two reversible counters gated with an arbitrary phase relationship to a sinusoidal excitation and 90° out of phase with respect to each other can be used to determine the phase between excitation and response of a system.

Figure 2 indicates diagramatically the excitation, response and the two counters. The phase between excitation and counters is ϕ_o. The equal time intervals ($\frac{1}{4}$ cycle) labelled A, B, C, and D represent periods during which the counters are counting positively or negatively. For instance, counter 1 adds any pulses arriving during A or B and subtracts pulses arriving during C or D. After many cycles the residual on counter 1 is Z1 = a+b-c-d where a represents the total counts during period A, and so forth. Since counter 2 lags counter 1 by 90° we have Z2 = -a+b+c-d.

The quantities a,b,c, and d must be evaluated as a function of the phase angle ϕ. An expression for the modulated concentration in a single excited state system was derived in the text. The modulated emission signal, E, is given by

$$\underset{\sim}{E} = \alpha k_f G I_o k_a \frac{1}{(\omega^2+k^2)^{1/2}} e^{i(\omega t+\phi)} \qquad (1)$$

where α includes all the detection factors.

Since the real part of the response is the only part detected we may write

$$\underline{E} = A \cos(\omega t + \phi) \tag{2}$$

where A includes all the constants in Eq. (1).

Since the counters are not necessarily in phase with the excitation Eq. (2) must be modified to reflect the fact that the phase being measured is the phase between the signal and the counters. Thus

$$\underline{E} = A \cos(\omega t + \psi) \tag{3}$$

where $\psi = \phi - \phi_o$.

The quantities a,b,c, and d are evaluated by integrating the signal over the appropriate time interval. (Note that $\tau = 2\pi/\omega$

$$a = \int_o^{T/4} A \cos(\omega t+\psi)dt = \frac{A}{\omega} (\cos \psi - \sin \psi)$$

$$b = \int_{T/4}^{2T/4} A \cos(\omega t+\phi)dt = \frac{A}{\omega} (-\sin \psi - \cos \psi)$$

$$c = \int_{2T/4}^{3T/4} A \cos(\omega t+\phi)dt = \frac{A}{\omega} (-\cos \psi + \sin \psi)$$

$$d = \int_{3T/4}^{4T/4} A \cos(\omega t+\phi)dt = \frac{A}{\omega} (\sin \psi + \cos \psi)$$

thus,

$$Z1 = \frac{A}{\omega} 4 \cos \psi \qquad Z2 = \frac{A}{\omega} 4 \sin \psi \tag{4}$$

and

$$\psi = \arctan \frac{Z_2}{Z_1}$$

Thus, Z1 and Z2 contain all the information needed to measure ψ.

Thus far we have considered the modulated excitation to be purely sinusoidal. However, as pointed out in the experimental section the second harmonic component of the modulated excitation was about 7% as large as the fundamental and the third harmonic was about 1% of the fundamental. We must consider the effect of these harmonics on the measured rate constants.

Consider the even harmonics in the excitation. Similarly to Eq. (3) we may write an expression for the component of the signal due to any even harmonic.

$$E_{j=even} = A(j) \cos(j\omega t + \psi_j) \qquad (5)$$

where w is the angular frequency of the fundamental. The quantities Z1 and Z2 can be evaluated for each of the even harmonics just as they were for the fundamental. For all values of even j both Z1 and Z2 are identically zero. Even harmonics in the modulated excitation make no contribution to the residual values on either counter. Consideration of the even harmonics may be neglected.

Z1 and Z2 are not, in general, zero when odd values of j are used in Eq. (5). In order to assess the effect of the small third harmonic in the modulated excitation we consider the phase vector of the fundamental of the signal compared to the phase vector of the third harmonic. Equation (1) indicates the two factors which determine the magnitude of the fundamental phase vector relative to the magnitude of the third harmonic phase vector.

$$\frac{|\hat{\underset{\sim}{E}}_3|}{|\hat{\underset{\sim}{E}}_1|} = \frac{I_{03}}{I_{01}} \left[\frac{\omega^2+k^2}{9\omega^2+k^2}\right]^{1/2} \tag{6}$$

Since $I_{03} = 0.01\ (I_{01})$ we can assert that the magnitude of the third harmonic phase vector is less than 1% of the fundamental phase vector. The phase of the third harmonic with respect to the fundamental was not determined so the direction of $\hat{\underset{\sim}{E}}_3$ is not known. If $\hat{\underset{\sim}{E}}_3$ is assumed to be perpendicular to $\hat{\underset{\sim}{E}}_1$ we can calculate the maximum error involved in neglecting $\hat{\underset{\sim}{E}}_3$ completely.

If $\hat{\underset{\sim}{E}}_1$ were at 45° the calculated lifetime would be 44.5 μsec. The addition of a vector 1% as long and perpendicular to $\hat{\underset{\sim}{E}}_1$ would result in a calculated lifetime of 46 μsec. It should be noted that this is an upper limit on the error involved in neglecting $\hat{\underset{\sim}{E}}_3$ since the direction of $\hat{\underset{\sim}{E}}_3$ was chosen to illustrate the greatest effect. Also from Eq. (6) $|\hat{\underset{\sim}{E}}_3|$ would be somewhat less then 1% of $|\hat{\underset{\sim}{E}}_1|$ depending on the value of k being measured.

The analysis in this experiment was in terms of pure sinusoidal excitation. Neglect of the third harmonic in the excitation could involve systematic errors of 3% or less.

APPENDIX B.

High Pressure Limits

To interpret the results of DC experiments, it is necessary to develop general expressions for concentrations in various states as a function of pressure. This discussion of the high pressure limit in fluorescence kinetics is an application of a more general discussion by Schwartz.[25]

Consider a set of states, one of which is populated optically, and the others are populated by a collisional stepladder process. In this discussion we will assume that each state is populated only by the state directly above it. From the usual steady state assumption the population of the first excited state, E_1, is

$$E_1 = I_o G k_a \frac{1}{k_{f1}+k_{q1}M} \tag{1}$$

where k_{f1} and k_{q1} are the fluorescence and quenching rate constants from state 1. Similarly, the population of the second state is

$$E_2 = \frac{E_1 b_1 M}{k_{f2}+k_{q2}M} = I_o G k_a \frac{1}{k_{f1}+k_{q1}M} \frac{b_1 M}{k_{f2}+k_{q2}M} \tag{2}$$

where b_1 is the rate constant for collisional deactivation from state 1 to state 2.

The population of state n is

$$E_n = I_o G k_a \frac{\prod_{j=1}^{j=n-1} (b_j M)}{\prod_{j=1}^{n} (k_{fj} + k_{qj} M)} \tag{3}$$

At high pressures where $k_{qj} M \gg k_{fj}$ expression (3) reduces to

$$E_n = \frac{I_o G k_a}{M} \frac{\prod_{1}^{n-1} b_j}{\prod_{1}^{n} k_{qj}} \tag{4}$$

Expression (4) can be placed in a form for direct comparison with the high pressure form of the Stern-Volmer relationship.

$$E_n = \frac{I_o G k_a}{k_{qn} M} \prod_{1}^{n-1} \left(\frac{b_j}{k_{qj}} \right) \tag{5}$$

This is to be compared with the high pressure Stern-Volmer relationship.

$$E = \frac{I_o G k_a}{k_q M}$$

Equation (5) illustrates the interesting result that conventional Stern-Volmer plots, at high enough pressure, are linear even for multistat systems. This result does not seem to be widely appreciated and has led to misinterpretation of Stern-Volmer data.

The analysis of the AC case is similar to the DC analysis. The differential equations describing the modulated concentrations are

linear if it is assumed that reactions between excited species are negligible. Solutions of the nonlinear case have been discussed previously.[49]

The simple case of a single excited state was discussed in the text. It was shown that

$$\underset{\sim}{E}_1 = I_o G k_a \frac{1}{k_1+i\omega} e^{i\omega t} \tag{6}$$

where

$$k_1 = k_{q1}M + k_{f1} \quad .$$

We now consider two state kinetics. The result for $\underset{\sim}{E}_1$ is known from Eq. (6). The differential equation governing $\underset{\sim}{E}_2$ is

$$\frac{d\underset{\sim}{E}_2}{dt} = \underset{\sim}{E}_1 b_1 M - k_2 \underset{\sim}{E}_2 \tag{7}$$

Equation (7) for $\underset{\sim}{E}_2$ is analogous to the equation for $\underset{\sim}{E}_1$, with $\underset{\sim}{E}_1$ taking the place of $\underset{\sim}{I}_o$ in the equation defining the time dependence of the second excited state. Therefore, the solution of Eq. (7) follows by analogy from the solution for $\underset{\sim}{E}_1$. The relationships for states of subsequent generations can be found in a similar manner.

$$\underset{\sim}{E}_2 = \underset{\sim}{I}_o G k_a \frac{1}{k_1+i\omega} \frac{b_1 M}{k_2+i\omega} \tag{8}$$

This result illustrates the generalization that the phase lag between two successive states must be between 0° and -90° depending on the magnitude of k for the second state.

Expressions for the modulated populations of the excited states at high pressure are particularly relevant. If the quenching rates constants are sufficiently large compared to the rate of fluorescence the k_{fi} may be omitted. The expression for $\underset{\sim}{E}_1$ then takes the form

$$\hat{\underset{\sim}{E}}_1 = \frac{\frac{I_o G k_a}{k_{q1} M}\left[1 - \frac{i\omega}{M}\frac{1}{k_{q1}}\right]}{1 + \left(\frac{\omega}{k_{q1} M}\right)^2} \tag{9}$$

The quantity $(\frac{\omega}{k_{q1}M})^2$ may be omitted if it is small compared to 1. This quantity is directly measured in a high pressure modulation experiment since

$$\frac{\omega}{k} = \frac{z_2}{z_1} = \tan^{-1}\phi$$

With a chopping frequency of 3600 cps the quantity $(\frac{\omega}{k_q M})^2$ may be omitted at measured values of k greater than 70×10^3 sec^{-1}. With this approximation the expression for the high pressure population of state 1 is

$$\hat{\underset{\sim}{E}}_1 = \frac{I_o G k_a}{M k_{q1}}\left[1 - \frac{i\omega}{M}\frac{1}{k_{q1}}\right] \tag{10}$$

Equation (10) agrees with the DC Stern-Volmer expression. At $\omega=0$ (the DC case) the out of phase (imaginary) component vanishes and the in phase component assumes the conventional form

$$E_1 = \frac{I_o G k_a}{M k_q}$$

The expression for E_2 is treated in the same manner. From Eq. (8) we write (neglecting k_{f2})

$$\hat{E}_2 \quad \frac{I_o G k_a}{M} \quad \frac{b_1}{k_{q1} k_{q2}} \quad \frac{\left[1 - \left(\frac{\omega}{M}\right)^2 \left(\frac{1}{k_{q1}} \frac{1}{k_{q2}}\right) - \frac{i\omega}{M}\left(\frac{1}{k_{q1}} + \frac{1}{k_{q2}}\right)\right]}{\left[1 + \left(\frac{\omega}{k_{q1} M}\right)^2\right]\left[1 + \left(\frac{\omega}{k_{q2} M}\right)^2\right]} \tag{11}$$

Again neglecting terms of the order $\left(\frac{\omega}{k_q M}\right)^2$ we obtain

$$\hat{E}_2 = \frac{I_o G k_a}{M} \quad \frac{b_1}{k_{q1} k_{q2}} \quad \left[1 - \frac{i\omega}{M}\left(\frac{1}{k_{q1}} + \frac{1}{k_{q2}}\right)\right] \tag{12}$$

In a similar manner we can write a general expression for the modulated population of state n

$$\hat{E}_n = \frac{I_o G k_a}{M} \quad \frac{b_1 \, b_2 \, \cdots \, b_{n-1}}{k_{q1} k_{q2} \cdots k_{qn}} \quad \left[1 - \frac{i\omega}{M}\left(\frac{1}{k_{q1}} + \frac{1}{k_{q2}} + \cdots + \frac{1}{k_{qn}}\right)\right] \tag{13}$$

APPENDIX C.

The data from the pressure dependent lifetime experiments are tabulated in this appendix. λ_{ex} and λ_{obs} are the excitation and observation wavelengths, respectively. ΔW is the difference between the excitation and observation energies.

λ_{ex} = 2760 Å

λ_{obs} = 2820 Å	ΔW = 770 cm^{-1}	λ_{obs} = 2839 Å	ΔW = 1000 cm^{-1}
Pressure, mTorr	$1/\tau \times 10^4$, sec^{-1}	Pressure, mTorr	$1/\tau \times 10^4$, sec^{-1}
3.30	49	6.51	69
5.00	65	9.03	93
6.61	74	13.5	126
7.93	89	14.5	142
9.38	97	15.9	157
10.6	115	17.7	170
12.7	138	20.3	191

λ_{obs} = 2879 Å	ΔW = 1500 cm^{-1}	λ_{obs} = 2921 Å	ΔW = 2000 cm^{-1}
Pressure, mTorr	$1/\tau \times 10^4$, sec^{-1}	Pressure, mTorr	$1/\tau \times 10^4$, sec^{-1}
6.15	64	6.15	54
9.13	86	9.11	77
11.1	109	11.1	96
13.0	136	13.0	115
15.7	142	15.7	129
16.9	140	16.9	125
19.1	174	19.1	142
20.2	177	20.2	157

λ_{obs} = 2965 Å	ΔW = 2500 cm^{-1}
Pressure, mTorr	$1/\tau \times 10^4$, sec^{-1}
6.15	51
9.14	70
11.1	88
13.0	100
15.7	122
16.9	121
19.1	142
20.2	139

λ_{obs} = 3009 Å	ΔW = 3000 cm^{-1}
Pressure, mTorr	$1/\tau \times 10^4$, sec^{-1}
5.02	42
7.28	55
9.29	65
10.9	74
13.1	87
15.2	101
20.7	115
21.4	133

λ_{obs} = 3055 Å	ΔW = 3500 cm^{-1}
Pressure, mTorr	$1/\tau \times 10^4$, sec^{-1}
7.37	51
9.35	60
11.0	72
13.0	80
15.2	96
18.3	107
20.7	123

λ_{obs} = 3103 Å	ΔW = 4000 cm^{-1}
Pressure, mTorr	$1/\tau \times 10^4$, sec^{-1}
6.00	41
8.02	50
10.1	61
13.2	73
15.7	92
18.2	97
19.4	110
20.5	113

λ_{obs} = 3152 Å	ΔW = 4500 cm^{-1}
Pressure, mTorr	$1/\tau \times 10^4$, sec^{-1}
5.03	36
8.02	45
10.1	57
13.2	70
15.7	80
18.2	98
19.4	101
20.5	105

λ_{obs} = 3202 Å	ΔW = 5000 cm^{-1}
Pressure, mTorr	$1/\tau \times 10^4$, sec^{-1}
5.02	35
6.01	39
7.97	47
10.1	56
13.2	70
15.7	84
18.2	90
19.4	94

λ_{obs} = 3254 Å	ΔW = 5500 cm^{-1}
Pressure, mTorr	$1/\tau \times 10^4$, sec^{-1}
5.11	30
6.32	37
8.24	47
10.7	56
11.4	65
13.1	70
17.3	90
19.2	100
21.2	106

λ_{obs} = 3308 Å	ΔW = 6000 cm^{-1}
Pressure, mTorr	$1/\tau \times 10^4$, sec^{-1}
5.11	31
6.33	38
8.22	45
10.7	57
11.4	63
13.1	72
17.3	89
19.2	98
21.2	106

λ_{obs} = 3364 Å	ΔW = 6500 cm^{-1}
Pressure, mTorr	$1/\tau \times 10^4$, sec^{-1}
6.32	37
8.88	47
11.2	58
13.4	69
14.4	71
16.1	80
17.6	86
20.2	97

λ_{ex} = 2960 Å

λ_{obs} = 3044 Å	ΔW = 910 cm^{-1}	λ_{obs} = 3067 Å	ΔW = 1153 cm^{-1}
Pressure, mTorr	$1/\tau \times 10^4$, sec^{-1}	Pressure, mTorr	$1/\tau \times 10^4$, sec^{-1}
5.01	51	6.21	73
6.22	63	8.05	92
6.87	64	9.92	110
8.01	79	10.6	107
8.78	79	13.1	124
9.92	92	15.1	137
10.6	96	17.0	175
13.2	117		
15.0	137		
17.0	158		

λ_{obs} = 3102 Å	ΔW = 1525 cm^{-1}	λ_{obs} = 3130 Å	ΔW = 1820 cm^{-1}
Pressure, mTorr	$1/\tau \times 10^4$, sec^{-1}	Pressure, mTorr	$1/\tau \times 10^4$, sec^{-1}
5.15	56	4.11	40
6.07	60	4.95	47
7.94	76	6.18	55
10.1	100	8.13	70
13.1	113	9.94	83
15.0	137	18.9	182
17.0	145		
19.2	167		

λ_{obs} = 3168 Å	ΔW = 2193 cm^{-1}
Pressure, mTorr	$1/\tau \times 10^4$, sec^{-1}
4.14	42
5.13	51
6.09	55
7.92	69
10.1	85
18.9	182

λ_{obs} = 3213 Å	ΔW = 2653 cm^{-1}
Pressure, mTorr	$1/\tau \times 10^4$, sec^{-1}
4.21	37
5.23	44
6.15	51
7.87	65
10.1	79
18.9	150

λ_{obs} = 3251 Å	ΔW = 3000 cm^{-1}
Pressure, mTorr	$1/\tau \times 10^4$, sec^{-1}
4.11	36
5.14	41
6.02	49
7.87	59
10.1	76
12.2	96
14.9	113
18.9	141

λ_{obs} = 3291 Å	ΔW = 3374 cm^{-1}
Pressure, mTorr	$1/\tau \times 10^4$, sec^{-1}
4.32	36
5.48	43
6.42	48
8.21	57
9.82	67
14.5	101

λ_{obs} = 3328 Å	ΔW = 3712 cm^{-1}
Pressure, mTorr	$1/\tau \times 10^4$, sec^{-1}
4.32	36
5.48	41
6.42	49
8.21	56
9.82	67
14.5	100

λ_{obs} = 3397 Å	ΔW = 3712 cm^{-1}
Pressure, mTorr	$1/\tau \times 10^4$, sec^{-1}
4.57	34
6.38	45
8.02	54
9.75	62
12.9	81
16.4	106
19.0	120

λ_{ex} = 3023 Å

λ_{obs} = 3089 Å	ΔW = 703 cm^{-1}	λ_{obs} = 3122 Å	ΔW = 1047 cm^{-1}
Pressure, mTorr	$1/\tau \times 10^4$, sec^{-1}	Pressure, mTorr	$1/\tau \times 10^4$, sec^{-1}
4.92	51	5.20	59
6.68	66	7.00	72
8.93	82	9.15	93
10.7	101	11.0	119
12.4	117	12.9	136
12.8	124	14.7	160
14.3	134	17.0	180
15.4	149		

λ_{obs} = 3147 Å	ΔW = 1302 cm^{-1}	λ_{obs} = 3182 Å	ΔW = 1650 cm^{-1}
Pressure, mTorr	$1/\tau \times 10^4$, sec^{-1}	Pressure, mTorr	$1/\tau \times 10^4$, sec^{-1}
5.15	64	5.32	51
6.90	83	7.25	67
9.10	113	9.05	80
11.2	138	11.4	100
13.1	154	13.1	114
17.0	183	15.1	134
19.5	219	17.2	149
		19.5	180

λ_{obs} = 3251 Å	ΔW = 2320 cm^{-1}
Pressure, mTorr	$1/\tau \times 10^4$, sec^{-1}
5.32	48
7.23	61
9.05	73
11.4	94
13.1	103
15.1	126
17.2	144
19.5	164

λ_{obs} = 3286 Å	ΔW = 2645 cm^{-1}
Pressure, mTorr	$1/\tau \times 10^4$, sec^{-1}
5.20	46
7.00	61
9.25	77
11.0	94
12.9	100
14.6	117
16.6	135
19.5	158

λ_{obs} = 3328 Å	ΔW = 3032 cm^{-1}
Pressure, mTorr	$1/\tau \times 10^4$, sec^{-1}
5.32	45
7.23	58
9.05	69
11.4	90
13.1	101
15.1	117
17.2	133
19.5	154

λ_{obs} = 3397 Å	ΔW = 3641 cm^{-1}
Pressure, mTorr	$1/\tau \times 10^4$, sec^{-1}
4.91	41
6.72	52
8.85	69
11.9	83
12.6	97
14.3	111
16.3	126
19.2	142

λ_{ex} = 3147 Å

λ_{obs} = 3211 Å	ΔW = 638 cm^{-1}	λ_{obs} = 3251 Å	ΔW = 1018 cm^{-1}
Pressure, mTorr	$1/\tau \times 10^4$, sec^{-1}	Pressure, mTorr	$1/\tau \times 10^4$, sec^{-1}
4.92	70	4.33	75
6.03	82	5.00	86
6.91	87	5.95	103
8.68	109	6.95	115
9.68	111	7.75	112
10.9	136	9.00	136
12.4	148	10.0	144
		11.5	182

λ_{obs} = 3283 Å	ΔW = 1313 cm^{-1}	λ_{obs} = 3314 Å	ΔW = 1603 cm^{-1}
Pressure, mTorr	$1/\tau \times 10^4$, sec^{-1}	Pressure, mTorr	$1/\tau \times 10^4$, sec^{-1}
6.34	106	5.11	70
7.51	130	7.13	89
9.18	151	10.0	132
10.4	171	11.5	137
11.4	180	14.3	175
11.8	187	16.7	183

λ_{obs} = 3340 Å	ΔW = 1838 cm^{-1}
Pressure, mTorr	$1/\tau \times 10^4$, sec^{-1}
5.62	73
7.25	93
9.50	115
10.5	129
13.2	145
14.5	145

λ_{obs} = 3397 Å	ΔW = 2339 cm^{-1}
Pressure, mTorr	$1/\tau \times 10^4$, sec^{-1}
5.01	80
6.12	91
7.19	106
8.23	118
8.93	117
9.52	126
10.2	133
11.0	145
12.6	167

REFERENCES

1. a. H. S. Johnston, Gas Phase Reaction Rate Theory (Ronald Press, New York, 1966).

   b. V. N. Kondrat'ev, Chemical Kinetics of Gas Reactions (Addison-Wesley, Massachusetts, 1964).

2. G. W. Robinson, J. Chem. Phys. 47, 1967 (1967).

3. A. E. Douglas, J. Chem. Phys. 45, 1007 (1966).

4. M. Bixon and J. Jortner, J. Chem. Phys. 50, 3284 (1969).

5. H. Kemper and M. Stockburger, J. Chem. Phys. 53, 268 (1970).

6. J. Steinfeld, Accts. of Chem. Res. 3, 313 (1970).

7. P. Pringsheim, Fluorescence and Phosphorescence (Interscience, New York, 1949).

8. K. Greenough and A. Duncan, J. Am. Chem. Soc. 83, 555 (1961).

9. P. Sackett and J. Yardley, J. Chem. Phys. 57, 152 (1972).

10. S. Strickler and D. Howell, J. Chem. Phys. 49, 1947 (1968).

11. H. D. Mettee, J. Phys. Chem. 73, 1071 (1969).

12. H. D. Mettee, J. Chem. Phys. 49, 1784 (1968).

13. G. Herzberg, Electronic Spectra of Polyatomic Molecules (D. Van Nostrand Co., New York 1966).

14. N. Metropolis, Phys. Rev. 60, 295 (1941).

15. J. H. Clements, Phys. Rev. 47, 224 (1934).

16. P. Warneck, F. F. Marmo and J. O. Sullivan, J. Chem. Phys. 40, 1132 (1963).

17. R. A. Cox, J. Phys. Chem. 6, 814 (1972).

18. S. Okuda, T. N. Rao, D. Slater and J. Calvert, J. Phys. Chem. 73, 4412 (1969).

19. A. Chutjian, J. Link and L. Brewer, J. Chem. Phys. 46, 2666 (1967).

20. A. B. Harker (Ph.D. thesis) University of California, Berkeley, California (1972).

21. J. J. Brophy, Basic Electronics for Scientists, (McGraw Hill, New York, 1966).

22. E. Kreyszig, Advanced Engineering Mathematics, (John Wiley and Sons, Inc., New York, 1962).

23. E. D. Morris,Jr. and H. S. Johnston, Rev. Sci. Inst. 39, 620 (1968).

24. O. Stern and M. Volmer, Physik. Z. 183 (1919).

25. S. Schwartz and H. S. Johnston, J. Chem. Phys. 51, 1286 (1969).

26. J. Rodman and H. Smith, Appl. Opt. 2, 181 (1963).

27. G. A. Morton, Appl. Opt. 7, 1 (1968).

28. S. Strickler and Berg, J. Chem. Phys. 37, 814 (1962).

29. P. Warneck, F. Marmo and J. Sullivan, J. Chem. Phys. 40, 1132 (1963).

30. C. J. Halstead and B. A. Thrush, Proc. Roy. Soc. A, 295, 380 (1966).

31. T. N. Rao, S. Collier and J. Calvert, J. Am. Chem. Soc. 91, 1609 (1968).

32. G. Kistiakowsky and C. Paramenter, J. Chem. Phys. 42, 2942 (1965).

33. M. Bixon and J. Jortner, J. Chem. Phys. 50, 3284 (1968).

34. D. Chock, J. Jortner and S. Rice, J. Chem. Phys. 49, 610 (1967).

35. G. Z. Whitten and B. S. Rabinovitch, J. Chem. Phys. 38, 2466 (1963).

36. P. B. Sackett and J. T. Yardley, Chem. Phys. Letters 6, 323 (1970).

37. G. W. Robinson and R. P. Frosch, J. Chem. Phys. 38, 1187 (1963).

38. M. Bixon and J. Jortner, J. Chem. Phys. 48, 715 (1968).

39. P. Gardner and M. Kasha, J. Chem. Phys. 50, 1453 (1968).

40. R. P. Frosch, personal communication.

41. L. F. Keyser, S. Z. Levine and F. Kaufman, J. Chem. Phys. 54, 355 (1971).

42. R. E. Harrington, B. S. Rabinovitch, and M. R. Hoare, J. Chem. Phys. 33, 744 (1960).

43. G. H. Kohlmaier and B. S. Rabinovitch, J. Chem. Phys. 38, 1692 (1962).

44. L. S. Kassel, Kinetics of Homogeneous Gas Reactions, (The Chemical Catalog Co., Inc., New York, 1932).

45. A. Messiah, Quantum Mechanics (John Wiley and Sons, Inc., New York, 1966), p. 836.

46. H. S. Heaps and G. Herzberg, Z. Physik, 133, 48 (1952).

47. T. N. Rao and J. G. Calvert, J. Phys. Chem. 74, 681 (1970).

48. H. W. Sidebottom, K. Otsuka, A. Horowitz, J. G. Calvert, B. R. Rabe and E. K. Damon, Chem. Phys. Letters 13, 337 (1972).

49. T. Paukert (Ph.D. thesis) University of California, Berkeley, California (1969).

TECHNICAL INFORMATION DIVISION
LAWRENCE BERKELEY LABORATORY
UNIVERSITY OF CALIFORNIA
BERKELEY, CALIFORNIA 94720